


8-2018

Unfolded protein response pathways in skeletal muscle homeostasis.

Kyle R. Bohnert
University of Louisville

Follow this and additional works at: <https://ir.library.louisville.edu/etd>

 Part of the [Cell Biology Commons](#), [Integrative Biology Commons](#), and the [Musculoskeletal System Commons](#)

Recommended Citation

Bohnert, Kyle R., "Unfolded protein response pathways in skeletal muscle homeostasis." (2018). *Electronic Theses and Dissertations*. Paper 3033.
<https://doi.org/10.18297/etd/3033>

This Doctoral Dissertation is brought to you for free and open access by ThinkIR: The University of Louisville's Institutional Repository. It has been accepted for inclusion in Electronic Theses and Dissertations by an authorized administrator of ThinkIR: The University of Louisville's Institutional Repository. This title appears here courtesy of the author, who has retained all other copyrights. For more information, please contact thinkir@louisville.edu.

UNFOLDED PROTEIN RESPONSE PATHWAYS IN SKELETAL MUSCLE
HOMEOSTASIS

By

Kyle R. Bohnert, M.S.

B.S., Hanover College, 2012

M.S., University of Kentucky, 2014

M.S., University of Louisville, 2016

A dissertation submitted to the Faculty of the School of Medicine of the University of
Louisville in Partial Fulfillment of the Requirements for the Degree of

Doctor of Philosophy in Anatomical Sciences and Neurobiology

Department of Anatomical Sciences and Neurobiology,

University of Louisville,

Louisville, Kentucky

August 2018

UNFOLDED PROTEIN RESPONSE PATHWAYS IN SKELETAL MUSCLE
HOMEOSTASIS

By

Kyle R. Bohnert, M.S.

A Dissertation Approved on

July 20, 2018

By the following Dissertation Committee:

Ashok Kumar, Ph.D.

Dissertation Director

Michal Hetman, MD, Ph.D.

J. Patrick Moore, Ph.D.

Jeffrey C. Petruska, Ph.D.

Scott R. Whittemore, Ph.D.

DEDICATION

To my wife

Mrs. Amanda Bohnert

For her unwavering support and unconditional love.

ACKNOWLEDGMENTS

Thank you to my committee members; Dr. Michal Hetman, Dr. J. Patrick Moore, Dr. Jeffrey C. Petruska, and Dr. Scott R. Whittemore. Thank you for your support and critical advice! I thank Dr. Shuichi Sato, Dr. Robert Friedland and once more Dr. Jeffrey C. Petruska, and Dr. Scott R. Whittemore for their impactful recommendation letters for the NRSA prize. Thank you to Dr. William Guido, Ms. Donna Bottorff, and all the ASNB faculty and staff for their continued support.

My lab members, currently and previously; Alex Straughn, Joe McMillan, Dr. Yann Gallott, Dr. Sajedah Hindi, Dr. Guangyan Xiong, Dr. Shuichi Sato, Dr. Marjan Tajrishi, Dr. Adriana Bankston, and Dr. Yuji Ogura, Thank you for creating a great working environment.

Thank you to the Bohnert family: my wife Amanda and our son Gibson, my parents Ken and Sharon Bohnert, my siblings and their significant others: Jennifer and Matthew King, Elizabeth and Peter Murphy, and Adam and Alyssa Bohnert, and my nephews: Jude, Davis, and Quinn Murphy and Declan Bohnert.

And last but most definite certainly not least, Dr. Ashok Kumar, my mentor, Thank You for all your hard work and support you have given me!

ABSTRACT

UNFOLDED PROTEIN RESPONSE PATHWAYS IN SKELETAL MUSCLE

HOMEOSTASIS

Kyle R. Bohnert

July 20, 2018

Skeletal muscle mass, contractile properties, and metabolic function are regulated through the coordinated activation of multiple intracellular signaling pathways and genetic reprogramming. The endoplasmic reticulum (ER) plays a pivotal role in protein folding and calcium homeostasis in many cell types, including skeletal muscle. Disruption of calcium levels or accumulation of misfolded proteins in the ER lumen leads to stress, which results in the activation of a signaling network called the unfolded protein response (UPR). Further, recent studies have suggested that in certain conditions, UPR pathways can be activated independent of ER stress. However, the role of ER stress and the UPR in the regulation of skeletal muscle mass and function had not been previously investigated.

This dissertation demonstrates that the markers of ER stress are increased in skeletal muscle of mouse models of cancer cachexia. Chronic administration of 4-phenylbutyrate (4-PBA), a molecular chaperon and an inhibitor of ER stress, leads to the loss of skeletal muscle mass and function in naïve conditions and in Lewis lung carcinoma (LLC) tumor-bearing mice. 4-PBA also causes atrophy in cultured primary myotubes. Further, our results demonstrate that the targeted deletion of X-box binding

protein (XBP1), a downstream target of the inositol-requiring enzyme 1 α (IRE1 α) arm of the UPR, attenuates the loss of skeletal muscle mass in LLC tumor-bearing mice. Overexpression of a spliced form of XBP1 causes atrophy and induces the gene expression of several proinflammatory cytokines and the components of ubiquitin proteasome system and autophagy in cultured myotubes. Our results also demonstrate that toll-like receptors-mediated signaling is responsible, at least in part, for the activation of the UPR in skeletal muscle of LLC tumor-bearing mice.

Finally, the role of the XBP1 in skeletal muscle growth and regeneration was also investigated. Results showed XBP1 mediates overload-induced myofiber hypertrophy and skeletal muscle regeneration potentially through augmenting the proliferation of satellite cells in a non-cell-autonomous manner. Altogether, this dissertation provides initial evidence that while basal levels of ER stress/UPR is essential for the maintenance of skeletal muscle mass and strength, supra-physiological activation of the UPR, especially the IRE1/XBP1 arm, causes skeletal muscle wasting.

TABLE OF CONTENTS

	PAGE
DEDICATIONS.....	iii
ACKNOWLEDGMENTS.....	iv
ABSTRACT.....	v
LIST OF FIGURES.....	vii
CHAPTERS	
CHAPTER 1.....	1
1.1 INTRODUCTION.....	1
1.2 THE UNFOLDED PROTEIN RESPONSE.....	1
1.3 UPR AND MYOGENESIS.....	3
1.4 SKELETAL MUSCLE ATROPHY.....	7
1.5 UPR AND SKELETAL MUSCLE ATROPHY.....	8
1.6 UPR AND SKELETAL MUSCLE ADAPTATION TO EXERCISE.....	12
1.7 CLINICAL SIGNIFICANCE OF UPR IN SKELETAL MUSCLE DISEASES.....	14
1.7 CONCLUDING REMARKS.....	19
CHAPTER 2.....	25
2.1 INTRODUCTION.....	25
2.2 MATERIALS AND METHODS.....	29
2.3 RESULTS.....	35
2.3.1 MARKERS OF ER STRESS ARE INDUCED IN SKELETAL MUSCLE OF MOUSE MODELS OF CANCER CACHEXIA.....	35
2.3.2 TUMOR-DERIVED FACTORS INCREASE MARKERS OF ER STRESS IN SKELETAL MUSCLE.....	36
2.3.3 INHIBITION OF ER STRESS DIMINISHES MUSCLE STRENGTH IN NORMAL AND LLC-BEARING MICE.....	37
2.3.4 INHIBITION OF ER STRESS CAUSES SKELETAL MUSCLE WASTING IN NORMAL AND LLC-BEARING MICE.....	38
2.3.5 ER STRESS IS NECESSARY FOR MAINTAINING THE OXIDATIVE PHENOTYPE OF SKELETAL MUSCLE.....	40
2.3.6 INHIBITION OF ER STRESS ACTIVATES PROTEOLYTIC PATHWAYS IN SKELETAL MUSCLE.....	41
2.3.7 ROLE OF ER STRESS IN THE ACTIVATION OF THE AKT/MTOR PATHWAY AND AMPK IN SKELETAL MUSCLE.....	42
2.3.8 INHIBITION OF ER STRESS CAUSES ATROPHY IN CULTURE MYOTUBES.....	43
2.4 DISCUSSION.....	45

CHAPTER 3.....	67
3.1 INTRODUCTION.....	67
3.2 MATERIALS AND METHODS.....	71
3.3 RESULTS.....	77
3.3.1 LEVELS OF TLRs AND MYD88 ARE INCREASED IN SKELETAL MUSCLE OF LLC TUMOR-BEARING MICE.....	77
3.3.2 TARGETED DELETION OF MYD88 INHIBITS LLC TUMOR- INDUCED SKELETAL MUSCLE WASTING IN MICE.....	78
3.3.3 INHIBITION OF MYD88 INHIBITS SLOW-TO-FAST TYPE TRANSITION IN SKELETAL MUSCLE DURING CACHEXIA.....	79
3.3.4 MYD88 MEDIATES THE ACTIVATION OF CATABOLIC PATHWAYS IN SKELETAL MUSCLE OF LLC TUMOR BEARING MICE.....	80
3.3.5 MYD88 MEDIATES THE ACTIVATION OF THE UPR IN SKELETAL MUSCLE DURING CANCER CACHEXIA.....	83
3.3.6 TARGETED ABLATION OF XBP1 INHIBITS SKELETAL MUSCLE IN LLC TUMOR-BEARING MICE.....	84
3.3.7 ACTIVATION OF XBP1 INDUCES ATROPHY OF CULTURED MYOTUBES.....	86
3.4 DISCUSSION.....	87
CHAPTER 4.....	108
4.1 INTRODUCTION.....	108
4.2 MATERIALS AND METHODS.....	111
4.3 RESULTS.....	117
4.3.1 MYOFIBER-SPECIFIC DELETION OF XBP1 INHIBITS SKELETAL MUSCLE REGENERATION IN ADULT MICE.....	117
4.3.2 ABLATION OF XBP1 INHIBITS THE EXPRESSION OF MYOGENIC MARKERS DURING SKELETAL MUSCLE REGENERATION IN MICE.....	118
4.3.3 TARGETED DELETION OF XBP1 REDUCES THE NUMBER OF SATELLITE CELLS IN REGENERATING SKELETAL MUSCLE.....	119
4.3.4 XBP1 MEDIATES POST-NATAL SKELETAL MUSCLE GROWTH.....	120
4.3.5 XBP1 MEDIATES MYOFIBER HYPERTROPHY IN RESPONSE TO FUNCTIONAL OVERLOAD.....	122
4.3.6 GENETIC ABLATION OF XBP1 INHIBITS SATELLITE CELL PROLIFERATION DURING OVERLOAD-INDUCED MYOFIBER HYPERTROPHY.....	123
4.3.7 XBP1 IS ESSENTIAL FOR MYOBLAST FUSION IN VITRO..	125
4.3.8 FORCED EXPRESSION OF XBP1 REDUCES MYOBLAST FUSION IN VITRO.....	126
4.4 DISCUSSION.....	126
CHAPTER 5.....	150
5.1 REVIEW OF DISSERTATION.....	150

5.2 SCIENTIFIC CONTRIBUTION AND FUTURE IMPLEMENTAT.....	157
5.3 LIMITATIONS OF FUTURE IMPLEMENTATION.....	159
REFERENCES.....	163
APPENDICES.....	181
APPENDIX 1.....	181
APPENDIX 2.....	182
APPENDIX 3.....	184
CURRICULUM VITAE.....	187

LIST OF FIGURES

FIGURE	PAGE
1. FIGURE 1.1.....	21
2. FIGURE 1.2.....	23
4. FIGURE 2.1.....	53
5. FIGURE 2.2.....	55
6. FIGURE 2.3.....	56
7. FIGURE 2.4.....	57
8. FIGURE 2.5.....	59
9. FIGURE 2.6.....	61
10. FIGURE 2.7.....	63
11. FIGURE 2.8.....	65
12. FIGURE 3.1.....	94
13. FIGURE 3.2.....	96
14. FIGURE 3.3.....	98
15. FIGURE 3.4.....	100
16. FIGURE 3.5.....	102
17. FIGURE 3.6.....	104
18. FIGURE 3.7.....	106
19. FIGURE 4.1.....	132
20. FIGURE 4.2.....	134

21. FIGURE 4.3.....	136
22. FIGURE 4.4.....	138
23. FIGURE 4.5.....	140
24. FIGURE 4.6.....	142
25. FIGURE 4.7.....	144
26. FIGURE 4.8.....	146
27. FIGURE 4.9.....	148

CHAPTER 1

GENERAL INTRODUCTION

1.1 Introduction. The following section provides an extensive review of the literature pertaining to the mechanisms regulating skeletal muscle formation, growth, and atrophy with focuses on the role of the unfolded protein response (UPR). This chapter is adapted from a review article, in which I am first author, that was published in the Journal of Cellular Physiology [1].

1.2 The Unfolded Protein Response. The endoplasmic reticulum (ER) is a membrane-bound organelle in mammalian cells that is responsible for proper folding, processing, and trafficking of proteins. The ER also plays an important role in calcium homeostasis of the cell. Accumulation of misfolded proteins, viral infection, imbalances in calcium level, and many other perturbations that disrupt cell homeostasis lead to ER stress [2-4]. The ER deals with such stress through initiating the unfolded protein response (UPR) that is mediated by three ER transmembrane sensors: RNA-dependent protein kinase-like ER eukaryotic translation initiation factor 2 alpha kinase (PERK), inositol-requiring protein 1 (IRE1), and activating transcription factor 6 (ATF6) [5-7].

Under normal physiological conditions, PERK, IRE1, and ATF6 proteins are maintained in an inactive state by binding to BiP/glucose-regulating protein 78 (GRP78),

an important ER chaperone. Upon ER stress, GRP78 disassociates from these proteins and preferentially binds to the misfolded proteins in the ER lumen (**Figure 1.1**). Upon release from GRP78, PERK is auto-phosphorylated leading to a cascade of signals including phosphorylation of eukaryotic translation initiation factor 2 α (eIF2 α) and translation of activating transcription factor-4 (ATF4), which induces transcription of C/EBP homologous protein (CHOP) [7-9]. The PERK/eIF2 α axis is also involved in the termination of the UPR after the stress has been relieved by activation of growth arrest and DNA damage-inducible protein, GADD34 [10]. Another ER transmembrane sensor, IRE1, also becomes activated by autophosphorylation during ER stress. Through its endonuclease activity, IRE1 promotes splicing of a 26-base intron from X-box-binding protein 1 (XBP1) mRNA [11]. Spliced XBP1 (sXBP1) increases ER chaperones and other components to assist in the folding capacity of the ER [12]. Lastly, once activated, ATF6 moves from the ER to the Golgi apparatus to be cleaved by site-1 proteases [13]. The cleaved N-terminal fragment of ATF6 is then transported to the nucleus where it acts in combination with sXBP1 to increase the levels of proteins that function to alleviate ER stress [11]. Activation of all three pathways alleviates ER stress by regulating gene expression and protein synthesis. The main purpose of the UPR is to increase the protein folding capacity of the cell while decreasing the unfolded protein load [7-9].

While chronic unmitigated ER stress can lead to cell death, accumulating evidence suggests that a low level of ER stress may be protective to cells by eliciting an adaptive UPR that ‘preconditions’ the cell to a subsequent pathological insult, a process named as ER hormesis. The UPR has been found to regulate autophagy, mitochondrial biogenesis and function, and the expression of various anti-oxidant molecules to protect

mammalian cells under stress conditions [14]. Low level of ER stress and UPR also play an important role in the survival, self-renewal, and differentiation of stem cells in various organs [15]. Moreover, it is increasingly evident that different arms of the UPR may have a distinct role in regulation of cell fate in naïve and diseased states [5-7].

In recent years, several articles have been published highlighting the potential role of ER stress in the regulation of skeletal muscle development, regeneration, and adaptation in response to external stimuli. In the following section, we provide a succinct review of the role and mechanisms of action of ER stress-induced UPR pathways in the regulation of various aspects of skeletal muscle function. We also provide potential avenues for future research that will elucidate the role of individual arms of the UPR in the regulation of skeletal muscle mass.

1.3 UPR and Myogenesis: Myogenesis is a complex and highly regulated process that involves the determination of multi-potential mesodermal cells to give rise to myoblasts, exit of these myoblasts from the cell cycle, and their differentiation into muscle fibers [16]. Myogenesis is regulated by the sequential expression of myogenic regulatory factors (MRFs), a group of basic helix-loop-helix transcription factors that include Myf5, MyoD, myogenin, and MRF4 (**Figure 1.2**). Many steps of myogenesis can be recapitulated *in vitro* through incubation of primary myogenic cells or C2C12 myoblasts, which form multi-nucleated myotubes in low serum conditions [16, 17].

An essential feature of skeletal muscle formation is selective apoptosis that eliminates differentiation-incompetent myoblasts during myogenesis [18, 19]. Activation of ER stress initiates the activation of caspase-12, which leads to the downstream

activation of caspase-9 and caspase-3 and subsequent apoptosis. An earlier study demonstrated that the ATF6 arm of the UPR and other markers of ER stress such as CHOP and BiP as well as caspase-12 are increased in the myoblasts undergoing apoptosis upon induction of myogenic differentiation [20]. Inhibition of ATF6 or caspase-12 reduced myoblast apoptosis and attenuated the formation of multi-nucleated myotubes in C2C12 cultures. Interestingly, a similar increase in caspase-12 is also observed in skeletal muscle during embryonic development suggesting that the ATF6 arm of the UPR leads to selective apoptosis of a subpopulation of cells that may be vulnerable to cellular stresses both *in vitro* and *in vivo* [20]. In support of these findings, a subsequent study demonstrated that forced activation of ER stress could be beneficial to improve myofiber formation [21]. Treatment of myoblasts with the ER stressors tunicamycin or thapsigargin leads to increased apoptosis in C2C12 cultures after induction of differentiation. Interestingly, the remaining myoblasts were resistant to apoptosis and were able to efficiently differentiate into healthy and functional myotubes that were morphologically distinct from the untreated cells, further suggesting that ER stress plays an important role in selectively removing differentiation incompetent myoblasts during myogenesis [21].

While the ATF6 arm of UPR appears to promote selective apoptosis of myoblasts, other arms of the UPR also appear to have a role in the regulation of myogenesis. The PERK/eIF2 α arm of the UPR and its downstream targets such as CHOP are transiently activated in a subset of myoblasts after initiation of the differentiation program [22]. Increased expression of CHOP inhibits myogenic differentiation through repressing the transcription of MyoD, which could be a mechanism to prevent premature differentiation

of myoblasts during myogenesis. Interestingly, overexpression of a phosphorylation resistant mutant of eIF2 α (i.e. eIF2 α S51A) also causes increase cell death during myogenesis even though the mechanisms remain unknown [22]. ER stress transducer IRE1 is an endonuclease, which removes an intron from XBP1 resulting in synthesis of the potent transcription factor, sXBP1 [5]. Previously, it has been reported that *Xbp1* is a direct target gene of MyoD and myogenin transcription factors, thus, providing an important link between XBP1 and myogenesis [23]. Recently, XBP1 has been found to regulate the expression of a large subset of genes in both myoblasts and myotubes including those involved in maintenance of ER function, growth, and DNA damage and repair pathways [24]. Overexpression of sXBP1 inhibits the expression of several markers of myogenesis and leads to formation of smaller myotubes in C2C12 cultures after their incubation in differentiation medium. Interestingly, XBP1 directly activates the expression of Mist1 transcription factor, a critical negative regulator of MyoD, which is essential for myogenesis. Although genetic evidence about the role of XBP1 in skeletal muscle formation is still missing, these cell culture studies suggest that XBP1 regulates differentiation of myoblasts into multinucleated myotubes [24].

Myogenesis is also required for the regeneration of skeletal muscle upon injury. Satellite cells are the adult muscle stem cells that contribute to skeletal muscle repair in adults. In normal conditions, these cells reside between the sarcolemma and the basal lamina in a quiescent state. Upon muscle injury, satellite cells get activated, proliferate and give rise to myoblasts/myocytes which eventually fuse with injured myofibers [25, 26]. While the majority of satellite cells differentiate into the myogenic lineage, a fraction of them undergo self-renewal and return to quiescent state. The paired box 7 (Pax7)

transcription factor is essential for self-renewal and maintenance of the myogenic potential of satellite cells [16, 17]. Our group recently investigate the role of PERK in satellite cell homeostasis. We generated mice in which PERK was ablated in satellite cells of adult mice using a tamoxifen-inducible Pax7-Cre line. Surprisingly, we could not find any significant difference in the number of quiescent satellite cells in skeletal muscle of control and satellite cell-specific PERK-knockout (i.e. scPERK-KO) mice. We also found that PERK is required for the survival of satellite cells and regeneration of myofibers upon injury [27]. Our cell culture studies also showed that deletion of PERK causes satellite cell death during myogenesis, which could be attributed to precocious activation of p38 MAPK. Pharmacological inhibition of p38 MAPK prevents cell death and improves myotube formation in PERK^{-/-} satellite cell cultures and augments the regeneration of myofibers in scPERK-KO mice [27]. Similar to our study, Zismanov et al recently reported that PERK and its downstream target eIF2 α are constitutively phosphorylated in quiescent satellite cells and this phosphorylation is reduced upon activation of the satellite cells [28]. Interestingly, targeted inducible expression of a phosphorylation resistant mutant of eIF2 α (i.e. eIF2 α S51A) or deletion of PERK leads to loss of quiescence in satellite cells, characterized by the increased expression of Myf5 and MyoD. While unable to undergo self-renewal, satellite cells expressing the eIF2 α S51A mutant are capable of undergoing terminal differentiation and subsequent fusion with myofibers. The study also showed that inhibition of eIF2 α dephosphorylation using small molecule such as Sal003 promotes satellite cell self-renewal *ex vivo*. Remarkably, satellite cells treated with Sal003 retain their myogenic capacity when transplanted in skeletal muscle *in vivo* [28]. However, the results of this study are

somewhat contradictory to a previously published where it was found that overexpression of eIF2 α S51A causes cell death and diminishes the differentiation of cultured myoblasts [22]. This could be attributed due to the different experimental approaches and myogenic cell types utilized in these two studies [22, 28]. However, it remains unknown whether the inhibition of PERK dephosphorylation will also promote satellite cell self-renewal and maintenance of their differentiation potential when transplanted into injured skeletal muscle. It is notable that in addition to PERK, eIF2 α can also be phosphorylated by other kinases such as double stranded RNA-activated protein kinase R, heme-regulated inhibitor eIF2 α kinase, and general control nonderepressible-2 (GCN2) in different conditions [29]. Furthermore, PERK also has several eIF2 α -independent functions, which are collectively known to promote cell survival in stress conditions [14, 30-32]. Finally, the role of the IRE1/XBP1 and the ATF6 arms of the UPR in the regulation of satellite cell self-renewal, proliferation, and differentiation is yet to be investigated through molecular and genetic approaches. Nevertheless, these published results suggest that the UPR plays an important role in the regulation of myogenesis both *in vitro* and *in vivo*.

1.4 Skeletal Muscle Atrophy: Skeletal muscle atrophy is a devastating complication which contributes to both morbidity and mortality [33]. Skeletal muscle mass is maintained through a delicate balance between the rate of protein synthesis and the rate of degradation. The ubiquitin-proteasome system (UPS) is a major proteolytic mechanism in skeletal muscle [34, 35]. Several E3 ubiquitin ligases such as MuRF1, MAFBx (Atrogin-1), Nedd4.1, TRAF6, and MUSA1 have now been identified which mediate proteolytic degradation of both thick and thin filament proteins in skeletal

muscle [33, 36]. The autophagy-lysosomal system (ALS) is another proteolytic mechanism involved in the degradation of defunct organelles and misfolded proteins [37]. While inhibition of basal autophagy can lead to myopathy due to the accumulation of dysfunctional organelles and oxidative stress [38, 39], excessive activation of autophagy can lead to muscle wasting [33, 40-42].

The activity of the UPS and ALS is regulated through the activation of a number of signaling pathways such as p38 MAPK, AMP-activated protein kinase (AMPK), and nuclear factor-kappa B (NF- κ B), which function through modulating the activity of various transcriptional regulators [33, 43]. The IGF-1/PI3K/Akt/mTOR cascade is a major signaling pathway that increases the rate of protein synthesis in skeletal muscle [44]. Activation of this pathway also inhibits protein degradation in skeletal muscle [33, 44]. Accumulating evidence also suggests that changes in mitochondrial content, integrity, and function also play a critical role in the regulation of skeletal muscle mass [33, 45].

1.5 UPR and Skeletal Muscle Atrophy. Activation of ER stress and the UPR occurs in skeletal muscle due to exercise, aging, and many other perturbations. However, their role in the regulation of skeletal muscle mass and function remain poorly understood. Moreover, in most of the conditions, all the three arms of the UPR are activated making it difficult to ascertain the contribution of each pathway to skeletal muscle adaptation. To understand the ER stress independent role of the PERK arm of the UPR in skeletal muscle, Miyake et al recently generated Fv2E-PERK transgenic (Tg) mice. In this mouse line, a fusion protein of artificial dimerization domain (Fv2E) and PERK kinase domain

were overexpressed in skeletal muscle [46]. The Fv2E-PERK Tg mouse serves as a model for ligand-dependent PERK activation. Interestingly, adult Fv2E-PERK Tg mice showed reduced body and individual hind limb muscle weight. Accordingly, grip strength was also significantly reduced in Fv2E-PERK Tg mice compared to littermate control mice. While Fv2E-PERK Tg mice show signs of muscle atrophy, constitutive activation of PERK in skeletal muscle leads to increased expression of metabolic and antioxidant genes. Moreover, PERK stimulates the production of fibroblast growth factor 21 (FGF21), which induces energy expenditure in brown adipose tissue and prevents adiposity [46]. These findings suggest that PERK plays a role in skeletal muscle. While it reduces muscle mass potentially due to inhibition of translation, it also improves muscle health through augmenting anti-oxidant mechanisms. While the floxed PERK mice have been generated, the effect of deletion of PERK in skeletal muscle in naïve as well as catabolic conditions has not been yet investigated. Similarly, the role of IRE1 and ATF6 α in skeletal muscle homeostasis using genetic mouse models has to be investigated. Based on their divergent downstream targets, it will not be surprising that individual arms of the UPR play distinct roles in skeletal muscle in various physiological and pathological conditions.

The activation of the markers of ER stress and UPR in skeletal muscle has been studied in multiple atrophy conditions. An earlier study reported no significant changes in the expression of ER stress proteins such as GRP78, calreticulin, CHOP, vinculin, the type I D-myoinositol 1,4,5-trisphosphate receptor, protein kinase R, and eIF2 α in skeletal muscle in response to hind limb unloading, a model of disuse atrophy [47]. However, BiP and CHOP are shown to be increased 14 days after reloading the muscle.

This effect was more pronounced in the older mice [48]. Furthermore, several markers of ER stress including CHOP are increased in skeletal muscle in response to denervation and in the AR113Q mice, an established model of spinal and bulbar muscular atrophy (SBMA) [49]. Interestingly, deletion of CHOP accentuated muscle atrophy in normal mice on denervation and in the AR113Q mice. There wasn't a noticeable difference in the activity of the UPS; however, autophagy was significantly increased upon deletion of CHOP in skeletal muscle of both these models. In contrast, inhibition of autophagy through Beclin-1 haplosufficiency attenuated muscle atrophy in response to denervation in normal mice and increased the lifespan of AR113Q mice [49]. Although the mechanisms by which CHOP inhibits autophagy remain unknown, these findings suggest that downstream of ER stress, the induction of CHOP is a mechanism to prevent excessive loss of muscle mass in response to denervation and during SBMA. ER stress and UPR pathways are also activated in SOD1 models of ALS [50, 51]. Interestingly, it was found that induction of autophagy following XBP1 deletion ameliorated pathology of SOD1 mice. In this model, autophagy promoted the degradation of mutant SOD1 resulting in the clearance of aggregates [51]. These reports emphasize that the activation of specific UPR pathways may have differential outcomes on skeletal muscle mass depending on the underlying condition and muscle wasting stimuli.

ER stress has also been found to be elevated in the skeletal muscle of the elderly, which could be due to the reduced expression of ER chaperones [52-55]. Anabolic resistance is considered one of the important mechanisms in age-associated muscle atrophy. However, a recent study has shown that ER stress may not contribute to age-associated anabolic resistance in skeletal muscle of mice [52]. Additionally, activation of

ER stress has been implicated in diaphragm contractile dysfunction in a mouse model of sepsis [56].

One of the important consequences of ER stress is the induction of autophagy in skeletal muscle. However, the signaling link between the UPR and autophagy remains less understood. Protein Kinase C theta (PKC θ) appears to be essential for the induction of autophagy in response to ER stress [57]. The ER stressors thapsigargin or tunicamycin strongly activate PKC θ in cultured myoblasts and myotubes. PKC θ activation was localized to LC3-positive autophagosomes in thapsigargin-treated myotubes. The role of PKC θ in ER stress-induced autophagy was evident by the findings that inhibition of PKC θ *in vitro* prevented ER stress-induced activation of autophagy, but had no effect on activation of ER stress [57]. *In vivo*, the lack of PKC θ prevented the activation of autophagy and skeletal muscle atrophy in response to starvation or immobilization. These findings suggest that PKC θ functions as an ER stress sensor and is required for the ER stress-dependent autophagy activation in skeletal muscle [57].

TRAF6 is an E3 ubiquitin ligase, and through association with the dimeric ubiquitin-conjugating enzyme Ubc13/Uev1A, it catalyzes lysine 63 (K63)-linked polyubiquitination of several target proteins. TRAF6 functions as a central regulator in multiple signaling pathways, such as NF- κ B, MAPK, and PI3K/Akt, in response to certain cytokines and microbial products. Targeted deletion of TRAF6 prevents skeletal muscle wasting in distinct catabolic conditions including starvation, denervation, and cancer cachexia [58, 59]. TRAF6 appears to be one of the upstream regulators for the induction of UPR in skeletal muscle, especially in response to starvation. Our studies have shown that deletion of TRAF6 reduces the levels of multiple markers of ER stress

such as ATF4, CHOP, GRP94, and GADD34 in skeletal muscle in fasting mice [58]. However, the molecular interactions through which TRAF6 induces ER stress and UPR pathways in skeletal muscle remain to be investigated.

Taken together, it is now increasingly evident that ER stress and the UPR pathways are activated in numerous conditions that lead to skeletal muscle atrophy and depending on the stimulus, it can have positive and negative effects in the regulation of skeletal muscle mass.

1.6 UPR and Skeletal Muscle Adaptation to Exercise: Exercise training has been shown to preserve the aerobic fitness of skeletal muscle as well as skeletal muscle strength. These adaptations can ameliorate metabolic dysfunction and prevent chronic disease. Aerobic and resistance exercise pose different challenges to skeletal muscle and elicit different molecular mechanisms in skeletal muscle. Published reports suggest that exercise activates all three ER stress-responsive UPR pathways [46, 60]. ER stress markers such as BiP, GRP94, GADD34, ATF4, CHOP, and sXBP1 are induced after one bout of exhaustive treadmill running [60]. An additional study showed that ER stress markers p-IRE1, p-PERK, and p-eIF2 α are increased in skeletal muscle of mice trained on a downhill treadmill [61]. However, the mice that had received previous training in the exercise paradigm, only the ER chaperones BiP and GRP94 were found to be increased in skeletal muscle, suggesting that the activation of the UPR is a mechanism for skeletal muscle adaptation after initial exercise training [60]. A similar rapid increase in the markers of the UPR was observed when rats were subjected to chronic contractile activity and this increase was attenuated with repeated bouts [62]. Furthermore, increases in ER

stress markers such as BiP and sXBP1 have been characterized in human muscle biopsies after a bout of running [63].

The transcriptional coactivator peroxisome proliferator-activated receptor gamma coactivator-1 alpha (PGC-1 α) is a key regulator of mitochondrial biogenesis and metabolic function [64, 65]. Levels of PGC-1 α are induced in skeletal muscle following an acute exercise bout or prolonged exercise training [66, 67]. Moreover, overexpression of PGC-1 α in the skeletal muscle has been found to improve performance capacity during voluntary and forced exercise in mice [68]. Interestingly, PGC-1 α is necessary for the activation of the UPR during pharmacologically-induced ER stress and exercise training [60]. PGC-1 α interacts with cleaved ATF6 α to induce adaptive UPR in skeletal muscle after exercise [60]. The role of ATF6 α in exercise-induced adaptive response is also evidenced by the findings that ATF6 α null mice fail to efficiently recover from muscle damage that occurs after acute exercise. While the ATF6 α arm of the UPR promotes skeletal muscle adaptation in response to exercise, some parts of the UPR may also have detrimental effects on skeletal muscle adaptation and recovery following exercise training. This is evidenced by the findings that genetic deletion of CHOP improved exercise tolerance in skeletal muscle specific PGC-1 α knockout mice [60]. Although more studies are needed, it is plausible that the PERK-eIF2 α arm of the UPR which also leads to the induction of CHOP, negatively regulate skeletal muscle homeostasis following exercise training.

During resistance exercise, skeletal muscle is subjected to a short bout of maximal contraction. These exercises cause the skeletal muscle to adapt through augmenting protein synthesis and organelle biogenesis. Synergistic ablation is a model to study

skeletal muscle hypertrophy, similar to that seen from resistance exercise. In this model, the gastrocnemius and soleus muscles are partially ablated leaving the plantaris muscle as the lone hind limb extensor. It has been suggested that a high rate of protein synthesis, which occurs during muscle hypertrophy, results in ER stress and activation of the maladaptive UPR. This is characterized by an increase in CHOP and a decrease in IRE1 α at 12 days post-ablation, possibly leading to a decrease in protein synthesis in an attempt to halt the excessive muscle growth [69]. ER stress has also been examined in humans following resistance exercise where participants completed a unilateral single bout of resistance exercise using the knee extensors. The biopsies from these muscles indicated an increase in the protein levels of GRP78, PERK, and IRE1 α 48h post-exercise. However, the mRNA levels of IRE1 α as well as ATF6 were unchanged [70].

Altogether, these studies indicate that moderate exercise initially causes induction of ER stress and activation of UPR pathways. However, after multiple rounds of training these markers appear to be diminished, which suggests that the UPR becomes activated to novel or challenging exercises in skeletal muscle during both, endurance and resistance exercises. The activation of ER stress leads to some mode of adaption in skeletal muscle that allows the skeletal muscle to acclimate to the demands of a specific exercise. More investigations are needed to understand the molecular mechanisms by which ER stress-induced UPR pathways promote skeletal muscle adaptation following exercise.

1.7 Clinical Significance of UPR in Skeletal Muscle Diseases. Myopathy refers to a systemic clinical disease in which the myofiber's structure and metabolism are disrupted leading to varying degrees of weakness and dysfunction, especially in proximal muscles. Inherited myopathies (e.g. congenital, mitochondrial and metabolic myopathies and

muscular dystrophy) have an early age of onset with a relatively longer duration and more severe progression, whereas acquired myopathies (e.g. inflammatory, toxin- or drug-related myopathies, and myopathies associated with systemic conditions) are relatively less severe and generally present at a later age. Emerging evidence suggests that ER stress and the UPR are also activated in various types of myopathies.

Dermatomyositis (DM), polymyositis (PM) and inclusion body myositis (IBM) are heterogeneous inflammatory myopathies in which myofibers are damaged as a result of the immune response [71]. IBM is divided into sporadic-IBM (s-IBM) and hereditary-IBM (h-IBM). The s-IBM is the most common muscle disease that starts after age 50 years and leads to severe disability. The h-IBM is characterized by pathologic features that strikingly resemble those of s-IBM except that skeletal muscle do not involve lymphocyte infiltration. Upregulation of class I major histocompatibility complex (MHC) in skeletal muscle fibers is a prominent feature of human inflammatory myopathies. Several studies have shown that the levels of ER stress markers, such as: calreticulin, GRP75, GRP78, and GRP94, are elevated in muscle biopsies from human myositis patients and in mouse models of inflammatory myopathy [72-74]. Moreover, overexpression of mouse class I MHC (H-2K(b)) induces ER stress in cultured skeletal muscle cells [73]. While IBM involves inflammation in skeletal muscle, a few studies have indicated that inflammation alone does not cause myositis [75]. A conditional transgenic line in which class I MHC (H-2K(b)) is overexpressed specifically in skeletal muscle has been proposed as a mouse model of IBM. Interestingly, ER chaperone protein GRP78 is increased in the skeletal muscle of these transgenic mice [73]. In a separate study, mice overexpressing class I MHC (H-2K(b)) were crossed with the immunodeficient $Rag2^{-/-}$ mice to examine whether the upregulation of ER stress and myopathy are due to the

inflammatory response. Interestingly, even in the absence of significant inflammatory cell infiltrations, myopathic changes, muscle weakness, and elevated levels of ER stress markers GRP78 and ATF6 were present [76].

Major characteristics of s-IBM are vacuolar muscle fibers, intramuscular fiber inclusions, and various degrees of mononuclear cell inflammation [77, 78]. Like Alzheimer's disease, s-IBM also involves accumulation of amyloid- β ($A\beta$) and phosphorylated tau proteins [77, 78]. Interestingly, muscle biopsies from patients with s-IBM indicate that all major ER chaperones are increased and aggregate with the $A\beta$ proteins in skeletal muscle [79] suggesting a potential role of ER chaperone proteins in folding and trafficking of $A\beta$ in skeletal muscle. A more recent study also demonstrated the activation of the UPR in skeletal muscle of s-IBM patients [80]. In addition to IBM, elevated levels of ER stress-specific chaperone protein GRP74 have been observed in serum of patients with DM or PM suggesting that ER stress and activation of the UPR is a common feature in inflammatory myopathies [81]. While the exact role and mechanisms by which ER stress causes inflammatory myopathies remain unknown, it may be related to oxidative stress, mitochondrial dysfunction, and production of inflammatory cytokines [82].

Myasthenia gravis (MG) is an autoimmune neuromuscular disease that causes weakness in skeletal muscles, especially those that control eye and eyelid movement, facial expression, chewing, talking, and swallowing. The main cause for this disease is autoantibodies that block, alter, or destroy the acetylcholine receptors at the neuromuscular junction leading to impairment in muscle contraction, weakness, and fatigability [83]. It has been proposed that damage to acetylcholine receptor can induce ER stress in skeletal muscle. Indeed, elevated levels of GRP74 have been reported in muscle biopsies from patients with

MG [84]. Moreover, higher binding of autoantibodies to ER chaperone GRP94 has been found to be associated with a subset of MG patients [85]. ER stress alone may also contribute to a loss of acetylcholine receptor in skeletal muscle cells. A recent study demonstrated that the ER stressor tunicamycin stimulates the loss of the acetylcholine receptors in C2C12 myotubes through endocytosis and lysosomal degradation. Moreover, knockdown of XBP1 in C2C12 myotubes attenuates the degradation of acetylcholine receptor by endocytosis [86] suggesting that inhibition of ER stress and/or endocytosis can be a potential therapeutic approach for MG.

Muscular dystrophy is a group of skeletal muscle diseases that involves progressive degeneration of myofibers, myopathy, and fibrosis. Muscular dystrophy arises due to mutations in individual genes that encode extracellular matrix proteins, transmembrane and membrane-associated proteins, cytoplasmic enzymes, and nuclear matrix proteins [87, 88]. Duchenne muscular dystrophy (DMD) is one of the most prevalent forms of muscular dystrophies that results from total or partial deficiency of dystrophin protein [88]. Pathogenesis of DMD includes an inflammatory response, loss of calcium homeostasis, hypoxia, and oxidative stress, all of which can cause ER stress [87, 89]. Dystrophin-deficient mdx mice are widely used as a model to study the pathogenesis of DMD. ER stress markers, such as: GRP78, PERK, eIF2 α , IRE1 α , and sXBP1 and caspase-12, are increased in dystrophic muscle of mdx mice as well as in muscle biopsies from patients with DMD suggesting that dystrophin-deficiency disrupts ER homeostasis in skeletal muscle [90, 91]. ER stress specifically activates caspase-12, which leads to the activation of caspase-9 and caspase-3 to induce apoptosis. Interestingly, genetic ablation of caspase-12 significantly reduces myofiber degeneration and improves skeletal muscle strength in mdx mice [91].

Another study recently demonstrated that ER stress inhibitors restore ER-mitochondria links, mitochondrial Ca^{2+} uptake, and improve contractility of the diaphragm in mdx mice [92] further implying that heightened ER stress and UPR pathways contribute to the dystrophic phenotype.

Myotonic dystrophy (DM1) is an inherited autosomal-dominant muscular dystrophy caused by an abnormal amount of CTG trinucleotide repeats in the 3' untranslated region of the dystrophia myotonica protein kinase (*DMPK*) gene. The pathogenesis of DM1 involves conduction defects, myofiber atrophy, and abnormal Ca^{2+} homeostasis. Ikezoe et al analyzed the markers of ER stress and the UPR in skeletal muscle of patients with DM1. They reported a significant increase in the levels of GRP78 and calnexin, and phosphorylation of PERK and eIF2 α in atrophic myofibers of DM1 patients suggesting that enhanced ER stress may contribute to muscle wasting in DM1 patients [93]. There are also reports suggesting that ER stress is increased in dysferlin-related and collagen VI-related myopathies [94-96].

Tibial muscular dystrophy (TMD) is an autosomal dominant late-onset distal myopathy that results from heterogeneous mutations in the last two exons of the *Titin* gene. TMD is characterized by myofiber atrophy and weakness in the skeletal muscle of the anterior compartment of the lower leg [97]. Gene profiling studies provided evidence that ER stress could be one of the potential reasons for muscle weakness in TMD patients [98]. Altogether, available literature suggests that ER stress and the UPR could be important players in the pathogenesis of various types of muscular dystrophy.

1.8 Concluding Remarks. From the above discussion, it is clear that ER stress and the UPR are activated in skeletal muscle in multiple conditions. However, because of the complexity of multiple UPR pathways and several downstream targets, their exact role remains poorly understood. It is now increasingly evident that depending on the underlying condition, activation of ER stress-induced UPR may produce beneficial or deleterious effects. It is clear that the UPR plays an important physiological role in skeletal muscle adaptation in response to acute exercise. Furthermore, low levels of ER stress may be beneficial in maintaining the pool of satellite cells in adult skeletal muscle for regenerative myogenesis. While there are several studies suggesting that ER stress and UPR pathways are perturbed in skeletal muscle in the conditions of atrophy and hypertrophy, it remains unknown how these pathways regulate skeletal muscle mass. Consistent with the notion that chronic unresolved stress can lead to inflammation and cell death, the markers of ER stress have been found to be elevated in skeletal muscle in models of a number of muscle degenerative diseases. However, it remains unknown whether the inhibition of ER stress will improve skeletal muscle mass during various diseases. Altogether, available literature suggests that the modulation of ER stress and UPR pathways can have therapeutic importance for skeletal muscle in diverse conditions and disease states. Interestingly, a number of ER stress activators and inhibitors have now been developed which can potentially be used for skeletal muscle diseases as well.

The current dissertation will examine the effect of inhibiting ER stress using pharmacological agents on skeletal muscle atrophy during cancer cachexia. In addition to using pharmacological modulators of ER stress, more specific perturbation using molecular and genetic approaches is needed to tease out the mechanisms by which the

components of ER stress and UPR pathways alters skeletal muscle homeostasis. Thus, this dissertation will also investigate the role of the IRE1/XBP1 arm of the UPR in regulation of skeletal muscle mass during cancer cachexia using genetic and molecular approaches. Moreover, this dissertation will investigate the role of the XBP1 transcription factor in skeletal muscle growth and regeneration in diverse conditions. Our working hypothesis is that a basal/physiological level of activation of the UPR promotes the growth and maintenance of skeletal muscle in adult animals. By contrast, chronic activation of the IRE1 α /XBP1 arm of the UPR leads to the loss of skeletal muscle mass, especially in tumor-bearing mice.

FIGURE 1.1

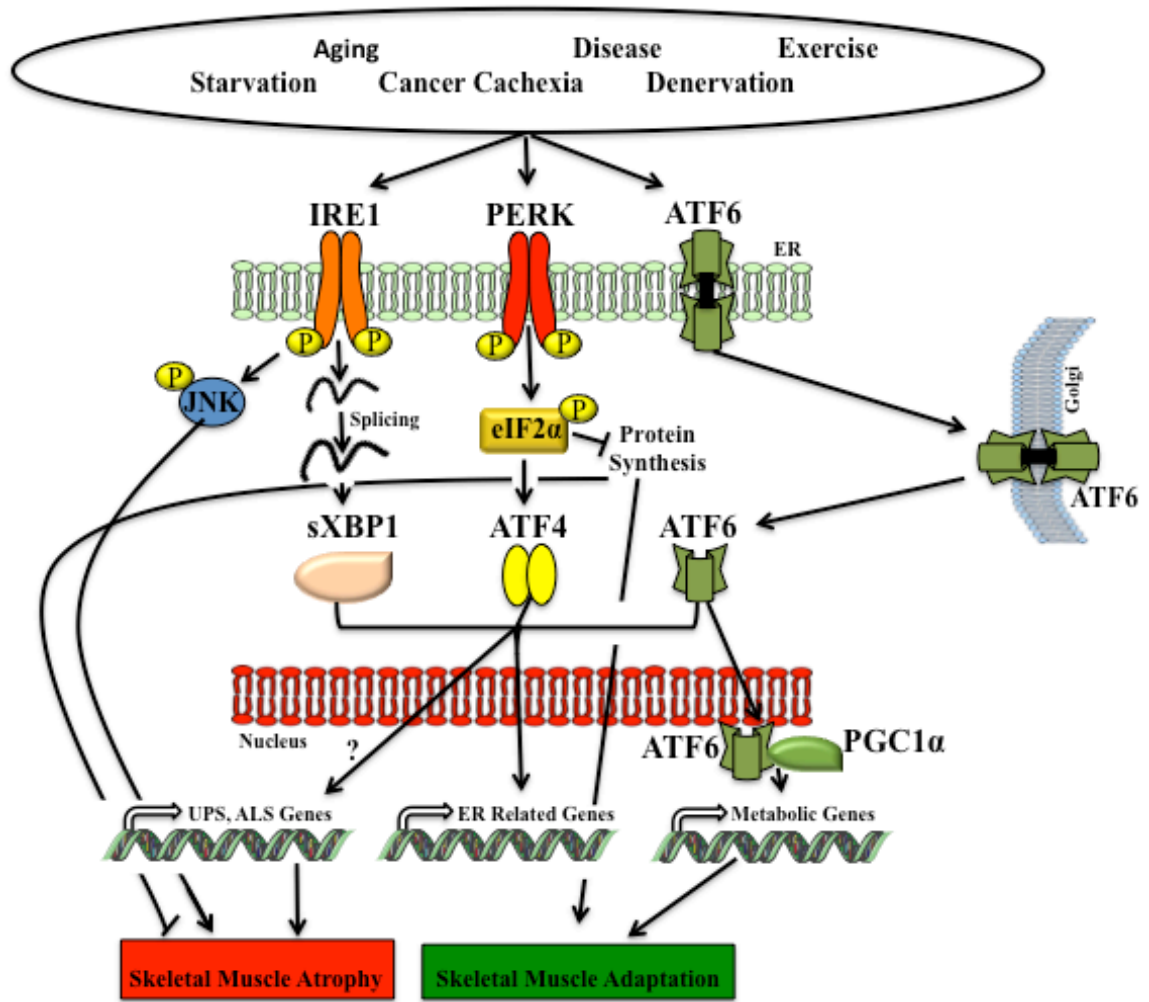


FIGURE 1.1: Schematic representation of the unfolded protein response pathways in skeletal muscle. Under normal physiological conditions, the PERK, IRE1, and ATF6 proteins are maintained in an inactive state by binding to BiP. Stress in skeletal muscle caused by aging, disease, exercise, starvation, cachexia, denervation, or high fat diet causes BiP to disassociate from these proteins and preferentially binds to the misfolded proteins in the ER lumen. Upon release from BiP, PERK is auto-phosphorylated leading to a cascade of signals including phosphorylation of eIF2 α and translation of ATF4, a potent transcription factor. Another ER transmembrane sensor, IRE1, also becomes activated by autophosphorylation during ER stress. Through its endonuclease activity, IRE1 promotes splicing of a 26-base intron from XBP1 mRNA as well as phosphorylation of JNK. Lastly, once activated, ATF6 moves from the ER to the Golgi apparatus to be cleaved by site-1 proteases. The cleaved N-terminal fragment of ATF6 is then transported to the nucleus where it acts in combination with sXBP1 and ATF4 to alleviate ER stress by regulating gene expression and protein synthesis. In addition to regulation of ER related genes, activation of ER stress has been shown to increase skeletal muscle atrophy by inhibition of protein synthesis through eIF2 α , activation of JNK through IRE1, and potentially through augmenting the expression of components of UPS and ALS. Activation of ATF6 increases skeletal muscle adaptation by increasing expression of metabolic genes through interaction with PGC1 α . ER stress has also been linked to insulin resistance through activation of ERK signaling and inhibition of AMPK. However, specific activation of PERK signaling leads to secretion of FGF21, which is shown to alleviate insulin resistance.

FIGURE 1.2

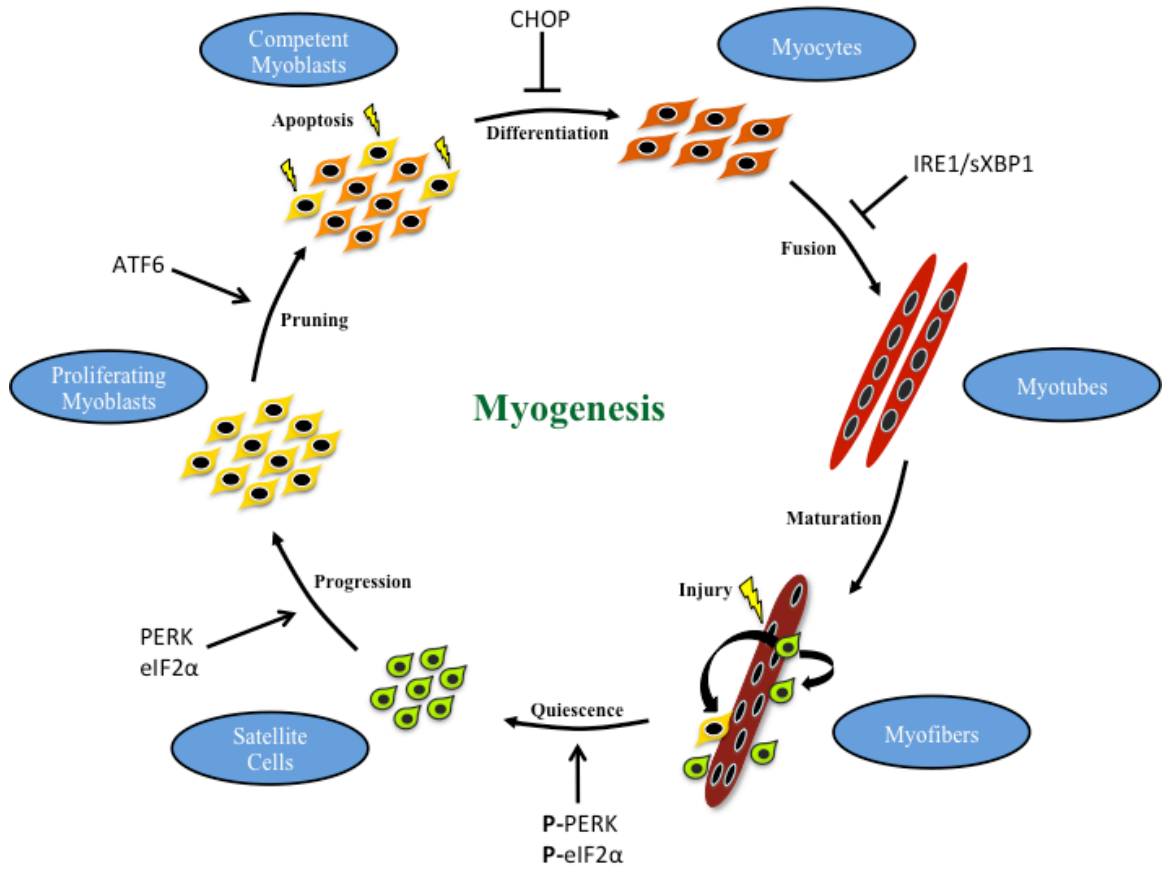


Figure 1.2 Schematic diagram illustrating the effect of ER stress pathways on myogenesis. Adult muscle stem cells or satellite cells reside between the sarcolemma and the basal lamina of mature muscle in a quiescent state and are maintained by constitutively phosphorylated PERK and phosphorylated eIF2 α . Dephosphorylation of PERK and eIF2 α promotes progression and commitment of satellite cells to the myogenic lineage. Prior to differentiation, myoblasts undergo an apoptotic pruning process facilitated by ATF6, ensuring that only differentiation-competent myoblasts proceed. Competent myoblasts differentiate into myocytes; however, CHOP has been found to inhibit this transition. Myocytes fuse with one another to form multi-nucleated myotubes. IRE1 and sXBP1 have been shown to disrupt the fusion process, resulting in thin, unhealthy cells through inhibition of MyoD and Myogenin. Myotubes undergo a maturation process to form adult myofibers with their own supply of quiescent satellite cells available for repair of damaged tissue due to injury or disease.

CHAPTER 2

INHIBITION OF ER STRESS AND UNFOLDED PROTEIN RESPONSE PATHWAYS CAUSES SKELETAL MUSCLE WASTING DURING CANCER CACHEXIA

2.1 Introduction

Cachexia is a multifactorial syndrome that affects majority of patients with advanced cancer especially colon, lung, and pancreatic cancer [99]. The syndrome is characterized by progressive weight loss due to significant loss of skeletal muscle mass with or without adipose tissue wasting [100]. The occurrence of cachexia is correlated with poor prognosis and negatively impacts on patient management, tolerance to antineoplastic therapies and quality of life. Cancer cachexia cannot be reversed by nutritional support alone [99]. Therefore, the development of therapy for cancer cachexia is critical to enhance the quality of life and survival of cancer patients [99-101].

Skeletal muscle wasting during cancer cachexia occurs through multiple mechanisms including an imbalance in the rate of protein synthesis and degradation and satellite cell dysfunction, which can limit the regeneration of myofibers upon injury [100, 102]. The ubiquitin proteasome system (UPS) is the primary mechanism that causes the degradation of thin and thick filament proteins in many wasting conditions, including cancer cachexia [103-105]. Inhibition of the UPS or its specific components have

been found to attenuate muscle loss in many experimental animal models of chronic diseases including cancer [104, 106, 107]. The autophagy-lysosomal system (ALS) is another important mechanism by which many misfolded proteins and defunct organelles are cleared within the cells. While a basal level of autophagy is critical for skeletal muscle homeostasis, spurious activation of autophagy can lead to muscle wasting in many conditions [37]. A recent study has shown that the activation of the ALS contributes to loss of skeletal muscle mass in models of cancer cachexia [42]. The activity of these proteolytic systems is regulated by the activation of nuclear factor-kappa B (NF- κ B), 5' AMP-activated protein kinase (AMPK), and p38 MAPK pathways [103-105, 108]. In contrast, phosphoinositide 3-kinase (PI3K)/Akt/mammalian target of rapamycin (mTOR) is the major signaling pathway which increases the rate of protein synthesis in skeletal muscle in response to growth factors and functional overload [44]. Activation of this pathway also inhibits protein degradation through inhibiting the activation of the UPS and ALS [44]. In recent years, several inflammatory cytokines and other host- or tumor-derived factors have been identified which mediate the activation of various proteolytic systems and inhibits protein synthesis in skeletal muscle in models of cancer cachexia [109-111]. However, molecular mechanisms which leads to the loss of muscle mass during cancer cachexia remain less understood.

The endoplasmic reticulum (ER) is a membrane bound organelle that is responsible for proper folding, processing, and trafficking of proteins within the cell. Accumulation of misfolded protein in the ER may induce ER stress. To deal with this stress, cells initiate the unfolding protein response (UPR), which is mediated by three types of ER-transmembrane protein: inositol-requiring protein 1 (IRE1), RNA-dependent

protein kinase-like ER eukaryotic translation initiation factor 2 alpha kinase (PERK), and activating transcription factor 6 (ATF6) [2-4]. When the cell is in an unstressed state, these proteins are maintained in relatively inactive state by binding to immunoglobulin heavy chain binding protein/glucose-regulating protein 78 (BiP/GRP78), an important ER chaperone. In response ER stress, BiP disassociates from these proteins and preferentially binds to the misfolded proteins in the ER lumen [6]. Upon release from BiP, PERK autophosphorylates leading to a cascade of signals including phosphorylation of eukaryotic translation initiation factor 2 α (eIF2 α) and translation of activating transcription factor-4 (ATF4), which induces transcription of C/EBP homologous protein (CHOP) [8, 9]. The PERK/eIF2 α axis is also involved in the termination of the UPR after the stress has been relieved by activation of growth arrest and DNA damage-inducible protein (GADD34) [10] which dephosphorylates p-eIF2 α . Upon ER stress, IRE1 becomes activated by auto-phosphorylation, which promotes splicing of a 26-base intron from X-box-binding protein 1 (XBP1) mRNA [11]. Spliced XBP1 (sXBP1) increases ER chaperones and other components to assist in the folding capacity of the ER [12]. Once activated, ATF6 moves from ER to the Golgi apparatus to be cleaved by site-1 protease (S1P) and site-2 protease (S2P) [13]. The cleaved N-terminal fragment of ATF6 is then transported to the nucleus where it acts in combination with ATF4 and sXBP1 to increase the levels of proteins that function to alleviate the ER protein folding capacity [6]. Activation of all three pathways executes ER stress by regulating gene expression (16, 17). While the primary role of UPR is to restore ER function, the failed recovery from ER stress leads to UPR-mediated cell death (16, 17). Indeed, the contribution of

UPR-activated cell death has now been reported in various disease states including ischemic stroke, multiple sclerosis, and Alzheimer's disease (16-19).

The ER-induced UPR appears to play an important role in myogenesis as evidenced by the findings that the ATF6 arm of the UPR is activated during myogenic differentiation. ATF6 mediates selective apoptosis of a subpopulation of myoblasts that may be vulnerable to cellular stresses. Inhibition of ER stress signaling blocked apoptosis and myoblast differentiation [20] whereas inducers of ER stress selectively eliminated vulnerable myoblasts in cultures and the surviving cells more efficiently differentiated into contracting myofibers [21]. In adult skeletal muscle, increased expression of ER stress markers such as BiP, GRP94, GADD34, ATF4, CHOP, and sXBP1 has been observed after one bout of exhaustive treadmill running [60]. The role of ER stress in exercise-induced muscle adaptation is supported by the findings that recovery from acute exercise is compromised in ATF6 α null mice [60]. Conversely, activation of ER stress is also linked with inflammation and insulin resistance in skeletal muscle. Attenuation of ER stress enhances insulin sensitivity, increases glucose uptake, and reduces glucose concentration in diabetic mice. Recently, ER stress has been observed in myopathies such as myotonic dystrophy type1 [93], sporadic inclusion body myositis [73, 79], and limb-girdle muscular dystrophy 1C [112]. ER stress has also been found to be induced in skeletal muscle of aged mice [52]. We have previously reported that the markers of ER stress and UPR are highly activated in skeletal muscle in response to starvation [58]. However, the role of ER stress in regulation of skeletal muscle mass in catabolic conditions including cancer cachexia remains largely unknown.

The major goal of this study was to investigate whether ER stress is activated and what role it plays in cancer cachexia. To evaluate the role of ER stress we used 4-phenylbutanoate (4-PBA), a chemical chaperon, which is known to attenuate ER stress both in vivo and in vitro [113, 114]. Our results demonstrate that ER stress is highly activated in skeletal muscle of Lewis lung carcinoma (LLC) and $Apc^{Min/+}$ models of cancer cachexia. Our results also demonstrate that 4-PBA hastens the loss of skeletal muscle mass in the LLC model. More importantly, we have found that the inhibition of ER stress using 4-PBA causes muscle wasting in naïve mice as well as in cultured primary myotubes providing initial evidence that ER stress is critical to maintaining muscle mass in both physiological and pathophysiological conditions.

2.2 Material and Methods

Animals. C57BL/6J and $Apc^{Min/+}$ mice were originally purchased from Jackson Laboratories (Bar Harbor, ME, USA), and breeding was maintained at the University of Louisville animal resource facility. $Apc^{Min/+}$ mice were killed at the age of 26 wk to study the activation of markers of ER stress. For the cancer cachexia model, LLC cells (2-3 $10E6$ cells in 100 ml saline; American Type Culture Collection, Manassas, VA, USA) were injected subcutaneously into the flanks of 3-mo-old C57BL/6 mice [59]. For the study of muscle atrophy, the mice were weighed daily and euthanized 18 d after implantation of LLC cells. In one experiment, the mice were given an injection of 4-PBA (100 mg/kg body weight, i.p.) daily until the end of the experiment.

Histology and morphometric analysis. Individual TA and soleus muscles were isolated from mice, snap frozen in liquid nitrogen, and sectioned with a microtome cryostat. For the assessment of muscle morphology and to quantify fiber cross-sectional area (CSA), 10-mm-thick transverse sections of TA and soleus muscle were stained with hematoxylin and eosin (H&E). The sections were examined under an Eclipse TE 2000-U microscope (Nikon, Tokyo, Japan). Fiber CSA was analyzed in H&E-stained muscle sections using ImageJ software [National Institutes of Health (NIH), Bethesda, MD, USA]. For each muscle, the distribution of fiber CSA was calculated by analyzing 220 myofibers.

Muscle fiber-type immunostaining. To determine the composition of different types of fibers in the soleus muscle of mice, transverse cross sections were made and blocked in 5% goat serum and 2% bovine serum albumin (BSA) for 30 min, followed by incubation for 1 h with monoclonal antibodies against type I, IIA, and IIB MyHC isoforms using clone BA-D5, SC-7, and BF-F3, respectively (Developmental Studies Hybridoma Bank, Iowa City, IA, USA). Secondary antibody used was goat anti-mouse IgG2b conjugated with Alexa-350, goat anti- mouse IgG1 conjugate with Alexa-568 and goat anti-mouse IgM conjugated with Alexa-488. Finally, the fluorescence was captured with an Eclipse TE 2000-U microscope (Nikon), the images were merged, and the percentage of each type of fibers in whole muscle section was recorded.

Preparation of LLC cell conditioned medium. LLC cells were seeded in 100 mm cell culture plates in growth medium (DMEM containing 10% fetal bovine serum) at a density of 5000 cells/cm². Supplementary growth medium was added to each plate after 2

d of plating. LLC cell cultures contain a heterogeneous mix of adherent and floating cells. After 4 d, we removed growth medium, and floating cells were harvested by centrifugation at 800 g, 5 min. Pelleted cells and 10 ml differentiation medium were added back to the plate containing the adherent cells. After 24 h, conditioned medium (CM) was harvested and cleared of cells and debris by centrifugation (800 g, 5 min). The CM was passed through 0.45 mm filters, and aliquots were frozen in liquid nitrogen for later use. For myotube treatments, CM was diluted 1:4 with fresh differentiation medium.

Indirect immunofluorescence and analysis of myotube size. Mouse primary myotubes were prepared according to a published protocol [115]. After treatment with LLC-CM and/or 4-PBA, the myotubes were fixed with paraformaldehyde and blocked in 1% BSA in PBS for 1 h and incubated with anti-MF20 (1:250; Developmental Studies Hybridoma Bank, Iowa City, IA, USA) in blocking solution at 4°C overnight. A brief PBS wash was applied before incubation with Alexa Fluor 568-conjugated secondary antibody (1:3000; Thermo Fisher Scientific Life Sciences, Carlsbad, CA, USA) for 1 h at room temperature. The cultures were washed 3 times for 15 min with PBS followed by incubation with DAPI (1:5000) for 3 min and subsequent PBS washes. The myotubes were then visualized at room temperature on an Eclipse TE 2000-U microscope equipped with a Digital Sight DS-Fi1 camera (Nikon). Images were captured, and the diameter of the myotubes was measured with ImageJ software (NIH). The myotube diameter was quantified as follows: 10 fields were chosen randomly, and 10 myotubes were measured per field. The average diameter per myotube was calculated as the mean of the 3 measurements taken along the length of the myotube.

Surface sensing of translation assay. Protein synthesis was measured by nonisotope labeled surface sensing of translation (Sunset), a validated method [116]. Myotubes were treated with LLC-CM and/or 4-PBA for 12 h, followed by addition of 0.1 mM puromycin for 30 min. The cells were collected, protein extracts were made, and newly synthesized protein was detected by Western blot with anti-puromycin (1:1000; EMB Millipore Darmstadt, Germany) as the primary antibody.

AMPK assay. Enzymatic activity of AMPK in skeletal muscle tissue extracts was measured with a commercially available kit, according to the protocol suggested by the manufacturer (MBL International, Woburn, MA, USA).

Total RNA extraction and QRT-PCR assay. RNA isolation and QRT-PCR were performed by using a published method [59, 117]. In brief, total RNA was extracted from gastrocnemius (GA) and TA muscles of mice or cultured primary myotubes isolated with TRIzol reagent (Thermo Fisher Scientific Life Sciences) and an RNeasy Mini Kit (Qiagen, Valencia, CA, USA) according to the manufacturers' protocols. First-strand cDNA for PCR analyses was made with a commercially available kit (Thermo Fisher Scientific Life Sciences). The quantification of mRNA expression was performed using the SYBR Green dye (Thermo Fisher Scientific Life Sciences) method on a sequence-detection system (model 7300; Thermo Fisher Scientific Life Sciences). Primers were designed with Vector NTI software (Thermo Fisher Scientific Life Sciences) and are available in Appendix 1. Data normalization was accomplished with the endogenous

control (β -actin), and the normalized values were subjected to a $2^{-\Delta\Delta C_t}$ formula to calculate the fold change between control and experimental groups.

Analysis of sXBP1. To measure the unspliced (u)XBP1 and spliced (s)XBP1, we prepared cDNA from skeletal muscle of control and LLC cell-bearing mice and subjected it to a semi-quantitative RT-PCR (QRT-PCR) assay [58]. The sequences of the primers were 5'-TTA CGG GAG AAA ACT CAC GGC-3' (forward) and 5'-GGG TCC AAC TTG TCC AGA ATG C-3' (reverse). The primer's annealing temperature was 56°C, and reaction mixtures containing 100 ng of cDNA proceeded for 35 cycles. The PCR products were run on a 2% agarose gel to identify the presence of uXBP1 and sXBP1 cDNA.

Western blot analysis. Estimation of the presence of various proteins was quantitated by performing Western blot analysis. TA or GA muscle of mice or primary myotubes were washed with sterile PBS and homogenized in lysis buffer: 50 mM Tris-Cl (pH 8.0), 200 mM NaCl, 50 mM NaF, 1 mM dithiothreitol, 1 mM sodium orthovanadate, 0.3% IGEPAL, and protease inhibitors. Approximately 100 mg protein was resolved in each lane on 10% SDS-polyacrylamide gels, electrotransferred onto nitrocellulose membranes, and probed with the following antibodies: anti-phospho-eIF2 α (1:1000; Cell Signaling Technology, Danvers, MA, USA), anti-eIF2 α (Cell Signaling Technology 1:1000), anti-CHOP (1:500; Cell Signaling Technology), anti-GADD34 (1:500; Santa Cruz Biotechnology, Santa Cruz, CA, USA), anti-ATF6 (1:500; Santa Cruz

Biotechnology), anti-MyHC (1:1000; DSHB), anti-troponin T (1:500; Sigma-Aldrich, St. Louis, MO, USA), anti-tropomyosin (1:500; Sigma-Aldrich), anti-sarcomeric α -actin (1:500; Sigma-Aldrich), anti-IRE1a (1:1000; Cell Signaling Technology), anti-sXBP1 (1:1000; Cell Signaling Technology), anti-ubiquitin (1:500; Santa Cruz Biotechnology), anti-LC3B1/2 (1:500; Cell Signaling Technology), anti-Beclin1 (1:500; Cell Signaling Technology), anti-p62 (1:500; MBL International), anti-phospho-Akt (Ser473) (1:500; Cell Signaling Technology), anti-Akt(1:500; Cell Signaling Technology), anti-phospho-mTOR (1:500; Cell Signaling Technology), anti-mTOR (1:500; Cell Signaling Technology), anti-phospho-p70S6K (1:500; Cell Signaling Technology), anti-p70S6K (1:500; Cell Signaling Technology), anti-phospho-ribosomal protein (rp)S6 (1:500; Cell Signaling Technology), anti-rpS6 (1:000; Cell Signaling Technology), anti- α -tubulin (1:1000; Cell Signaling Technology), and anti-GAPDH (1:2000; Cell Signaling Technology). Antibodies were detected by chemiluminescence. Quantitative estimation of the bands' intensity was performed with ImageJ software (NIH).

Grip-strength test. We used a digital grip-strength meter (Columbus Instruments, Columbus, OH, USA) to measure forelimb or total 4-limb grip strength of mice by following a known protocol [118]. Mice were acclimatized for 5 min before the grip-strength test began. The mouse was allowed to grab the metal pull bar with the forepaws and in a separate experiment with all 4 paws. The mouse tail was then gently pulled backward in the horizontal plane until it could no longer grasp the bar. The force at the time of release was recorded as the peak tension. Each mouse was tested 5 times with a 20–40

s break between tests. The average peak tension from 3 best attempts normalized against total body weight was defined as forelimb grip strength.

Statistical analysis. Results are expressed as mean \pm standard deviation (SD). For statistical analyses, we used unpaired two-tailed Student's t-test. A value of $P < 0.05$ was considered statistically significant, unless otherwise specified.

2.3 Results

2.3.1 Markers of ER stress are induced in skeletal muscle of mouse models of cancer

cachexia. We first investigated how the expression of ER stress markers is altered in skeletal muscles of mice in response to cancer growth. There are several mouse models, but LLC and *Apc*^{Min/+} mice are commonly used to study cancer cachexia [103, 105, 108, 119, 120]. C57BL/6 mice were inoculated with 2×10^6 LLC cells in the left flank. The mice were euthanized 18 d after implantation of LLC cells and right hindlimb muscles were analyzed. Markers of ER stress were measured by performing QRT-PCR and Western blot. As shown in **Figure 2.1A**, mRNA levels of IRE1 α , XBP1, ATF6, and DR5 were significantly increased in the GA muscle of LLC-bearing mice. Western blot analysis showed that levels of phosphorylated eIF2 α (p-eIF2 α), a downstream phosphorylation target of PERK, were significantly elevated in skeletal muscle of LLC-bearing mice. Moreover, the protein levels of CHOP were significantly increased in skeletal muscle of LLC-bearing mice (**Figure 2.1B, C**). In response to ER stress, XBP1 mRNA is spliced by IRE1 to produce a highly active transcription factor that induces UPR genes [121]. We evaluated the splicing of XBP1 mRNA by performing semi-QRT-

PCR using primers that detect both unspliced and spliced mRNAs. As shown in **Figure 2.1D**, there was a considerable increase in levels of sXBP1 in GA muscle of LLC-bearing mice. We next used an $Apc^{Min/+}$ genetic mouse model of cancer cachexia to determine whether the induction of markers of ER stress was limited to a specific type of cancer. Results showed that mRNA levels of PERK, IRE1a, XBP1, ATF6, GRP78, GRP94, GADD34, and DR5 were significantly increased in GA muscle of 4-mo-old $Apc^{Min/+}$ transgenic mice compared to littermate control mice (**Figure 2.1E**). These results suggest that ER stress is elevated in skeletal muscle in models of cancer cachexia.

2.3.2 Tumor-derived factors increase markers of ER stress in skeletal muscle.

Although we found increased activation and expression of markers of ER stress in skeletal muscle of the models of cancer cachexia, it is not clear whether host- or tumor-derived factors mediate such activation. To resolve this question, we investigated whether treatment with LLC-CM can also activate markers of ER stress in cultured myotubes. Fully differentiated mouse primary myotubes were treated with LLC-CM in a 1:4 ratio for 24 h, followed by a study of the markers of ER stress. Treatment of myotubes with LLC-CM significantly increased the mRNA levels of PERK, ATF6, GRP94, GADD34, CHOP, ATF4, and DR5 measured by the QRT-PCR technique (**Figure 2.2A**). We also performed Western blot analysis to determine the levels of phosphorylated eIF2a protein. This analysis showed that the levels of phosphorylated eIF2a were significantly elevated in myotubes upon treatment with LLC-CM (**Figure 2.2B, C**). Moreover, the levels of CHOP and ATF6 proteins were also significantly increased in myotubes treated with LLC-CM. By contrast, the levels of GADD34 protein remained comparable between

control and LLC-CM-treated myotubes (**Figure 2.2B**). These results suggest that tumor-derived factors are responsible for the increased ER stress in skeletal muscle in models of cancer cachexia.

2.3.3 Inhibition of ER stress diminishes muscle strength in normal and LLC-bearing mice.

Although we observed increased activation of the markers of ER stress in models of cancer cachexia, it is not known whether ER stress works to promote muscle wasting or it antagonizes atrophying signals. We next investigated the effect of inhibition of ER stress in normal and LLC-bearing mice. In several previous studies, 4-PBA has been used to block ER stress in animal models of various diseases [79, 112]. Mice were given intraperitoneal injections of 4-PBA (100 mg/kg body weight, i.p.) daily until 18 d after inoculation of LLC cells. Control mice received only PBS. The average body weight of LLC cell-bearing mice was significantly lower than that of control mice at 18 d (**Figure 2.3A**). Treatment with 4-PBA significantly reduced the body weight of normal mice. Furthermore, there was a trend toward further reduction in average body weight of LLC cell-bearing mice upon treatment with 4-PBA. We next measured the muscle strength of these mice using a grip strength meter. As expected, LLC cell-bearing mice displayed a significant decrease in maximum and average forelimb, as well as total (4 paw) grip strength compared to control mice (**Figure 2.3B–E**). Consistent with body weight, treatment of normal mice with 4-PBA resulted in a significant loss in grip strength. Indeed, loss of grip strength was comparable between control mice treated with 4-PBA and untreated LLC cell-bearing mice. Moreover, treatment with 4-PBA further reduced grip strength in LLC cell-bearing mice.

We next isolated individual hindlimb muscles and measured their wet weight. Wet weights of tibialis anterior (TA) and soleus muscle were significantly reduced in 4-PBA-treated normal mice; LLC cell-bearing mice; or 4-PBA-treated, LLC cell-bearing mice compared to control mice treated with vehicle alone (**Figure 2.3F, G**). Furthermore, wet weight of the GA muscle was significantly reduced in 4-PBA-treated, LLC-bearing mice compared to mice in the other 3 groups (**Figure 2.3H**). We also investigated whether increased muscle loss in 4-PBA-treated, LLC-bearing mice was due to increase in tumor growth. We found unexpectedly that treatment with 4-PBA reduced the size of tumors in mice (**Figure 2.3I**). These results suggest that inhibition of ER stress in naive and LLC-bearing mice exaggerates the loss of skeletal muscle mass and strength.

2.3.4 Inhibition of ER stress causes skeletal muscle wasting in normal and LLC-bearing mice. Skeletal muscle wasting is characterized by loss of fiber CSA without having any effect on number of fibers [44]. We next investigated how inhibition of ER stress using 4-PBA affects fiber CSA in normal and LLC-bearing mice. For this analysis, we prepared TA and soleus muscle transverse sections and performed H&E staining followed by quantification of average fiber CSA. This analysis showed that average fiber CSA of TA (**Figure 2.4A, B**) and soleus muscle (**Figure 2.4C, D**) decreased significantly in LLC-bearing mice compared to control mice confirming a cachectic phenotype in these mice. Consistent with wet muscle weight, we found that treatment with 4-PBA alone significantly reduced fiber CSA in both TA and soleus muscle of normal mice. Moreover, treatment with 4-PBA further reduced average fiber CSA in both these muscles of LLC-bearing mice (**Figure 2.4A–D**).

Studies have shown that skeletal muscle wasting in response to multiple stimuli including cancer cachexia involves degradation of specific muscle proteins, such as MyHC fast type [117, 122]. Protein extracts were prepared from GA muscle of mice, and levels of various thin and thick filament proteins were measured by Western blot analysis. Levels of MyHC were significantly reduced in skeletal muscle of LLC-bearing mice and 4-PBA-treated normal or LLC-bearing mice compared with that in normal mice treated with vehicle alone (**Figure 2.4E, F**). By contrast, the levels of Troponin, Tropomyosin, and Sarcomeric α -actin were comparable between all the groups (**Figure 2.4E, quantification not shown**). Our Western blot analysis also confirmed that the major markers of ER stress (i.e., p-eIF2, IRE1, sXBP1, and ATF6) were considerably reduced in skeletal muscle of 4-PBA-treated mice (**Figure 2.4G**). ATF4 is regulated by the PERK arm of ER stress [6]. One study has shown that ATF4 is involved in starvation-induced muscle atrophy [123]. By performing QRT-PCR, we measured mRNA levels of ATF4 and found that the levels of ATF4 were drastically increased in skeletal muscle of LLC-bearing mice. Treatment with 4-PBA blunted the LLC-induced expression of ATF4 in skeletal muscle of mice. Whether ATF4 has any role in regulation of muscle mass during cancer growth remains unknown, but inhibition of expression of ATF4 confirms that 4-PBA effectively inhibits the markers of UPR in skeletal muscle of mice. The collective results suggest that inhibition of ER stress/UPR pathways causes muscle wasting in normal mice and produces a more severe cachetic phenotype in LLC-bearing mice.

2.3.5 ER stress is necessary for maintaining the oxidative phenotype of skeletal

muscle. Skeletal muscle wasting in many conditions is associated with a slow-to-fast

fiber type transition [124]. There are also several reports suggesting that fast-type

(glycolytic) fibers undergo atrophy at a faster rate than do slow-type (oxidative) fibers

[125]. Induction of cancer cachexia through C-26 tumor cells in mice has been shown to

cause a transition from slow-to-fast type fibers in soleus muscle [126]. To investigate

whether inhibition of ER stress affects the composition of slow- and fast-type fibers in

skeletal muscle, we prepared soleus muscle cross sections and stained them with anti-

myosin heavy chain (MyHC) types I, IIA, and IIB. Representative images of all 4 groups

are presented in (**Figure 2.5A**). Consistent with published reports, soleus muscle of

normal mice contained mainly type I and IIA (both oxidative) fibers with almost no type

IIB (glycolytic) fibers. Treatment of mice with 4-PBA alone or inoculation with LLC

cells significantly increased the number of type IIB fibers in soleus muscle of mice.

Moreover, treatment of LLC cell-bearing mice with 4-PBA further increased the pro-

portion of type IIB fibers in soleus muscle (**Figure 2.5B**). We also investigated whether

the inhibition of ER stress reduces the CSA of type I or IIA fibers or of both. Quantitative

estimation of stained soleus muscle section showed that 4-PBA or inoculation of LLC

alone significantly reduced average CSA of type I and IIA fibers in mice. The

combination of 4-PBA and LLC had no additional effects on the reduction of average

CSA of type I fibers. By contrast, the average CSA of type IIA fibers was significantly

reduced compared to 4-PBA alone or LLC alone (**Figure 2.5C**). These results suggest

that ER stress/UPR maintains the proportion and size of slow-type fibers in skeletal

muscle.

2.3.6 Inhibition of ER stress activates proteolytic pathways in skeletal muscle. The UPS and autophagy are 2 major proteolytic systems that cause degradation of muscle protein during cancer growth and in many other catabolic conditions [42, 103]. We next investigated whether inhibition of ER stress affects the activation of these pathways in skeletal muscle of mice. To understand the overall levels of ubiquitinylation, we prepared muscle extracts and performed immunoblot analysis with an antibody against ubiquitin. There was a significant increase in the conjugation of muscle proteins to ubiquitin in LLC cell-bearing mice. Furthermore, the levels of ubiquitinated proteins were considerably increased in skeletal muscle of 4-PBA-treated mice compared with those treated with vehicle alone. Treatment with 4-PBA reduced the levels of ubiquitinated protein in LLC-bearing mice (**Figure 2.6A**). We also measured mRNA levels of the E3 ubiquitin ligases MAFBx, MuRF1, MUSA1, and TRAF6, which are induced in skeletal muscle and have been shown to mediate degradation of muscle proteins in multiple catabolic conditions [44, 58, 103, 127, 128]. Consistent with published reports, there was a significant increase in the mRNA levels of MAFBx, MuRF1, and TRAF6 in skeletal muscle of LLC-bearing mice compared to control mice. In contrast, the mRNA levels of MUSA1 were reduced in LLC-bearing mice (**Figure 2.6B**). There was also a trend toward increased expression of MAFBx in skeletal muscle of mice treated with 4-PBA, although it was not statistically significant. Transcript levels of MuRF1 remained unchanged, whereas the levels of TRAF6 and MUSA1 were significantly reduced in skeletal muscle of mice treated with 4-PBA alone compared to vehicle alone. Treatment with 4-PBA significantly

reduced the mRNA levels of MAFBx, MuRF1, and TRAF6 in skeletal muscle of LLC-bearing mice.

We next measured the markers of autophagy in skeletal muscle of mice in each group. During autophagy, microtubule-associated protein 1A/1B LC3B-I is converted to LC3B-II through lipidation, allowing LC3B to become associated with autophagic vesicles. Furthermore, p62 is a bona fide substrate of autophagy, and its levels are reduced upon activation of autophagy [37]. Our analysis showed that there was no significant difference in the ratio of LC3B-II/LC3B-I protein in skeletal muscle of control and 4-PBA-treated mice. However, the ratio of LC3B-II to -I was significantly higher in skeletal muscle of LLC-bearing mice and was further increased by treatment with 4-PBA. We did not find a significant difference in the protein levels of another autophagy-related protein, Beclin1 (**Figure 2.6C, D**); however, the levels of p62 protein were significantly reduced in skeletal muscle of mice treated with 4-PBA alone, LLC alone, or LLC+4-PBA, suggesting activation of autophagy in all the 3 groups (**Figure 2.6C, D**). Our collective results suggest that inhibition of ER stress leads to the activation of the UPS and autophagy system in skeletal muscle.

2.3.7 Role of ER stress in the activation of the Akt/mTOR pathway and AMPK in skeletal muscle. Akt/mTOR is one of the most important signaling pathways that promote protein synthesis in skeletal muscle. Furthermore, activation of this pathway inhibits the activity of UPS and ALS in skeletal muscle [44]. We next sought to determine whether the inhibition of ER stress affects the activity of the Akt/mTOR pathway in skeletal muscle. There was no significant difference in phosphorylated or

total levels of Akt in different groups (**Figure 2.7A, B**). Treatment with 4-PBA significantly reduced the levels of phosphorylated mTOR, p70S6K, and rpS6 in skeletal muscle of mice. Levels of phosphorylated p70S6K and rpS6 were also found to be significantly reduced in LLC-bearing mice, and 4-PBA further reduced the levels of phosphorylated rpS6 protein. AMPK is an important signaling protein that induces the activity of proteolytic pathways and inhibits protein synthesis through negatively regulating mTOR [44]. Using a commercially available AMPK activity assays kit, we measured the enzymatic activity of AMPK in skeletal muscle of mice in all 4 groups. We found that the activity of AMPK increased significantly in skeletal muscle of mice in the 4-PBA alone, LLC, or LLC+4-PBA groups, compared to the mice treated with vehicle alone (**Figure 2.7C**).

2.3.8 Inhibition of ER stress causes atrophy in cultured primary myotubes. LLC-CM has been shown to induce atrophy in cultured myotubes [105]. To further understand the role of ER stress and tumor-derived factors in induction of atrophy, we treated primary myotubes with 4-PBA (5 mM), with or without LLC-CM (1:4 ratio), for 24 h. Results showed that treatment with 4-PBA alone or LLC-CM caused a significant reduction in myotube diameter. Loss of myotube diameter was further increased by combination of 4-PBA and LLC-CM (**Figure 2.8A, B**). By performing Western blot analysis, we confirmed that the markers of ER stress/UPR, such as phosphorylation of eIF2 α and levels of sXBP1 and total XBP1 are reduced upon treatment of myotubes with 4-PBA (**Figure 2.8C**). We also measured the mRNA levels of some of the markers of UPS and autophagy at 12 and 24 h after treatment of myotubes with 4-PBA and LLC-CM. The

mRNA levels of MuRF1, MAFBx, MUSA1, TRAF6, LC3B, and Beclin1 were significantly increased at 12 h after treatment of myotubes with 4-PBA (**Figure 2.8D**). Levels of MAFBx, MUSA1, TRAF6, and LC3B (but not MuRF1 and Beclin1) remained significantly elevated at 24 h after start of 4-PBA treatment. LLC-CM alone significantly increased the mRNA of only Beclin1 after 12 h of treatment. However, at 24 h, the mRNA levels of MuRF1, MAFBx, and LC3B were significantly higher in the myotubes treated with LLC-CM compared with the control cultures. We found that 4-PBA significantly reduced the mRNA levels of MuRF1 in LLC-CM-treated myotubes without having a significant effect on the mRNA levels of MAFBx, TRAF6, and LC3B at 12 or 24 h. We also measured the rate of protein synthesis in cultured myotubes using the Sunset assay. As shown in Fig. 8E, treatment with 4-PBA for 12 h considerably reduced the rate of protein synthesis in cultured myotubes. Studies have shown that the addition of LLC-CM initially increases protein synthesis, potentially to counter atrophy signals, whereas long-term (48 h) treatment inhibits protein synthesis in myotubes [129]. We found a modest up-regulation in protein synthesis by treatment of myotubes with LLC-CM. However, 4-PBA reduced the LLC-CM-induced protein synthesis in cultured myotubes. We also measured the phosphorylation of Akt, mTOR, and rpS6 proteins. As shown in **Figure 2.8F**, treatment with 4-PBA increased the phosphorylation of Akt but reduced the levels of phosphorylated mTOR and rpS6 proteins in myotubes. Consistent with protein synthesis, LLC-CM increased the activation of mTOR and rpS6 in myotubes within 12 h, which was blunted by treatment with 4-PBA. The collective results suggest that the inhibition of ER stress causes atrophy in cultured myotubes potentially through perturbing the activity of various proteolytic pathways and suppressing protein synthesis.

2.4 Discussion

Recent studies have shown that ER stress and UPR pathways get activated in skeletal muscle in response to both physiologic and pathologic stimuli [130]. With the exception of a study in which the role of the ATF6 arm of UPR in an acute exercise-induced adaptive response was investigated [60], there has been no published report investigating the direct role of ER stress in regulation of skeletal muscle mass in adult animals. In this study, many markers of ER stress were significantly increased in skeletal muscle of 2 mouse models of cancer cachexia (**Figure 2.1**). 4-PBA effectively inhibits ER stress and is one of the most commonly used agents to block all 3 arms of UPR in different conditions [113, 114], and we therefore used this chemical chaperon to identify the potential role of ER stress in regulation of skeletal muscle in both naive conditions and the LLC model of cancer cachexia. We found that inhibition of ER stress through prolonged administration of 4-PBA caused loss of skeletal muscle mass and strength in adult animals (**Figures 2.3&4**). Our study also provided initial evidence that the activation of ER stress and the UPR may be an important mechanism for preventing additional loss of skeletal muscle mass during cancer cachexia. These findings are consistent with the presumption that the main role of UPR is to restore ER function and hence improve proper protein folding in stress conditions [5, 6]. The requirement of individual UPR pathways in homeostasis is evident by the findings that genetic ablation of PERK, IRE1 or ATF6 causes growth retardation, pancreatic dysfunction, and embryonic lethality in mice [12, 131-133]. Therefore, inhibition of ER stress-induced UPR may disrupt homeostasis, which eventually results in loss of skeletal muscle mass.

Alternatively, it is possible that the components of UPR pathways engage in cross-talk with other signaling pathways that are important for the acquisition and maintenance of skeletal muscle mass. Indeed, our results demonstrate that the inhibition of ER stress using 4-PBA inhibits the phosphorylation of mTOR and its downstream phosphorylation targets in skeletal muscle both in vivo and in vitro (**Figures 2.7A, B, and 2.8E**).

Although we observed increased expression of the markers of ER stress in skeletal muscle of mouse models of cancer cachexia, it remains unknown whether increased ER stress is a common phenomenon in atrophying skeletal muscle in all catabolic conditions. Another report has suggested that the markers of ER stress are not altered during unloading-induced skeletal muscle atrophy [47]. The prototypical markers of ER stress and UPR in skeletal muscle are induced during starvation-induced skeletal muscle atrophy [58]. The increased expression of markers of ER stress in atrophying skeletal muscle during cancer (**Figures 2.1, 2.2**) and starvation [58] suggests that ER stress is associated with the regulation of skeletal muscle mass in certain conditions, especially those that involve chronic inflammation and metabolic perturbations. Indeed, there are reports suggesting increased ER stress in muscle diseases such as myositis, which involves chronic inflammation, swelling, and weakness of skeletal muscle [73, 79]. Increased expression of ER stress markers has also been observed in the myopathy associated with myasthenia gravis [84, 130].

Prolonged activation and unresolved ER stress can lead to many pathologic conditions in different tissues, including skeletal muscle. For example, activation of ER stress has been associated with development of insulin resistance in skeletal muscle [134]. Indeed, we have reported that treatment with tunicamycin or thapsigargin, the

inducers of ER stress, significantly increases the transcript levels of the components of UPS (e.g., MAFBx and MuRF1) and autophagy (e.g., LC3B and Beclin1) and represses expression of MyHC in cultured myotubes [58]. Compared to the UPS and autophagy markers, tunicamycin or thapsigargin caused a dramatic increase in the markers of ER stress, suggesting that very high levels of ER stress can initiate the atrophy program leading to loss of skeletal muscle mass [58]. However, it is also possible that a small (in physiologic range) elevation of ER stress-associated UPR protects cells from undergoing further damage. Indeed, our results in this study demonstrate that activation of ER stress/UPR in skeletal muscle preserves skeletal muscle mass and strength. Treatment of LLC cell-bearing mice with 4-PBA led to a further reduction in both muscle strength and weight (**Figure 2.3**). Similar results were obtained when cultured myotubes were treated with a combination of LLC-CM and 4-PBA (**Figure 2.8A, B**). Inhibition of ER stress using 4-PBA resulted in lower tumor weight in mice (**Figure 2.3I**), suggesting that the additional loss of muscle mass with administration of 4-PBA in LLC cell-implanted mice is not caused by the additional growth of the tumor. These results further emphasize the protective role of ER stress and UPR in tumor-induced muscle wasting.

Skeletal muscle atrophy is also associated with a change in expression of myosin isoforms. Specifically, cancer growth has been shown to cause a shift toward type IIB muscle fibers in the soleus muscle [126]. Our results confirm a slow-to-fast fiber type transition in soleus muscle of LLC-bearing mice (**Figure 2.5**). We found that treatment with 4-PBA also causes a slow-to-fast fiber type transition in the naive conditions and leads to an even higher number of type IIB fibers in soleus muscle of LLC-bearing mice (**Figure 2.5**). Although the underpinning mechanisms remain unknown, these results

suggest that ER stress plays an important role in maintenance of oxidative fibers in skeletal muscle *in vivo*.

Activation of the UPS and ALS has been observed in numerous catabolic states [37, 103, 107]. It has been observed that E3 ubiquitin ligases such as MuRF1, MAFBx, MUSA1, and TRAF6 are necessary in catalyzing the conjugation of ubiquitin to target protein [44, 59, 103, 127]. Once the protein is tagged with ubiquitin chains, they are subjected to degradation in the proteasome [103]. As expected, implantation of LLC cells in mice resulted in an increase in the levels of ubiquitinated proteins (**Figure 2.6A**) and significantly higher expression of MAFBx, MuRF1, and TRAF6. We found that the levels of MUSA1 were significantly reduced in skeletal muscle of LLC cell-bearing mice (**Figure 2.6B**). Treatment of wild-type mice with 4-PBA alone also increased the levels of ubiquitinated proteins (**Figure 2.6A**). Although statistical significance could not be achieved with the number of animals used in each group, there was a trend toward increased mRNA levels of MAFBx and MuRF1 in skeletal muscle of mice treated with 4-PBA (**Figure 2.6B**). By contrast, the levels of MUSA1 and TRAF6 were significantly reduced in skeletal muscle of mice treated with 4-PBA alone (**Figure 2.6B**). Treatment with 4-PBA reduced the levels of ubiquitinated proteins (**Figure 2.6A**) and mRNA levels of MAFBx, MuRF1, and TRAF6 (**Figure 2.6B**) in LLC-implanted mice. Myotubes treated with LLC-CM and 4-PBA exhibited similar inhibition in MAFBx and MuRF1 (**Figure 2.8C**). These results indicate that the inhibition of ER stress perturbs homeostasis in skeletal muscle in naive conditions, leading to enhanced protein degradation, potentially through UPS. It is also possible that some components of ER stress are involved in the activation of UPS in tumor-bearing animals and the inhibition of ER

stress/UPR attenuates the activity of UPS in tumor-bearing mice. However, more severe muscle atrophy in LLC cell-bearing mice upon treatment with 4-PBA indicates that, even though the UPS is inhibited, other catabolic mechanisms may get activated, resulting in overall higher loss of skeletal muscle mass. One such mechanism appears to be the activation of autophagy. The markers of autophagy are increased in skeletal muscle of normal mice treated with 4-PBA alone or in LLC-bearing mice. Although 4-PBA reduced the levels of ubiquitinated proteins, it did not inhibit the markers of autophagy in LLC cell-bearing mice (**Figure 2.6C, D**).

Although we observed muscle atrophy and increased levels of polyubiquitinated proteins, we found no significant increase in the mRNA levels of MAFBx, MuRF1, TRAF6, or MUSA1 in skeletal muscle of 4-PBA-treated mice. We cannot rule out the possibility that the inhibition of physiologic ER stress leads to the increased activity of some other E2 and E3 enzymes of the UPS leading to elevated levels of polyubiquitinated proteins in skeletal muscle. Moreover, it is possible that continued inhibition of some E3 ubiquitin ligases, such as MUSA1 and TRAF6, as observed in 4-PBA-treated mice (**Figure 2.6B**) upregulates other E3 ligases in skeletal muscle as a part of a compensatory mechanism. In fact, a few recently published reports demonstrate that proteasome activity is significantly increased in the MuRF1 knockout mice compared to that in control mice in 14 d denervated muscle or during aging, even though muscle atrophy is significantly rescued in MuRF1 knockout mice [135, 136]. There is also a possibility that the expression of some of these E3 ubiquitin ligases is increased at an early time point after treatment of mice with 4-PBA. This hypothesis is partly supported by our results demonstrating that 4-PBA significantly increased the levels of MAFBx, MuRF1, TRAF6,

and MUSA1 within 12 h (**Figure 2.8D**). Nevertheless, the results presented in this study suggest that ER stress/UPR pathways differentially regulate polyubiquitination and the expression of various E3 ubiquitin ligases in skeletal muscle in naive and cachectic conditions.

Another potential mechanism by which inhibition of ER stress causes muscle atrophy is through inhibition of the mTOR signaling pathway. Akt is known to regulate skeletal muscle hypertrophy through phosphorylation and activation of downstream targets, such as mTOR and rpS6, leading to increased protein synthesis [137]. Although Akt is an upstream activator in response to growth factors, mTOR can also be activated through Akt-independent mechanisms [138]. Our results suggest that although phosphorylation of Akt was not much affected, the phosphorylation of mTOR, p70S6K, and rpS6 kinase was significantly reduced in LLC cell-bearing mice (**Figure 2.7A, B**). Similar to the muscle atrophy phenotype, we found that 4-PBA further reduced the phosphorylation of mTOR, p70S6K, and rpS6 protein in normal and LLC-bearing mice (**Figure 2.7A, B**). AMPK, a highly conserved heterotrimeric kinase complex composed of a catalytic (α) subunit and 2 regulatory (β and γ) subunits, is activated under conditions of energy stress when intracellular ATP levels decline and intracellular AMP increases, as occurs during nutrient deprivation, hypoxia, and physical exercise [139]. Accumulating evidence suggests that mTOR and AMPK represent 2 antagonistic forces governing muscle adaptation in response to different stimuli. Specifically, activation of AMPK inhibits mTOR in skeletal muscle, leading to reduced protein synthesis and increased activation of proteolytic pathways [40]. Our analysis showed that the activity of AMPK is significantly increased in skeletal muscle of mice treated with 4-PBA, LLC

cells, or the combination of LLC cells and 4-PBA (**Figure 2.7C**). Although the exact mechanisms by which inhibition of ER stress increases the activation of AMPK and inhibits mTOR remain unknown, interplay between AMPK and mTOR through the components of UPR could be an important mechanism of the regulation of muscle mass in the naive and catabolic states.

We also found that treatment with 4-PBA drastically reduced protein synthesis in cultured myotubes (**Figure 2.8E**). Furthermore, 4-PBA significantly reduced the phosphorylation of mTOR and rpS6 protein in cultured myotubes (**Figure 2.8F**). However, when treated with LLC-CM alone, protein synthesis and phosphorylation of mTOR and rpS6 protein were increased (**Figure 2.8E, F**), perhaps because of the short time (12 h) during which the myotubes were subjected to the LLC CM. The myotubes could have been attempting to rescue the atrophy after addition of LLC CM. However, treatment with 4-PBA reduced LLC CM-induced protein synthesis and phosphorylation of mTOR and rpS6 protein in cultured myotubes. Taken together, these results further support a physiologic role of ER stress in promoting activation of the mTOR pathway and protein synthesis in skeletal muscle.

One caveat of the present study is that we used 4-PBA to block ER stress and UPR pathways in vivo. Although 4-PBA is one of the most commonly used inhibitors of ER stress, prolonged use can influence other metabolic pathways in addition to inhibition of ER stress. 4-PBA is classically used as a treatment for urea cycle disorders. This compound also acts as a histone deacetylase (HDAC) inhibitor [140]. A recent study has demonstrated that 4-PBA increases the expression of glucose transporter-4 through inhibiting histone deacetylase 5, leading to increased glucose metabolism in cultured

C2C12 myotubes [141]. HDAC inhibitors are also known to suppress tumor growth [142], which could account for the decrease in overall LLC tumor size after chronic treatment with 4-PBA (**Figure 2.3**). Moreover, HDAC inhibitors have recently been investigated as a potential treatment for loss of skeletal muscle mass during aging [143]. Certainly, further investigation is needed to determine whether 4-PBA causes muscle wasting in mice mainly through inhibition of ER stress/UPR or also through perturbation of other pathways including those involved in the regulation of metabolism.

In summary, our results suggest that the ER stress-induced UPR is essential for maintenance of skeletal muscle mass and strength in both naive and tumor-bearing mice. Although the exact roles remain enigmatic, it is possible that different arms of the UPR provide different signaling outcomes in skeletal muscle. Moreover, different parts of the UPR may play distinct roles in naive and catabolic states, including cancer cachexia. It is also possible that an alteration in a specific arm of UPR would be beneficial to the muscle, even in catabolic states. Future research using genetic mouse models will tease out whether distinct mechanisms are used by different arms of UPR to regulate skeletal muscle mass in the conditions of muscle hypertrophy, atrophy, and disease. Because of the complexity of ER stress/UPR and its many targets, a better understanding of its regulatory role is of significant clinical importance for developing new therapeutic strategies for treatment of various skeletal muscle disorders.

FIGURE 2.1

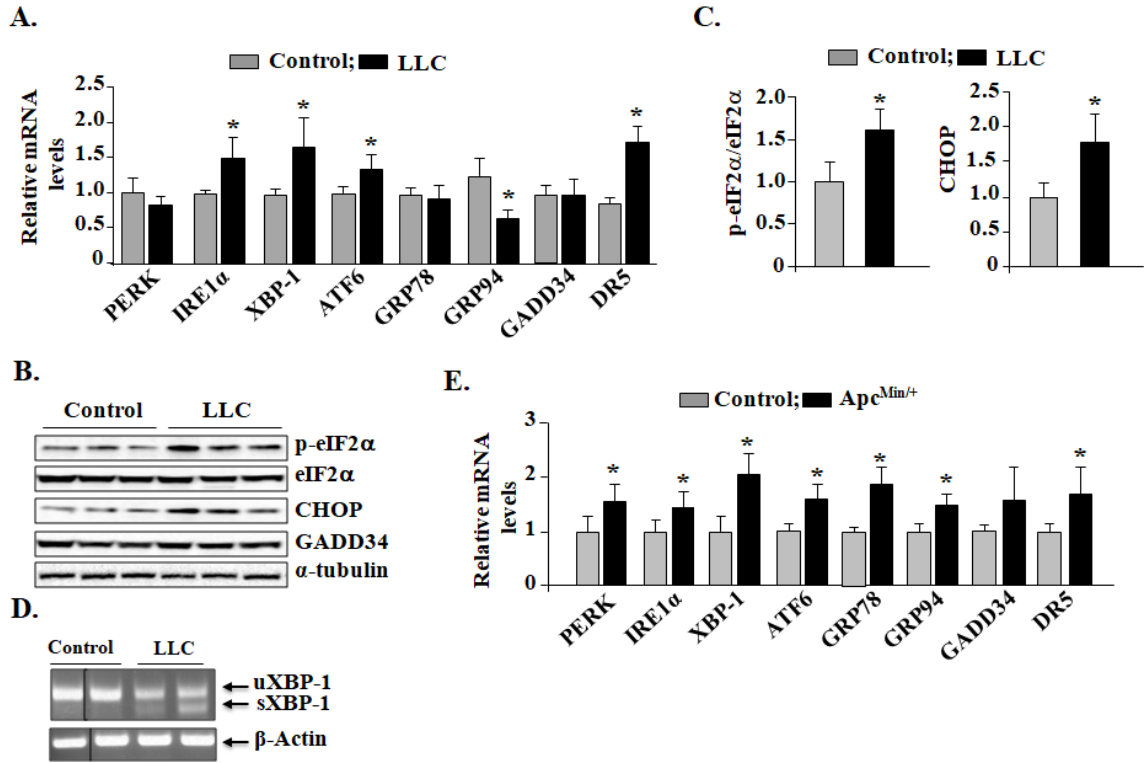


FIGURE 2.1 Activation of ER stress in mouse models of cancer cachexia. LLC cells were implanted in the left flank of wild-type mice, and tumor growth was monitored. Right hindlimb muscles were isolated and used to measure the levels of various markers of ER stress. **(A)** Relative mRNA levels of PERK, IRE1 α , XBP1, ATF6, GRP78, GRP94, GADD34, and DR5 in GA muscle of control and LLC-bearing mice. **(B)** Western blot analysis of levels of phosphorylated and total eIF2 α and total CHOP and of total GADD34 protein in GA muscle of control and LLC-bearing mice. **(C)** Densitometry quantification of phosphorylated vs. total eIF2 α ratio and CHOP in GA muscle of control and LLC-bearing mice. **(D)** Spliced (s)XBP1 and unspliced (u)XBP1 levels in control and LLC-bearing mice measured by semiquantitative RT-PCR assay using primers that detected both sXBP1 and uXBP1. Black vertical lines in gel images indicate that intervening lanes have been spliced out. **(E)** Relative mRNA levels of PERK, IRE1 α , XBP1, ATF6, GRP78, GRP94, GADD34, and DR5 in GA muscle of 4-mo-old control and Apc^{Min/+} mice measured by QRT-PCR. Error bars represent SD (n = 4/group); *P < 0.05, vs. control mice.

FIGURE 2.2

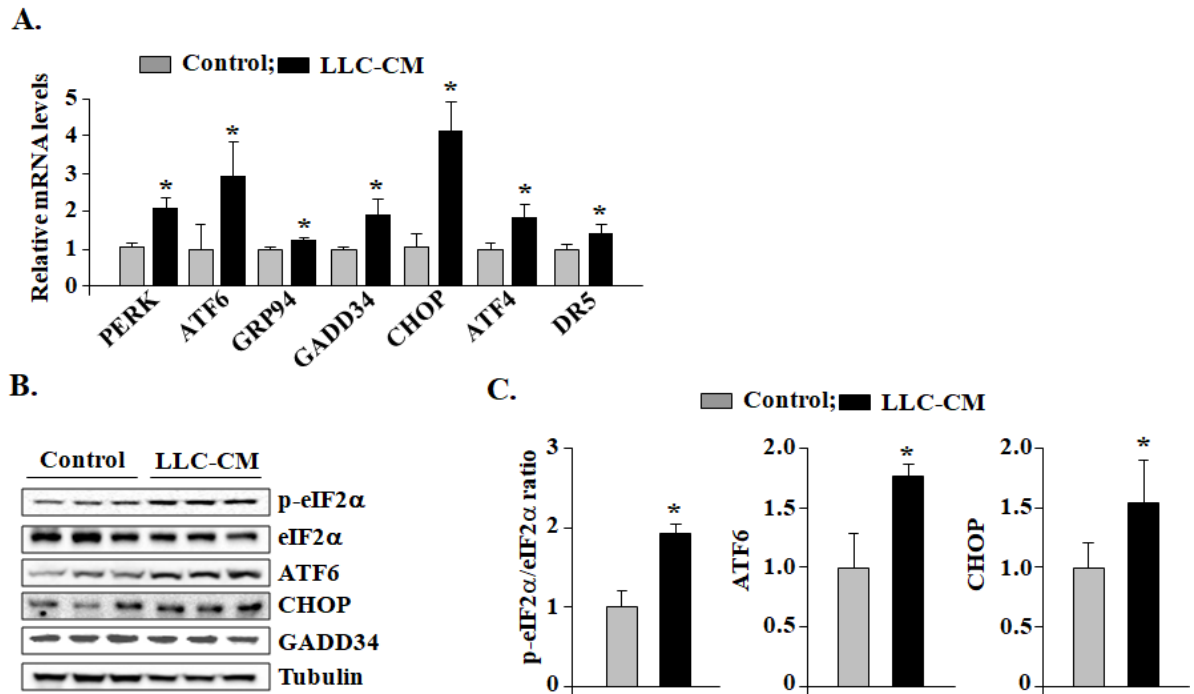


FIGURE 2.2: Activation of UPR markers in cultured myotubes treated with LLC-CM. Primary myotubes prepared from WT mice were treated with LLC-CM in a 1:4 ratio for 24 h and processed for a QRT-PCR assay or Western blot analysis. **(A)** Relative mRNA levels of PERK, ATF6, GRP94, GADD34, CHOP, ATF4, and DR5 in control and LLC-CM-treated myotubes. **(B)** Immunoblots demonstrate the levels of phosphorylated and total eIF2 α and ATF6, CHOP, and GADD34 protein in control and LLC-CM-treated myotubes. **(C)** Densitometry quantification of phosphorylated vs. total p-eIF2 α and total ATF6 and CHOP in control and LLC-CM-treated myotubes (n = 3/group). Error bars represent SD; *P < 0.05, vs. control cultures.

FIGURE 2.3

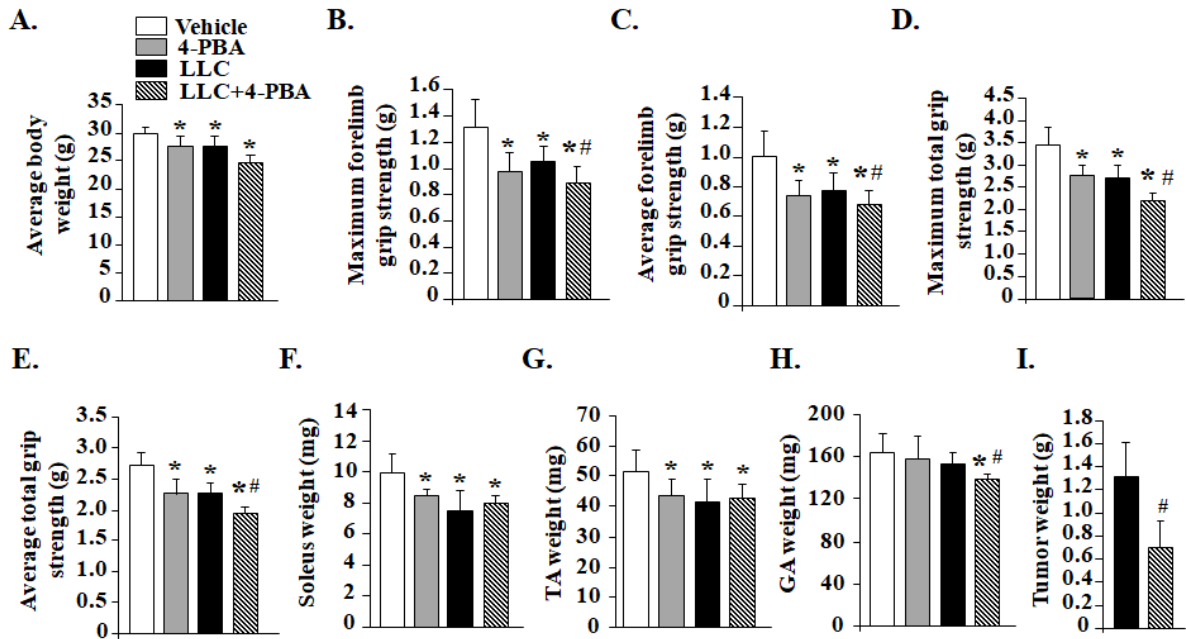


FIGURE 2.3: ER stress inhibitor 4-PBA causes loss of muscle strength and mass in naive conditions and in LLC-bearing mice. C57BL/6 12-wk-old mice were inoculated with 2×10^6 LLC cells in the left flank. They were also treated daily with 4-PBA (100 mg/kg body weight, i.p.). After 18 d, muscle strength, body weight, and wet muscle mass were measured. **(A)** Average body weight of mice in each group. **(B, C)** Maximum **(B)** and average **(C)** forelimb grip strength of mice in each group. **(D, E)** Maximum **(D)** and average **(E)** total 4-paw grip strength of mice in each group. **F–H)** Average wet weight of isolated soleus **(F)**, TA **(G)**, and GA **(H)** muscle in each group. **(I)** Wet weight of tumor after 18 d of inoculation with LLC in vehicle alone or 4-PBA-treated mice ($n = 5/\text{group}$). Error bars represent SD; * $P < 0.05$, vs. control mice; # $P < 0.05$, vs. LLC cell-inoculated mice.

FIGURE 2.4

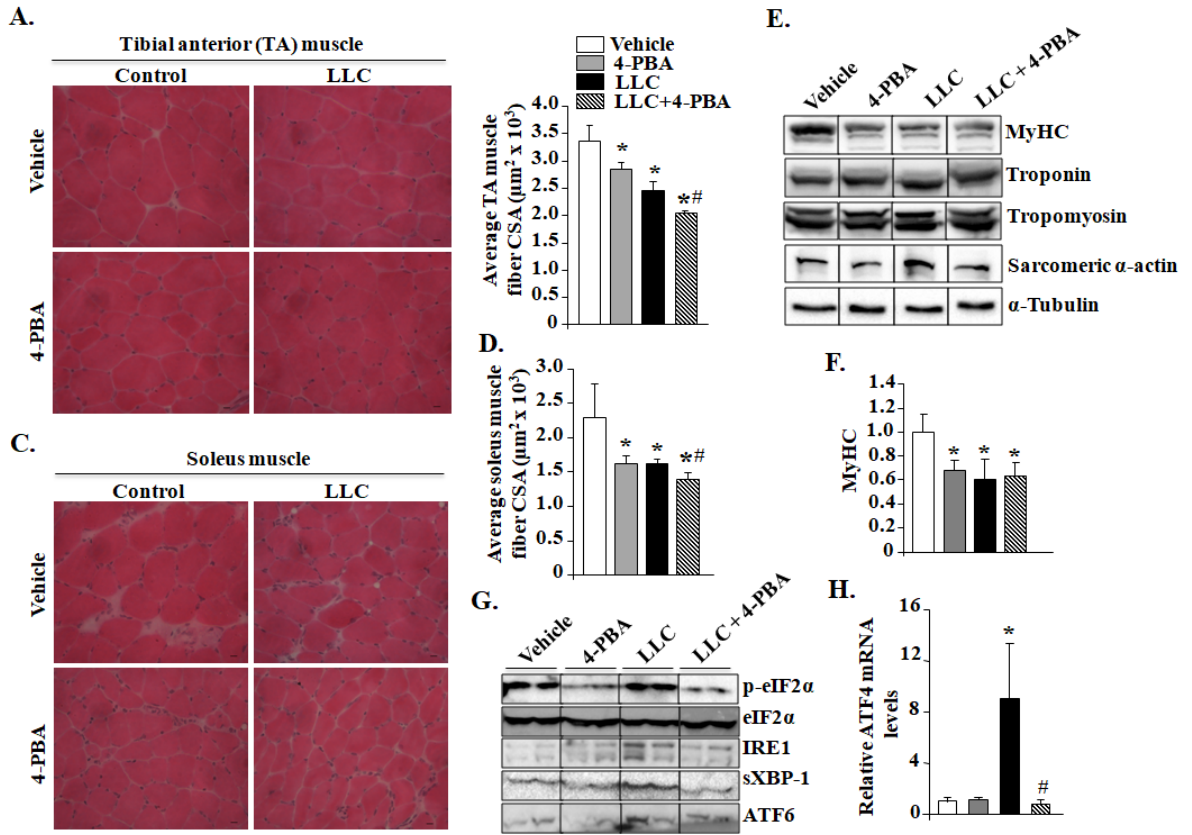


FIGURE 2.4: Inhibition of ER stress by 4-PBA exacerbates skeletal muscle atrophy in control and LLC-bearing mice. (A) Representative photomicrographs of H&E-stained sections of mouse TA muscle. Scale bar, 10 mm. (B) Quantification of average fiber CSA of TA muscle in control and LLC-bearing mice, with or without 4-PBA treatment. (C) Representative photomicrographs of H&E-stained sections of soleus muscle. Scale bar, 10 mm. (D) Quantification of average fiber CSA of soleus muscle in control and LLC-bearing mice, with or without 4-PBA treatment. (E) GA muscle of vehicle, 4-PBA, LLC, and LLC+4-PBA mice were processed for Western blot analysis to detect levels of specific muscle proteins. Representative immunoblots demonstrate the levels of MyHC, Troponin, Tropomyosin, Sarcomeric α -actin, and unrelated protein α -tubulin. (F) Densitometry quantification of MyHC. (G) Representative immunoblots demonstrate that the levels of phosphorylated and total eIF2 α , total IRE1, total sXBP1, and ATF6 were reduced by treatment with 4-PBA, confirming suppression of ER stress. (H) Transcript levels of ATF4 in GA muscle of vehicle, 4-PBA alone, LLC alone, and LLC+4-PBA groups measured by performing QRT-PCR assay. Black vertical lines in immunoblots indicate that intervening lanes have been spliced out (n = 5/group). Error bars represent SD; *P < 0.05, vs. mice treated with vehicle alone; #P < 0.05 vs. LLC-inoculated mice.

FIGURE 2.5

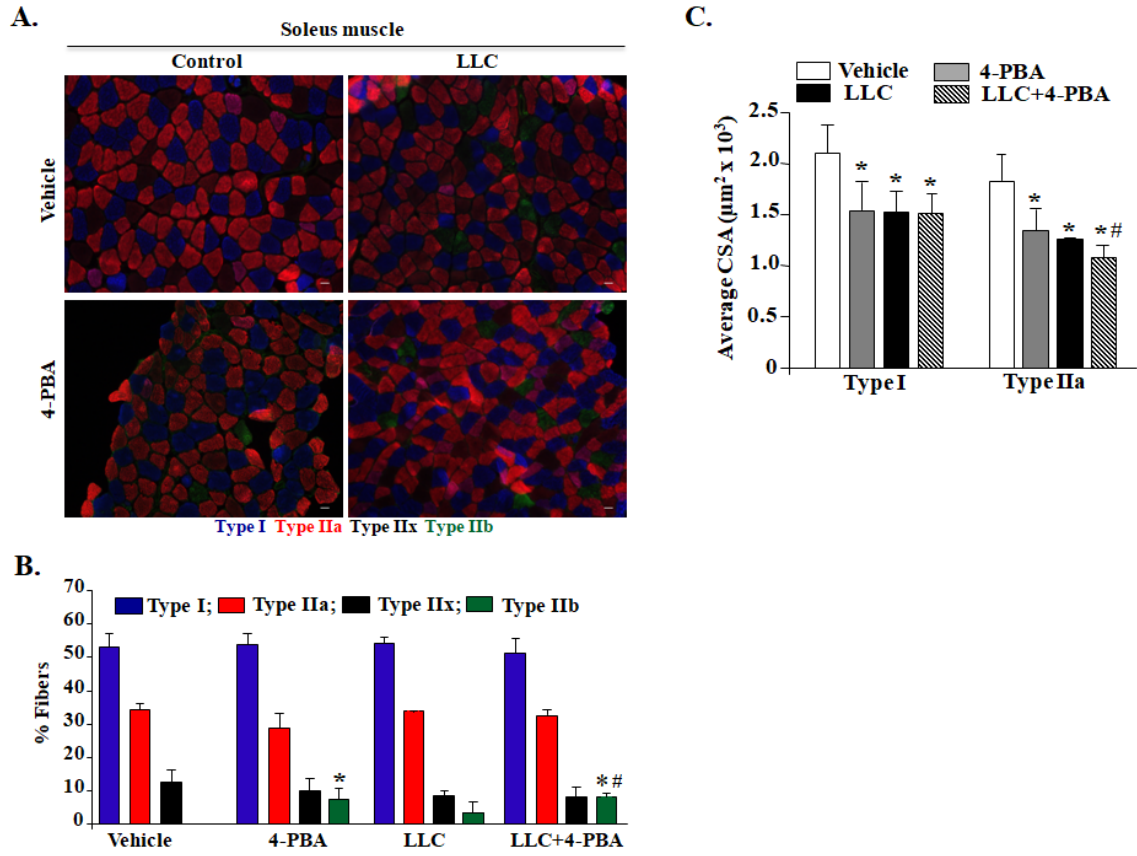


FIGURE 2.5: Blocking ER stress increases the proportion of fast-type fibers in normal and LLC-bearing mice. Soleus muscle sections prepared from vehicle, 4-PBA, LLC, and LLC+4-PBA mice were subjected to triple immunostaining against MyHC I, IIA, and IIB protein. **(A)** Representative photomicrographs of triple-stained sections of soleus muscle. Scale bar, 50 μ m. **(B)** Quantification of the percentage of each fiber type in different groups. **(C)** Average CSA of type I and IIA fibers in soleus muscle of mice in each group (n = 5 in each group). Error bars represent SD; *P < 0.05, vs. control mice; #P < 0.05, vs. LLC-inoculated mice.

FIGURE 2.6

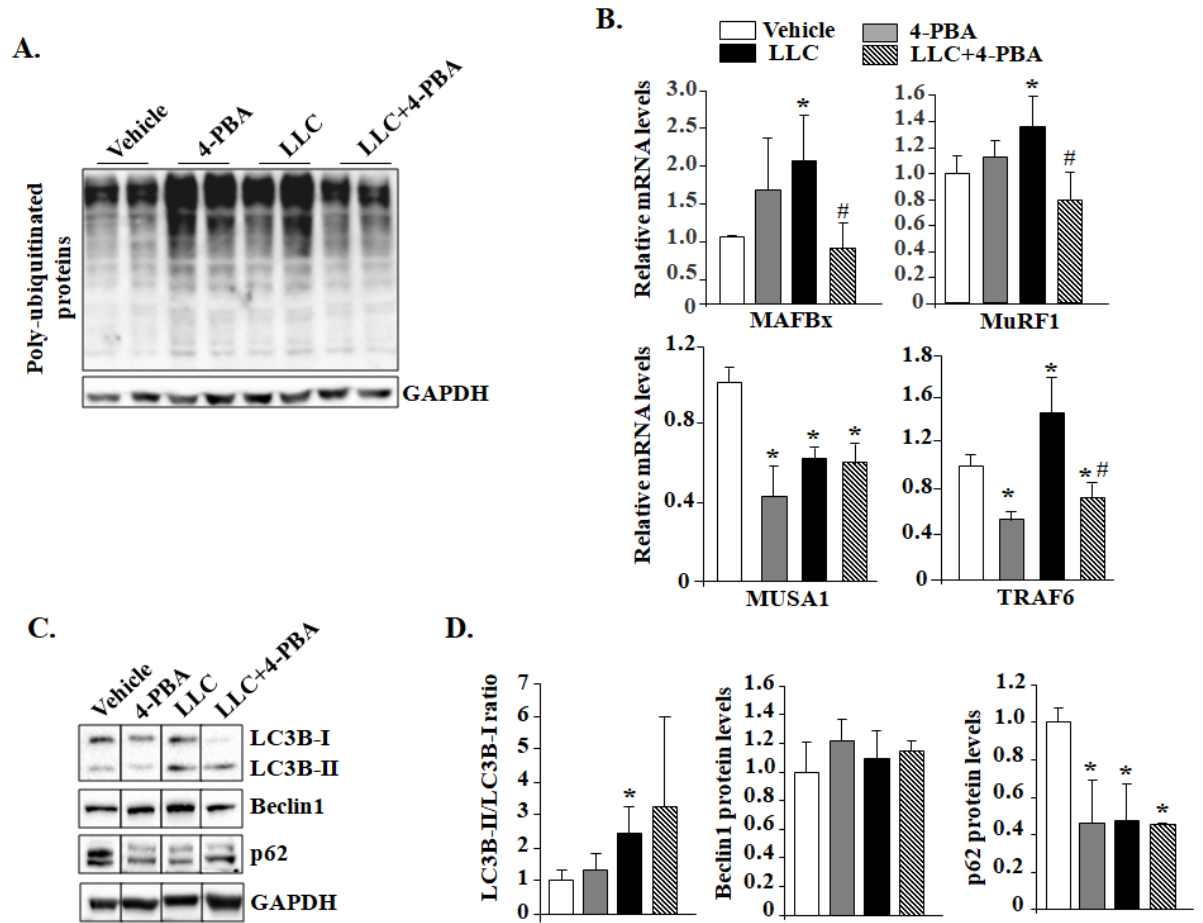


FIGURE 2.6: The effect of 4-PBA treatment on the activation of ubiquitin proteasome system and autophagy. GA muscle of vehicle, 4-PBA, LLC, and LLC+4-PBA mice were processed for Western blot and QRT-PCR analyses. **(A)** Representative immunoblots demonstrate the levels of ubiquitinated proteins in GA muscle of mice in each group. **(B)** Relative mRNA levels of MAFB_x, MuRF1, MUSA1, and TRAF6 in GA muscle measured by performing QRT-PCR assay. **(C)** Representative immunoblots demonstrates the levels of LC3B-I and -II, Beclin1, p62, and the unrelated protein GAPDH in GA muscle of mice. **(D)** Densitometry quantification of the ratio of LC3B-II vs. LC3B-I and total levels of Beclin1, and p62. Black vertical lines in immunoblots indicate that intervening lanes have been spliced out (n = 4/group). Error bars represent SD. *P < 0.05, vs. control mice; #P < 0.05, vs. LLC inoculated mice.

FIGURE 2.7

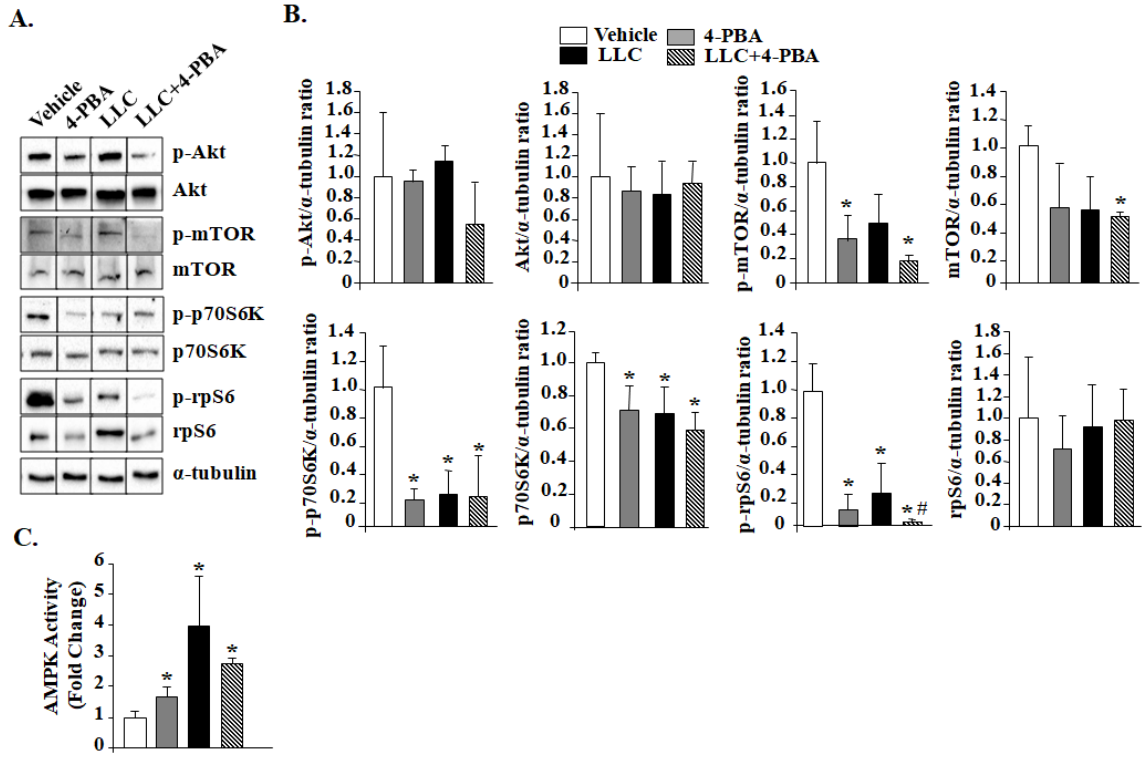


FIGURE 2.7: Effects of 4-PBA on activation of Akt/mTOR and AMPK signaling pathways in skeletal muscle of normal and LLC- bearing mice. GA muscle of vehicle-, 4-PBA-, LLC-, and LLC+4-PBA-treated mice were processed by Western blot analysis. **(A)** Representative immunoblots demonstrate the levels of phosphorylated and total Akt, mTOR, p70S6 kinase (p70S6K), rpS6, and the unrelated protein α -tubulin. Black vertical lines indicate that intervening lanes have been spliced out. **(B)** Quantification of phosphorylated and total Akt, mTOR, p70S6K, and rpS6 levels after normalizing with α -tubulin in GA muscle of vehicle-, 4-PBA-, LLC-, and LLC+4-PBA- mice. **(C)** Fold change in enzymatic activity of AMPK in GA muscle of vehicle-, 4-PBA-, LLC-, and LLC+4- PBA-treated mice measured with a commercially available kit (n = 4/group). Error bars represent SD; *P < 0.05, vs. control mice; #P < 0.05, vs. LLC-inoculated mice.

FIGURE 2.8

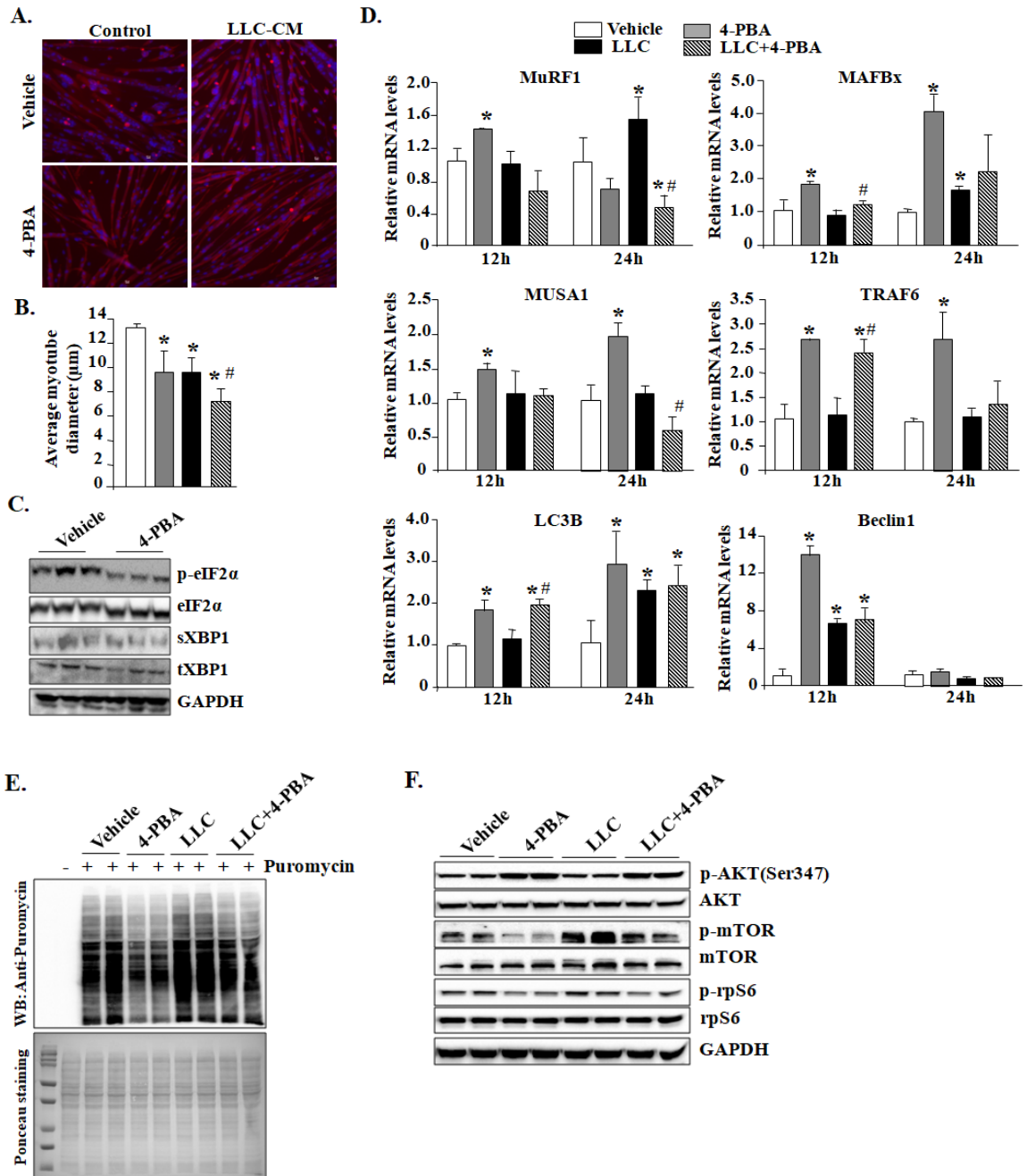


FIGURE 2.8: Inhibition of ER stress causes atrophy in cultured primary myotubes.

Differentiated myotubes were treated with vehicle alone, 4-PBA (5 mM), LLC-CM (1:4 ratio), or LLC-CM+4-PBA for 24 h. **(A)** Representative photomicrographs of myotubes in each group taken at 24 h. Scale bar, 10 μ m. **(B)** Average myotube diameter in each group. **(C)** Immunoblots demonstrate the levels of phosphorylated and total eIF2 α , sXBP1, and tXBP1 in cultured myotubes after treatment with 4-PBA (5 mM) for 24 h. **(D)** Relative mRNA levels of the E3 ubiquitin ligases MuRF1, MAFBx, MUSA1, and TRAF6 and the autophagy marker LC3B and Beclin1 in vehicle, 4-PBA, LLC-CM, or LLC-CM+4-PBA-treated myotubes measured after 12 and 24 h. **(E)** Representative immunoblot (top) from the Sunset assay demonstrating relative amounts of newly synthesized protein in each condition. Equal loading of protein in each lane was confirmed by staining nitrocellulose membrane with Ponceau S dye (bottom). **(F)** Immunoblots demonstrate the levels of phosphorylated and total Akt, mTOR, and rpS6 after 12 h in the indicated groups (n = 3/group). Error bars represent SD; *P < 0.05, vs. control cultures; #P < 0.05, vs. LLC-CM- treated myotube cultures at corresponding time points.

CHAPTER 3

TLRS-MYD88-XBP1 AXIS MEDIATES SKELETAL MUSCLE WASTING IN CANCER-ASSOCIATED CACHEXIA

3.1 Introduction. Cancer cachexia is a devastating syndrome that is characterized by the progressive loss of skeletal muscle mass and strength. Cachexia afflicts a vast majority of cancer patients and is responsible for about 30% of all cancer-related deaths [144]. In addition to the deterioration in quality of life, patients with cachexia show intolerance to chemotherapy and other anti-neoplastic treatments [101]. It is now evidenced that increased protein degradation due to stimulation of the ubiquitin-proteasome system (UPS) and autophagy are prominent mechanisms for skeletal muscle wasting in many catabolic states, including cancer [42, 103, 145]. Moreover, a systemic inflammatory response, which is triggered by factors generated by either the tumor or non-tumor cells, also plays an important role in skeletal muscle weakness in cancer-induced cachexia [100]. While a number of drugs have been tested in clinical trials, none of them showed a significant impact on the quality of life or weight gain emphasizing that a better understanding of molecular mechanisms is paramount for the development of effective therapies to preserve muscle mass in cancer patients [146, 147].

Proinflammatory cytokines are important mediators of skeletal muscle wasting in many chronic disease states, including cancer [100, 144]. Furthermore, cancer cells generate

danger-associated molecular patterns (DAMPs), as well as heat-shock proteins (Hsp), that stimulate muscle proteolysis through binding of the toll-like receptors (TLRs) [100, 148]. Indeed, recent studies have suggested that the genetic deletion of TLR4 inhibits skeletal muscle wasting in response to microbial products, as well as in a model of cancer cachexia [149, 150]. Myeloid differentiation primary response gene 88 (MyD88) is the key adaptor protein for the interleukin-1 (IL-1) receptor and TLR-mediated activation of downstream signaling pathways [151-153]. Accumulating evidence suggests that MyD88 plays an important role in the regulation of skeletal muscle mass in diverse conditions. We recently reported that MyD88 promotes myoblast fusion in a cell-autonomous manner during post-natal muscle growth and overload-induced hypertrophy [154]. By contrast, activation of TLRs and MyD88 promotes inflammation, leading to a worsening of muscle pathology in animal models of muscular dystrophy [155]. However, the role and mechanisms by which MyD88 regulates skeletal muscle mass in cancer-induced cachexia remains to be investigated.

The endoplasmic reticulum (ER) is a major site for the synthesis and proper folding, and maturation of cellular proteins in the mammalian cells. The ER also plays a critical role in the regulation of calcium levels in the cell. Accumulation of misfolded/unfolded proteins or disruption in calcium levels leads to stress in the ER. This stress is resolved through the activation of a signaling network commonly referred to as the unfolded protein response (UPR). The UPR is initiated by three ER transmembrane sensors: RNA-dependent protein kinase-like ER eukaryotic translation initiation factor 2 alpha kinase (PERK), inositol-requiring protein 1 α (IRE1 α), and activating transcription factor 6 (ATF6) [5-7]. In conditions of ER stress, PERK undergoes oligomerization and

auto-phosphorylation leading to its activation. PERK phosphorylates eukaryotic translation initiation factor 2 (eIF2 α), which represses general translation while selectively augmenting the translation of ATF4 and gene expression of stress-responsive genes, such as C/EBP homologous protein (CHOP) and BiP [7-9]. Similar to PERK, IRE1 α is also activated through auto-phosphorylation. IRE1 α possesses endonuclease activity that facilitates the splicing of a 26-base intron from X-box-binding protein 1 (XBP1) mRNA [11]. Spliced XBP1 (sXBP1) acts as a potent transcription factor to induce the gene expression of several ER chaperones involved in protein folding or ER-associated protein degradation [12]. Chronic ER stress also stimulates IRE1 α kinase activity, leading to the activation of c-Jun N-terminal kinase (JNK) and nuclear factor-kappa B (NF- κ B) pathways [7]. Finally, in stress conditions, ATF6 translocates from the ER to the Golgi apparatus, where it is cleaved by site-1 proteases resulting in the formation of an active ATF6 transcription factor [13]. The active ATF6 fragment is subsequently imported into the nucleus, where it increases the gene expression of various proteins that function to alleviate ER stress [7-9, 11]. While the main function of the UPR is to improve homeostasis, unmitigated ER stress and chronic activation of components of the UPR can also produce deleterious effects, such as inflammation and apoptosis [7]. Interestingly, a few studies have suggested that the UPR pathways can be activated in the absence of ER stress [89, 156, 157].

Recent studies have suggested that the markers of ER stress are increased in skeletal muscle under physiological and various pathological conditions [89, 157]. In Chapter 2, we reported that levels of several markers of ER stress and activation of UPR pathways are significantly increased in the skeletal muscle of mice in response to

starvation and during cancer-associated cachexia [58, 158]. Intriguingly, this chapter also demonstrated that chronic administration of 4-phenylbutyrate (4-PBA), a molecular chaperon and inhibitor of ER stress, in wild-type mice leads to skeletal muscle weakness and atrophy. Moreover, treatment with 4-PBA aggravated muscle wasting in the Lewis lung carcinoma (LLC) model of cancer cachexia [158]. These results highlighted that physiological levels of ER stress and the UPR may be important for the maintenance of skeletal muscle health in both naïve conditions and in cancer-induced cachexia. It is also possible that individual arms of the UPR play distinct roles in the regulation of skeletal muscle mass in various catabolic states, including during tumor growth. However, the role of different arms of the UPR in the regulation of skeletal muscle mass has not yet been investigated. Moreover, the signaling mechanisms that regulate the activation of the UPR in skeletal muscle during cancer cachexia remain completely unknown.

In the present study, we demonstrate that the levels of several TLRs and MyD88 are increased in skeletal muscle of LLC tumor-bearing mice. The targeted ablation of MyD88 blocks LLC tumor-induced muscle wasting in mice. Our results demonstrate that TLRs/MyD88 mediate the activation of the UPR in skeletal muscle during cancer cachexia. Similar to MyD88, the muscle-specific deletion of XBP1 attenuates LLC tumor-induced loss of muscle mass both *in vivo* and *in vitro*. Finally, our results demonstrate that forced expression of sXBP1 is sufficient to cause atrophy and increases the gene expression of various proinflammatory cytokines, specific components of UPS, and autophagy in cultured myotubes.

3.2 Materials and methods.

Mice. Floxed MyD88 (MyD88^{fl/fl}; Jax strain: B6.129P2 (SJL)-MyD88^{tm1Defr/J}) were purchased from Jackson Laboratory. Floxed XBP1 (XBP1^{fl/fl}) mice as described [7] were kindly provided by Prof. Laurie Glimcher. Myoblast-specific MyD88-knockout (MyD88^{myoKO}) mice were generated by crossing MyD88^{fl/fl} mice with MyoD-Cre (Jax strain: FVB.Cg-MyoD^{tm2.1(icre)Gh/J}) mice. Skeletal muscle-specific XBP1-knockout (XBP1^{mKO}) were generated by crossing XBP1^{fl/fl} mice with MCK-Cre mice (Jax strain: B6.FVB(129S4)-Tg (Ckmm-cre)5Khn/J). All mice were in the C57BL/6J background and their genotype was determined by PCR from tail DNA. For cancer cachexia studies, LLC cells (2 X 10⁶ cells in 100 µl saline) were injected subcutaneously into the left flanks of 3-month old similar to as described [59, 159]. Control mice were injected with saline only. The mice were weighed daily and euthanized on day 21 after injection of LLC cells or if the animal reached a predetermined endpoint. All experimental protocols with mice were approved in advance by the Institutional Animal Care and Use Committee (IACUC) and Institutional Biosafety Committee (IBC) at the University of Louisville.

Grip strength test. We used a digital grip-strength meter (Columbus Instruments, Columbus, OH, USA) to measure forelimb or total 4-limb grip strength of mice by following a protocol as described [118]. Mice were acclimatized for 5 min before the grip-strength test began. The mouse was allowed to grab the metal pull bar with the forepaws and in a separate experiment with all 4 paws. The tail of the mouse was then gently pulled backward in the horizontal plane until it could no longer grasp the bar. The

force at the time of release was recorded as the peak tension. Each mouse was tested 10 times with a 20–40 s break between tests. The average peak tension from the 10 repetitions was normalized against total body weight and was defined as the average grip strength. The maximum peak tension from the 10 repetitions was normalized against total body weight and was defined as the maximum grip strength.

Histology and morphometric analysis. Individual TA and soleus muscles were isolated from mice, snap frozen in liquid nitrogen, and sectioned with a microtome cryostat. For the assessment of muscle morphology, 10 μm thick transverse sections of TA and soleus muscle were stained with hematoxylin and eosin (H&E) dye. Muscle sections were also processed for immunostaining for Laminin protein to mark the boundaries of myofibers. The sections were examined under an Eclipse TE 2000-U microscope (Nikon, Tokyo, Japan). Average myofiber cross-sectional area (CSA) and minimal Feret's diameter were analyzed in anti-Laminin-stained muscle sections using ImageJ software (NIH, Bethesda, MD). For each muscle, CSA was calculated by analyzing approximately 75 fibers per image (20x magnification). Five images were randomly taken for each mouse, allowing for 375 fibers measured per mouse.

Immunohistochemistry and fiber typing. For immunohistochemistry studies, frozen TA or soleus muscle sections were fixed in acetone, blocked in 2% bovine serum albumin in PBS for 1 h and incubated with rabbit anti-Laminin, in blocking solution at 4 °C overnight under humidified conditions. The sections were washed briefly with PBS before incubation with goat anti-rabbit Alexa Fluor 468 secondary antibody for 1 h at

room temperature and then washed three times for 15 min with PBS. To determine the composition of different types of fibers in the TA and soleus muscle of mice, transverse cross sections were made and blocked in 5% goat serum and 2% bovine serum albumin (BSA) for 30 min, followed by incubation for 1 h with monoclonal antibodies against type I, IIA, and IIB MyHC isoforms using clone BA-D5, SC-7, and BF-F3, respectively (Developmental Studies Hybridoma Bank, Iowa City, IA). Secondary antibody used was goat anti-mouse IgG2b conjugated with Alexa-350, goat anti-mouse IgG1 conjugate with Alexa-568, and goat anti-mouse IgM conjugated with Alexa-488. Finally, the fluorescence was captured with an Eclipse TE 2000-U microscope (Nikon), the images were merged, and the percentage of each type of fibers in whole muscle section was recorded. Average CSA of each fiber type was analyzed using ImageJ software (NIH). For each muscle, CSA was calculated for approximately 100 Type I and Type IIA fiber and 300 Type IIB fibers for each mouse.

Cell culture. C2C12, a myoblastic cell line, was purchased from American Type Culture Collection (ATCC). These cells were grown in growth medium (GM, DMEM containing 10% FBS). To induce differentiation, the cells were incubated in differentiation medium (DM, DMEM supplemented with 2% horse serum) for 96h. After appropriate treatments, myotubes cultures were visualized at room temperature on an Eclipse TE 2000-U microscope equipped with a Digital Sight DS-Fi1 camera (Nikon). Images were captured and the diameter of the myotubes was measured with ImageJ software (NIH). The myotube diameter was quantified as follows: 4 fields were chosen randomly within each well, and 4 wells were measured. The average diameter per myotube was calculated as

the mean of the 3 measurements taken along the length of the myotube. Myotubes were then collected, frozen, and stored at -80°C for further experiments.

Preparation of LLC-conditioned medium (LLC-CM). LLC cells were seeded in 100 mm cell culture plates in growth medium (DMEM containing 10% fetal bovine serum) at a density of 5000 cells/cm². Additional growth medium was added to each plate after 48h of plating. LLC cell cultures contain a heterogeneous mix of adherent and floating cells. After 4 days, floating cells were harvested by centrifugation at 800 RPM for 5 min. Pelleted cells and 10 ml differentiation medium were added back to the plate containing the adherent cells. After 24 hours, conditioned medium (CM) was harvested and cleared of cells and debris by centrifugation (800 RMP, 5 min). The CM was passed through 0.45 μm filters and aliquots were frozen in liquid nitrogen for later use. CM was diluted 1:4 with fresh differentiation medium (DM) for treatment of cultured myotubes and subsequent analysis of LLC CM-induced myotube atrophy.

Generation and use of adenoviral vectors. Adenoviral vectors expressing Xbp1 shRNA or XBP1 cDNA were generated following a protocol as described [27, 160]. The target siRNA sequence for mouse XBP1 mRNA were identified using BLOCK-iT RNAi Designer online software (Life Technologies). The shRNA oligonucleotides were synthesized to contain the sense strand of target sequences for mouse Xbp1 shRNA (GCCAAGCTGGAAGCCATTAAT), a short spacer (CTCGAG), and the reverse complement sequences followed by five thymidines as an RNA polymerase III transcriptional stop signal. Oligonucleotides were annealed and cloned into pLKO.1-Puro

plasmid with AgeI/EcoRI sites. The insertion of shRNA sequence in the plasmid was confirmed by DNA sequencing. Adenovirus carrying XBP1 shRNA was generated following the manufacturer protocol (AdEasy Adenoviral Vector System, Agilent). In brief, Xbp1 shRNA was PCR amplified from pLKO.1 plasmid and ligated into the pAdTrack-CMV vector digested at KpnI and XbaI sites. For the generation of adenovirus expressing sXBP1, Flag tagged sXBP1 cDNA was isolated from pCMV5-Flag-XBP1s plasmid (Addgene, Plasmid # 63680) and ligated at KpnI and HindIII sites in pAdTrack-CMV plasmid. The resulting pAdTrack-CMV-XBP1 shRNA or pAdTrack-CMV-sXBP1 plasmid was linearized with PmeI and co-transformed into E. coli BJ5183 cells with the pAdEasy-1 plasmid. Clones undergoing Adtrack-Adeasy recombination were selected with kanamycin and confirmed by digestion with restriction endonuclease. The recombinant plasmid was linearized with PacI and transfected into 293T cell line (ATCC) using Effectene Transfection Reagent (Qiagen) to package into active virus particles. Viruses were amplified by serial passage to concentrate viral titer. The titer was monitored under a microscope by visualizing the GFP marker co-expressed with XBP1 shRNA or sXBP1 cDNA in the Adtrack-Adeasy recombinants. Adenoviral vectors were transduced in cultured myotubes at multiplicity of infection (MOI) of 1:50.

Quantitative real-time PCR (QRT-PCR). RNA isolation and QRT-PCR were performed following a protocol as described [58, 59]. In brief, total RNA was extracted from skeletal muscles of mice or cultured C2C12 myotubes using TRIzol reagent (Thermo Fisher Scientific Life Sciences) and an RNeasy Mini Kit (Qiagen, Valencia, CA, USA). First-strand cDNA was made with a commercially available kit (Thermo

Fisher Scientific Life Sciences). The quantification of mRNA expression was performed using the SYBR Green dye (Thermo Fisher Scientific Life Sciences) method on a sequence detection system (Model 7300; Thermo Fisher Scientific Life Sciences). Primers were designed with Vector NTI software (Thermo Fisher Scientific Life Sciences). Primers sequences are available in Appendix 1. Data normalization was accomplished using the endogenous control β -actin and the normalized values were subjected to a $2^{-\Delta\Delta Ct}$ formula to calculate the fold change between the control and experimental groups.

Western blot. Relative levels of various proteins were determined by performing Western blot analysis. Skeletal muscle of mice or cultured C2C12 myotubes were washed with sterile PBS and homogenized in lysis buffer: 50 mM Tris-Cl (pH 8.0), 200 mM NaCl, 50 mM NaF, 1 mM dithiothreitol (DTT), 1 mM sodium orthovanadate, 0.3% IGEPAL, and protease inhibitors. Approximately 100 μ g protein was resolved in each lane on 10-12% SDS-polyacrylamide gels, electrotransferred onto nitrocellulose membranes, and probed with the following antibodies: anti-Troponin T (1:500; Sigma-Aldrich, St. Louis, MO, USA), anti-Tropomyosin (1:500; Sigma-Aldrich), anti-sXBP1 (1:1000; Cell Signaling Technology), anti-LC3B (1:500; Cell Signaling Technology), anti- α -Tubulin (1:1000; Cell Signaling Technology), and anti-GAPDH (1:2000; Cell Signaling Technology). Bound antibodies were detected by secondary antibodies conjugated to horseradish peroxidase (Cell Signaling Technology). Signal detection was performed by an enhanced chemiluminescence detection reagent (Bio-Rad). Approximate molecular masses were determined by comparison with the migration of prestained

protein standards (Bio-Rad). Quantitative estimation of the bands' intensity was performed using ImageJ software (National Institute of Health, Bethesda, MD).

Statistical analysis. Results are expressed as mean \pm standard deviation (SD). For statistical analyses, we used unpaired two-tailed Student's t-test. A value of $P < 0.05$ was considered statistically significant, unless otherwise specified.

3.3 Results

3.3.1 Levels of TLRs and MyD88 are increased in skeletal muscle of LLC tumor-bearing mice. We first investigated how the gene expression of various TLRs and MyD88 are regulated in skeletal muscle of mice in response to tumor growth. Adult C57BL/6J mice were inoculated with 2×10^6 LLC cells in the left flank. After 21 days, the mice were euthanized and the right hind limb muscles were isolated and analyzed by performing QRT-PCR analysis and Western blot. We found that transcript levels of TLR1, TLR2, TLR4, TLR7, and TLR8 were significantly increased and there was a trend towards an increase in TLR9 in the GA muscle of LLC tumor-bearing mice compared with corresponding control mice (**Figure 3.1A**). Moreover, both mRNA and protein levels of MyD88 were found to be significantly increased in the GA muscle of LLC tumor-bearing mice compared to control mice (**Figure 3.1B, C**).

To understand whether factors secreted by tumor cells induce the gene expression of TLRs and MyD88 in skeletal muscle, we investigated the effect of LLC-conditioned medium (LLC-CM) on the expression levels of TLRs and MyD88 in cultured myotubes. Cultured C2C12 myotubes were treated with LLC-CM in a 1:4 ratio for 24h followed by

performing QRT-PCR. Interestingly, treatment of C2C12 myotubes with LLC-CM significantly increased the mRNA levels of *TLR1*, *TLR4*, *TLR7*, and *TLR8* (**Figure 3.1D**). Moreover, there was a significant increase in the mRNA (**Figure 3.1E**) and protein (**Figure 3.1F**) levels of MyD88 in myotubes upon treatment with LLC-CM, suggesting that factors produced by tumor cells stimulate gene expression of various TLRs and MyD88 in skeletal muscle during cancer cachexia.

3.3.2 Targeted deletion of MyD88 inhibits LLC tumor-induced skeletal muscle

wasting in mice. MyD88 is a critical adaptor protein that mediates the activation of downstream signaling from all TLRs, except TLR3. In fact, the deletion of MyD88 has been a widely used approach to investigate the role of TLRs in both physiological and pathological conditions. To investigate the role of MyD88 in cancer cachexia, we used the Myod1-Cre line that deletes the target gene in both myoblasts and differentiated skeletal muscle. Specifically, floxed MyD88 (*MyD88^{ff}*) mice were crossed with the Myod1-Cre line to generate littermate muscle-specific MyD88-knockout (*MyD88^{myoKO}*) and control (*MyD88^{ff}*) mice as described [154]. To understand the role of MyD88 in cancer cachexia, 3-month old *MyD88^{ff}* and *MyD88^{myoKO}* mice were injected with 2×10^6 LLC cells or saline alone (as a control) subcutaneously in the left flank and growth of LLC tumor was monitored every day. At day 20 post-LLC injection, the mice were analyzed for grip strength measurements. There was a significant decrease in forelimb and total four paw grip strength in LLC tumor-bearing *MyD88^{ff}* mice compared to corresponding mice injected with saline alone (**Figure 3.2A-D**). Interestingly, we found that *MyD88^{myoKO}* mice were protected from LLC tumor-induced reductions in grip

strength. Specifically, forelimb and total four paw grip strength was significantly higher in LLC tumor-bearing MyD88^{myoKO} mice compared with corresponding MyD88^{f/f} mice (**Figure 3.2A-D**).

We next investigated whether the genetic ablation of MyD88 has any effect on the myofiber size in LLC-tumor bearing mice. We generated transverse sections of TA and soleus muscles and performed H&E staining or immunostaining for the Laminin protein. There was no overt difference in skeletal muscle structure in control and LLC tumor-bearing MyD88^{f/f} and MyD88^{myoKO} mice (**Figure 3.2E**). Morphometric analysis of Laminin-stained sections revealed a significant improvement in average cross-sectional area (CSA), as well as minimal Feret's diameter in both TA and soleus muscle of LLC tumor-bearing MyD88^{myoKO} mice compared with corresponding MyD88^{f/f} mice (**Figure 3.2F-I**). This analysis also showed that there was a significant reduction in the LLC tumor-induced percentage loss in myofiber CSA in MyD88^{myoKO} mice compared with MyD88^{f/f} mice (**Figure 3.2H**). However, average tumor size was comparable between MyD88^{f/f} and MyD88^{myoKO} mice at day 21 after implantation of LLC cells (**Figure 3.2I**), suggesting that the targeted deletion of MyD88 inhibits LLC-induced muscle wasting without having any effect on tumor growth in mice.

3.3.3 Inhibition of MyD88 inhibits slow-to-fast fiber type transition in skeletal muscle during cachexia. In addition to the loss of myofiber diameter, skeletal muscle wasting is also associated with a slow-to-fast fiber type transition [159, 161]. We next investigated whether the genetic deletion of MyD88 affects the composition of slow- and fast-type fibers in skeletal muscle. Transverse sections generated from TA and soleus

muscles of MyD88^{ff} and MyD88^{myoKO} mice were processed for triple immunostaining using antibodies against Myosin Heavy Chain (MyHC) types I, IIA, and IIB. Unstained myofibers were considered as type IIX or a myofiber in transition from one type to another (**Figure 3.3A, B**). Consistent with published results [159], growth of LLC cell tumors resulted in a loss of oxidative fibers (Type I and IIA) in both the TA and soleus muscle of MyD88^{ff} mice. Interestingly, there was a significant increase in the proportion of type IIA myofibers in the TA muscle and type I and IIA myofibers in soleus muscle of LLC tumor-bearing MyD88^{myoKO} mice compared with corresponding MyD88^{ff} mice (**Figure 3.3C, D**). To understand whether the rescue in the loss of myofiber size in MyD88^{myoKO} mice upon inoculation of LLC cells is due to changes in the composition of fibers or the amelioration in myofiber atrophy, we quantified the average CSA of each myofiber type. Consistent with our previous study [159], there was a significant reduction in average CSA of each fiber type in LLC tumor-bearing MyD88^{ff} mice (**Figure 3.3E, F**). However, myofiber CSA of all fiber types was significantly higher in MyD88^{myoKO} mice compared with MyD88^{ff} mice inoculated with LLC cells (**Figure 3.3E, F**). Collectively, these results suggest that the specific inhibition of MyD88 preserves oxidative myofibers in skeletal muscle during cancer-induced cachexia.

3.3.4 MyD88 mediates the activation of catabolic pathways in skeletal muscle of LLC tumor-bearing mice. Skeletal muscle wasting in many catabolic conditions, including cancer growth, involves the degradation of muscle specific proteins [59, 122, 159]. To investigate the biochemical mechanisms by which MyD88 mediates muscle wasting, we first measured levels MyHC, Tropomyosin, and Troponin in skeletal muscle

of control and LLC tumor-bearing mice. There was a significant reduction in the levels of all three proteins in GA muscle of MyD88^{ff} mice compared with corresponding non-tumor control mice. Our analysis also showed that levels of MyHC and Troponin, but not Tropomyosin, were significantly higher in LLC-bearing MyD88^{myoKO} mice compared with corresponding MyD88^{ff} mice (**Figure 3.4A, B**).

Skeletal muscle wasting in multiple conditions is a result of accelerated protein degradation. The ubiquitin-proteasome system (UPS) and autophagy are two major proteolytic systems that cause the degradation of the bulk of muscle proteins in various catabolic states [40, 103, 162]. Indeed, gene expression of various components of the UPS and autophagy is increased in skeletal muscle in response to a number of catabolic stimuli, including cancer. We next measured relative mRNA levels of select markers of UPS and autophagy in GA muscle of MyD88^{ff} and MyD88^{myoKO} mice. Consistent with published mRNA levels of muscle-specific E3 ubiquitin ligase, MAFBx and MuRF1, were found to be significantly increased in skeletal muscle of LLC tumor-bearing MyD88^{ff} mice compared with control mice (**Figure 3.4C**). Importantly, mRNA levels of MAFBx were significantly reduced and a trend towards a decrease in MuRF1 was noticeable in GA muscle of MyD88^{myoKO} mice compared with MyD88^{ff} mice (**Figure 3.4C**). Similar to the UPS, there was also significant increase in transcript levels of autophagy markers LC3B and Beclin-1 in skeletal muscle of LLC-bearing MyD88^{ff} mice. However, transcript levels of both LC3B and Beclin-1 were found to be significantly reduced in skeletal muscle of MyD88^{myoKO} mice compared with MyD88^{ff} mice in response to tumor growth (**Figure 3.4D**). Furthermore, ratio of LC3BII/I was also significantly reduced in the GA muscle of LLC-bearing MyD88^{myoKO} mice compared

with corresponding MyD88^{ff} mice, further suggesting that the genetic ablation of MyD88 inhibits the activation of autophagy in skeletal muscle during cancer cachexia (**Figure 3.4E**).

Activation of the UPS and autophagy in skeletal muscle involves the upstream activation of specific signaling pathways [40]. Because MyD88 is a major adaptor protein involved in the activation of various signaling pathways, we next investigated whether MyD88 functions through the activation of specific signaling proteins in skeletal muscle of tumor-bearing mice. We first investigated whether MyD88 plays a role in the activation of nuclear factor kappa-B (NF- κ B) in skeletal muscle of LLC tumor-bearing mice. Interestingly, the phosphorylation of NF- κ B subunit, p65 (also called RelA), was significantly inhibited in LLC tumor-bearing MyD88^{myoKO} mice compared with corresponding MyD88^{ff} mice (**Figure 3.4F, G**). Inhibitor of κ B (I κ B α) protein masks the nuclear localization signals of NF- κ B proteins and keep them sequestered in an inactive state in the cytoplasm [43]. Levels of I κ B α protein are reduced due to its proteolysis in response to NF- κ B activating stimulus. Our results showed that levels of I κ B α proteins were significantly higher in the GA muscle of LLC tumor-bearing MyD88^{myoKO} mice compared with MyD88^{ff} mice (**Figure 3.4F, G**). We next investigated whether MyD88 regulates the activation of p38MAPK signaling in skeletal muscle of mice in response to tumor growth. While the phosphorylation of p38MAPK was significantly increased in skeletal muscle of MyD88^{ff} mice in response to tumor growth, there was no significant difference in the levels of phosphorylated p38 MAPK between MyD88^{ff} and MyD88^{myoKO} mice (**Figure 3.4F, G**). Altogether, these results suggest that the deletion of

MyD88 attenuates the activation of the proteolytic systems and catabolic signaling pathways in skeletal muscle of LLC tumor-bearing mice.

3.3.5 MyD88 mediates the activation of UPR in skeletal muscle during cancer

cachexia. The UPR pathways are employed by cells as a corrective measure to avoid an increase in the unfolded-protein load. It is generally believed that the PERK and IRE1 arms of the UPR are involved in mediating deleterious effects, whereas the ATF6 arm mediates adaptive responses [1]. We investigated whether MyD88 has any role in the activation of the UPR pathways in skeletal muscle of tumor bearing mice. Consistent with our previously published report [159], the markers of the PERK and IRE1/XBP1 arms of the UPR were found to be significantly increased in skeletal muscle of LLC tumor-bearing MyD88^{f/f} mice. Interestingly, LLC tumor-induced increases in the levels of p-eIF2 α , tXBP1, and sXBP1 were significantly inhibited in skeletal muscle of MyD88^{myoKO} mice compared with MyD88^{f/f} mice (**Figure 3.5A, B**). We also compared mRNA levels of various markers of ER stress in skeletal muscle of MyD88^{f/f} and MyD88^{myoKO} mice. This analysis showed that LLC tumor-induced increases in relative mRNA levels ATF4, CHOP, GRP78, and sXBP1 were significantly diminished in skeletal muscle of MyD88^{myoKO} mice compared with MyD88^{f/f} mice (**Figure 3.5C**).

A recent study demonstrated that tumor cells secrete heat shock protein (Hsp) 70 and Hsp90, which causes muscle wasting through binding to TLRs in mouse models of cancer cachexia [148]. We investigated whether recombinant Hsp70 can activate the PERK and IRE1/XBP1 arms of the UPR in cultured myotubes. Results showed that treatment with Hsp70 significantly increased the levels of p-eIF2 α and sXBP1 in cultured

C2C12 myotubes (**Figure 3.5D, E**). Furthermore, QRT-PCR analysis showed that mRNA levels of several ER stress markers CHOP, GADD34, and sXBP1 were significantly increased in C2C12 myotubes upon treatment with Hsp70 (**Figure 3.5F**). Collectively, these results suggest that tumor-derived factors activate the UPR through MyD88-dependent mechanisms in skeletal muscle.

3.3.6 Targeted ablation of XBP1 inhibits skeletal muscle wasting in LLC tumor-bearing mice. While both the PERK and IRE1/XBP1 arms of the UPR are activated during cancer cachexia, we found that targeted inhibition of PERK does not attenuate skeletal muscle wasting in response to the LLC tumor (**our unpublished results**). We then investigated whether inhibition of XBP1, the major effector of the IRE1 arm of the UPR, can attenuate skeletal muscle wasting in LLC model of cancer cachexia. Since XBP1 is also required for myogenic differentiation, we generated mice in which XBP1 was deleted only in differentiated skeletal muscle. Specifically, floxed XBP1 (XBP1^{f/f}) mice were crossed with the muscle creatine kinase (MCK)-Cre line to generate muscle-specific XBP1-knockout (henceforth XBP1^{mKO}) mice and littermate XBP1^{f/f} mice. Our QRT-PCR analysis confirmed that mRNA levels of XBP1 and its downstream targets, EDEM and SEC61, were significantly reduced in skeletal muscle of XBP1^{mKO} mice compared to littermate XBP1^{f/f} mice (**Figure 3.6A**).

To understand the role of XBP1 in muscle wasting in cancer cachexia, 3-month old XBP1^{f/f} and XBP1^{mKO} mice were implanted with 2×10^6 LLC cells. After 21 days, hind limb muscle of the mice were isolated and analyzed by morphometric and biochemical assays. We first generated transverse sections of TA and soleus and

performed H&E staining or anti-Laminin staining (**Figure 3.6B**). Intriguingly, our analysis showed that the average CSA and minimal Feret's diameter were somewhat reduced in skeletal muscle of XBP1^{mKO} mice compared with littermate XBP1^{f/f} mice in naïve conditions, suggesting that XBP1 may have a role in skeletal muscle growth (**Figure 3.6C, D**). However, we found that XBP1^{mKO} mice were protected from LLC cell-induced muscle wasting. The average CSA and minimal Feret's diameter of myofiber were significantly higher in TA and soleus muscle of LLC tumor-bearing XBP1^{mKO} mice compared to corresponding XBP1^{f/f} mice (**Figure 3.6B-E**). Our analysis also showed that the deletion of XBP1 in skeletal muscle had no effect on growth of LLC tumors in mice (**Figure 3.6F**). We next compared mRNA levels of components of UPS and autophagy in skeletal muscle of XBP1^{f/f} and XBP1^{mKO} mice. Results showed that the tumor-induced increases in the mRNA levels of MuRF1, MAFBx, LC3B, and Beclin-1 were significantly inhibited in GA muscle of XBP1^{mKO} mice compared with XBP1^{f/f} mice (**Figure 3.6G, H**).

Inflammatory cytokines are some of the important mediators of skeletal muscle wasting in various catabolic states, including cancer. Interestingly, sXBP1 binds to the promoter region of both TNF- α and IL-6 to enhance their gene expression in macrophages [156]. Thus, we next investigated whether the inhibition of XBP1 has any effect on the gene expression of inflammatory cytokines in skeletal muscle of LLC tumor-bearing mice. Results showed that the LLC tumor-induced increase in mRNA levels of IL-6, TWEAK, TNF- α and TNF receptor I (TNFRI) were significantly inhibited in XBP1^{mKO} mice compared to corresponding XBP1^{f/f} mice (**Figure 3.6I**). Collectively, these results suggest that the inhibition of XBP1 inhibits LLC tumor-induced muscle

wasting, potentially through the inhibition of the activity of proteolytic pathways and repressing levels of inflammatory cytokines.

3.3.7 Activation of XBP1 induces atrophy in cultured myotubes. While our results demonstrate that the inhibition of XBP1 can prevent skeletal muscle wasting in response to LLC, it remains unknown whether the activation of XBP1 is sufficient to cause skeletal muscle wasting. To address this issue, we generated an adenoviral vector expressing spliced XBP1 (sXBP1) cDNA. C2C12 myotubes were transduced with a control or sXBP1-expressing adenoviral vector. After 48h, the myotubes cultures were fixed and stained with DAPI (**Figure 3.7A**). Interestingly, we found that the overexpression of sXBP1 led to a significant decrease in the diameter of myotubes (**Figure 3.7B**). In a parallel experiment, we also measured mRNA levels of markers of the UPS and autophagy in control and sXBP1-overexpressing myotubes. Our analysis showed that mRNA levels of MAFBx, MuRF1, LC3B, and Beclin-1 were significantly increased in myotubes cultures transduced with sXBP1-expressing adenoviral vector (**Figure 3.7C, D**). Moreover, mRNA levels of IL-6, TNF- α , and TWEAK were also significantly increased sXBP1-overexpressing cultures compared to controls (**Figure 3.7E**). We also measured whether overexpression of sXBP1 affects the activation of NF- κ B and p38 MAPK. Results showed that levels of phosphorylated p65 and p38 MAPK were significantly increased in sXBP1-expressing cultures compared with control cultures (**Figure 3.7F, G**). Our Western blot analysis also showed that protein levels of sXBP1 were increased in cultures transduced with sXBP1-expressing adenoviral vector (**Figure 3.7F, G**).

We have recently shown that treatment of cultured myotubes with LLC-CM leads to the splicing of XBP1 [159]. We next sought to determine whether the inhibition of XBP1 can attenuate myotube atrophy in response to LLC-CM. We first generated adenoviral constructs expressing either a scrambled (control) shRNA or XBP1 shRNA. C2C12 myotubes were transduced with control or XBP1 shRNA-expressing adenoviral vector. After 24h, the myotubes were treated with LLC-CM for an additional 48h. As expected, the treatment of myotubes with LLC-CM caused a significant reduction in average myotube diameter (**Figure 3.7H**). Interestingly, shRNA-mediated knockdown of XBP1 prevented the loss of myotube diameter after treatment with LLC-CM (Figure 7I). Our QRT-PCR analysis confirmed a drastic reduction in mRNA levels of XBP1 in myotube cultures transduced with Ad.shXBP1 (**Figure 3.7J**). Altogether, these results indicate that *in vitro* overexpression of XBP1 promotes myotubes atrophy, whereas, knockdown of XBP1 can prevent LLC-CM induced myotube wasting.

3.4 Discussion.

Cancer cachexia is a complex syndrome that involves a severe loss of skeletal muscle mass [144]. Tumor cells secrete a number of factors, which have significant impacts on muscle proteolysis and function [100, 144]. The tumor itself or tumor-derived factors can also stimulate the production of certain molecules, such as proinflammatory cytokines, from non-tumor cells leading to systematic inflammation and metabolic dysfunction in various organs, including skeletal muscle [100, 138, 163]. TLRs, which mediate downstream signaling through the recruitment of MyD88 protein, are important regulators of the inflammatory response in many pathological conditions. A number of

molecules can bind to specific TLRs to initiate the inflammatory response [151-153]. Recently, it was reported that several types of cancer cells, which cause cachexia, constitutively secrete Hsp70 and Hsp90 proteins into the circulation. These proteins are packed in extracellular vesicles and delivered to skeletal muscle, where they bind to TLR4 to activate catabolic signaling pathways and production of inflammatory cytokines [148]. A recent study has also shown that skeletal muscle wasting is partially rescued in whole body TLR4-KO mice in response to growth of LLC tumor [149]. However, how the gene expression of other TLRs as well as MyD88 is regulated and their potential role and mechanisms of action in cancer-associated skeletal muscle wasting remained largely unknown.

Our study demonstrates that the gene expression of several TLRs and MyD88 is considerably increased in skeletal muscle of mice after inoculation with LLC cells. Since conditioned media from LLC cells was also able to induce the expression of TLRs and MyD88 in cultured myotubes (**Figure 3.1**), it is likely that factors of tumor origin induce the expression of TLRs in skeletal muscle during cancer cachexia. More importantly, our results showed that the inhibition of TLR-mediated signaling through the genetic ablation of MyD88 blunts the LLC tumor-induced loss of skeletal muscle strength and myofiber CSA in adult mice (**Figure 3.2**). Further, our results suggest that the inhibition of TLR/MyD88 signaling may prevent muscle wasting through inhibition of the UPS and autophagy. It has been consistently observed that gene expression of a number of components of the UPS and autophagy is increased through upstream activation of NF- κ B and MAPK signaling pathways [33, 43]. Consistent with reduced expression of markers of the UPS and autophagy, we found that the genetic ablation of MyD88 reduced

the activation of NF- κ B and p38MAPK in skeletal muscle of LLC tumor-bearing mice (**Figure 3.5F, G**). Braun et al. have previously reported that whole body, but not skeletal muscle-specific, deletion of MyD88 inhibits skeletal muscle atrophy after stimulation with Lipopolysaccharide (LPS), an agonist of TLR4 [164]. In contrast, our study demonstrates that muscle-specific inhibition of MyD88 effectively inhibits muscle wasting in LLC cell-associated cachexia. While the exact reasons remained unknown, it is possible that LPS and tumor-derived factors induce muscle wasting through recruitment of distinct TLR receptors. Indeed, our results demonstrate that multiple TLRs become activated in the LLC model of cachexia, not just TLR4 (**Figure 3.1**). TLR7 has been previously reported to mediate the loss of muscle mass during cancer cachexia [165]. Interestingly, our results demonstrate that the expression of TLR7 is significantly increased in skeletal muscle in LLC model of cancer cachexia (**Figure 3.1**). Another reason could be the mouse models used in the two studies. Braun et al used mice in which MyD88 was deleted only in differentiated myofibers [164], whereas in the present study, we used Myod1-Cre line which leads to the ablation of MyD88 in myoblasts as well as differentiated myofibers (15).

Accumulating evidence suggests that ER stress and the UPR pathways are activated in skeletal muscle under diverse conditions [89, 157]. We previously reported that the markers of ER stress are activated in skeletal muscle of two models of cancer cachexia: LLC and APC^{Min/+} mice. We have also demonstrated that the conditioned medium of LLC cells was able to induce the activation of the UPR pathways [158]. Our results in the present investigation suggest that Hsp70, which is produced by tumor cells in mouse models of cancer cachexia [148], can also induce the UPR pathways in cultured

myotubes (**Figure 3.5D-F**) suggesting that the factors of tumor origin, including Hsp70, are responsible, at least in part, for the activation of the UPR pathways in skeletal muscle *in vivo*. Intriguingly, a previous study has demonstrated that TLRs recruit IRE1 α to stimulate the splicing and activation of XBP1 in macrophages to boost the innate immune response [156]. Moreover, the TLR-mediated activation of IRE1/XBP1 occurs in the absence of ER stress and does not lead to the induction of gene expression of ER chaperones. Instead, the activation of XBP1 leads to the induction of proinflammatory cytokines, including IL-6 and TNF α in macrophages [156]. Our results suggest that TLR/MyD88 axis not only mediates the activation of IRE1/XBP1 but it also stimulates the activation of the PERK arm of the UPR in skeletal muscle in LLC-tumor bearing mice. (**Figure 3.5**). However, the exact molecular interactions through which the TLRs/MyD88 axis leads to the activation of the UPR in skeletal muscle remain to be investigated.

The role of ER stress and individual arms of the UPR in the regulation of skeletal muscle mass has just begun to be investigated. We have recently reported that the pan-inhibition of ER stress produces deleterious effects on muscle mass and function during LLC-induced cancer cachexia both *in vivo* and *in vitro* [158]. A previous study has demonstrated that the deletion of CHOP, which is induced by PERK/eIF2 α pathway in conditions of ER stress, accelerates denervation-induced skeletal muscle wasting potentially due to the increased activation of autophagy [49]. Recently, it was reported that that inducible activation of PERK leads to the loss of skeletal muscle mass in adult mice [46, 166]. Interestingly, a constitutively-active mutant form of PERK also augments gene expression of several enzymes involved in amino acid metabolism and stimulates

the gene expression and secretion of Fibroblast Growth Factor 21 (FGF21), an anti-obesity myokine that promotes energy expenditure in brown adipose tissue [46]. These findings suggest that while overexpression of PERK causes muscle atrophy, it also improves metabolic adaptation of whole body. Published reports also suggest that ATF4, a transcription factor that is also induced through the activation of PERK/eIF2 α , mediates muscle atrophy during starvation, immobilization, and aging [123, 167, 168]. While the PERK/eIF2 α axis is activated in skeletal muscle in models of cancer cachexia, our results showed that the genetic ablation of PERK does not have any significant effect on LLC tumor-induced muscle wasting in adult mice (**our unpublished results**). These findings suggest that different components of the UPR may have different roles in the regulation of skeletal muscle mass in catabolic conditions.

Activation of the IRE1/XBP1 pathway causes insulin resistance through the activation of JNK in mice fed with a high fat diet [89, 157]. However, the muscle-specific role of this pathway had not been investigated before. Our results demonstrate that XBP1 may have a role in skeletal muscle growth, evidenced by a slightly reduced myofiber size in XBP1^{mKO} mice compared to littermate control mice, in naïve conditions (**Figure 3.6B-D**). Interestingly, we found that the myofiber-specific ablation of XBP1 considerably inhibited the LLC tumor-induced skeletal muscle wasting in mice (**Figure 3.6B-F**). Similarly, we found that the shRNA-mediated knockdown of XBP1 inhibits atrophy in cultured myotubes in response to LLC-CM (**Figure 3.7H, I**). By contrast, the forced expression of sXBP1 causes atrophy in cultured myotubes, suggesting that increased activation of XBP1 is sufficient to induce muscle wasting (**Figure 3.7A, B**). Our results also demonstrate that similar to innate immunity, XBP1 induces the gene expression of

proinflammatory cytokines IL-6, TNF- α , and TWEAK in skeletal muscle, which may be an important mechanism for skeletal muscle atrophy. Indeed, IL-6 is one of the important mediators of muscle wasting in cancer-associated cachexia [119, 169-171]. Increased expression of proinflammatory cytokines can further stimulate muscle wasting through activation of catabolic signaling pathways and proteolytic systems [33, 43, 44, 100]. Consistently, we found that the forced activation of sXBP1 increases the activation of NF- κ B and p38 MAPK in cultured myotubes (**Figure 3.7F, G**). We also found that XBP1 regulates the gene expression of several important components of UPS and autophagy. Being a transcription factor, it is possible that sXBP1 directly binds to the promoter region of these genes to induce their expression. Alternatively, the increased expression of these molecules could be a result of the activation of other catabolic pathways, including NF- κ B and p38 MAPK. While our results demonstrate that ablation of XBP1 inhibits markers of autophagy in the skeletal muscle LLC model of cancer cachexia, a published report suggested that the genetic deletion of XBP1 ameliorates pathology of SOD1 mutant mice, a model of Amyotrophic lateral sclerosis. Interestingly, it was found that XBP1 deletion results in the increased activation of autophagy, which hastens the clearance of mutant SOD1 aggregates [51]. Taken together, these findings further emphasize that depending on the catabolic stimuli or pathological condition, inhibition of a specific arm of the UPR can have distinct downstream events. Further investigations are needed to precisely define the role of each arm of the UPR in skeletal muscle wasting during cancer cachexia.

In summary, our present study identifies the TLR-MyD88-XBP1 axis as a mediator of skeletal muscle wasting in a mouse model of cancer cachexia. However, it

remains to be determined whether this pathway promotes muscle wasting in other conditions as well. Targeting components of this pathway may be an important approach to inhibit muscle wasting in catabolic states, including cancer.

FIGURE 3.1

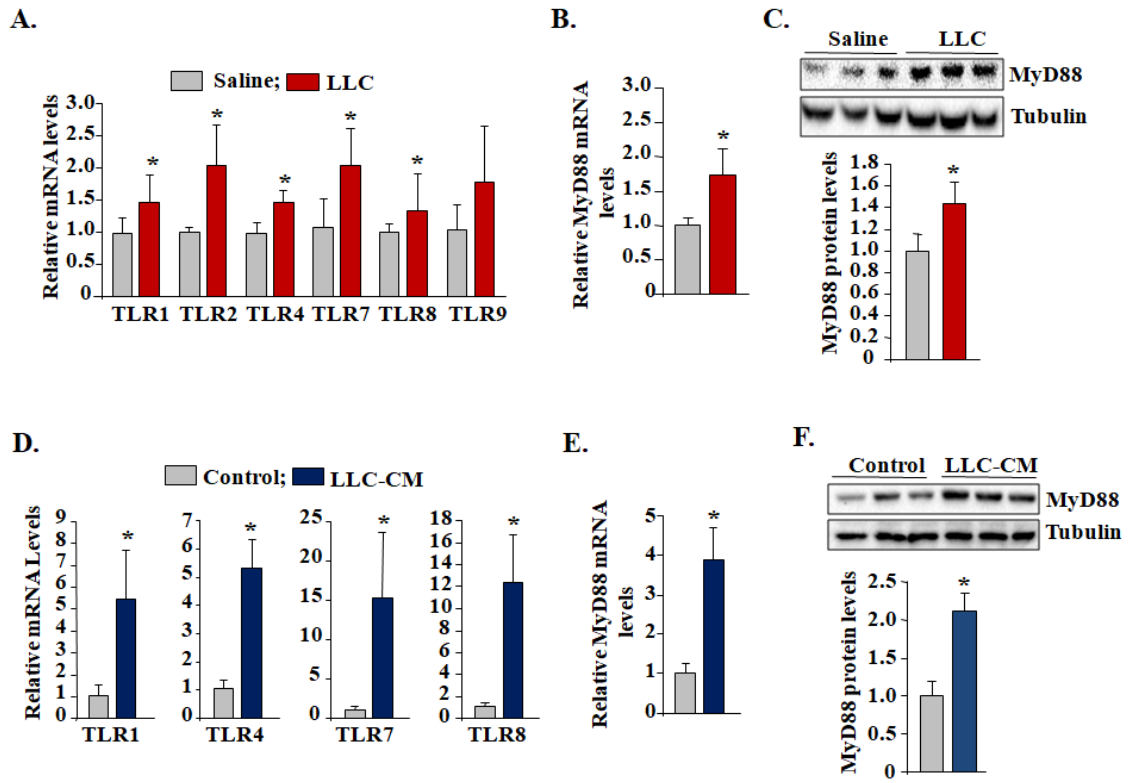


FIGURE 3.1: Increased gene expression of TLRs and MyD88 during cancer

cachexia. 3-month old C57BL6J mice were injected with saline alone or 2×10^6 Lewis lung carcinoma (LLC) cells in the left flank and tumor growth was monitored. After 21 days, right side hind limb muscle were isolated and analysed by QRT-PCR and Western blot. Relative mRNA of **(A)** TLR1, TLR2, TLR4, TLR7, TLR8, and **(B)** MyD88 in gastrocnemius (GA) muscle of control and LLC tumor-bearing mice. **(C)** Immunoblots demonstrating levels of MyD88 and an unrelated protein Tubulin in skeletal muscle of control and LLC tumor-bearing mice. Bar diagram represents densitometry quantification of bands in immunoblot. C2C12 myotubes were incubated in differentiation medium with or without LLC-condition medium (LLC-CM) for 24h followed by performing QRT-PCR and Western blot. Transcript levels of **(D)** TLR1, TLR4, TLR7, and TLR8 and **(E)** MyD88 in control and LLC-CM treated myotubes. **(F)** Representative immunoblots and densitometry analysis of MyD88 protein in control and LLC-CM treated myotubes. N= 3/group. Error bars represent SD. * $p < 0.05$, values significantly different from corresponding controls.

FIGURE 3.2

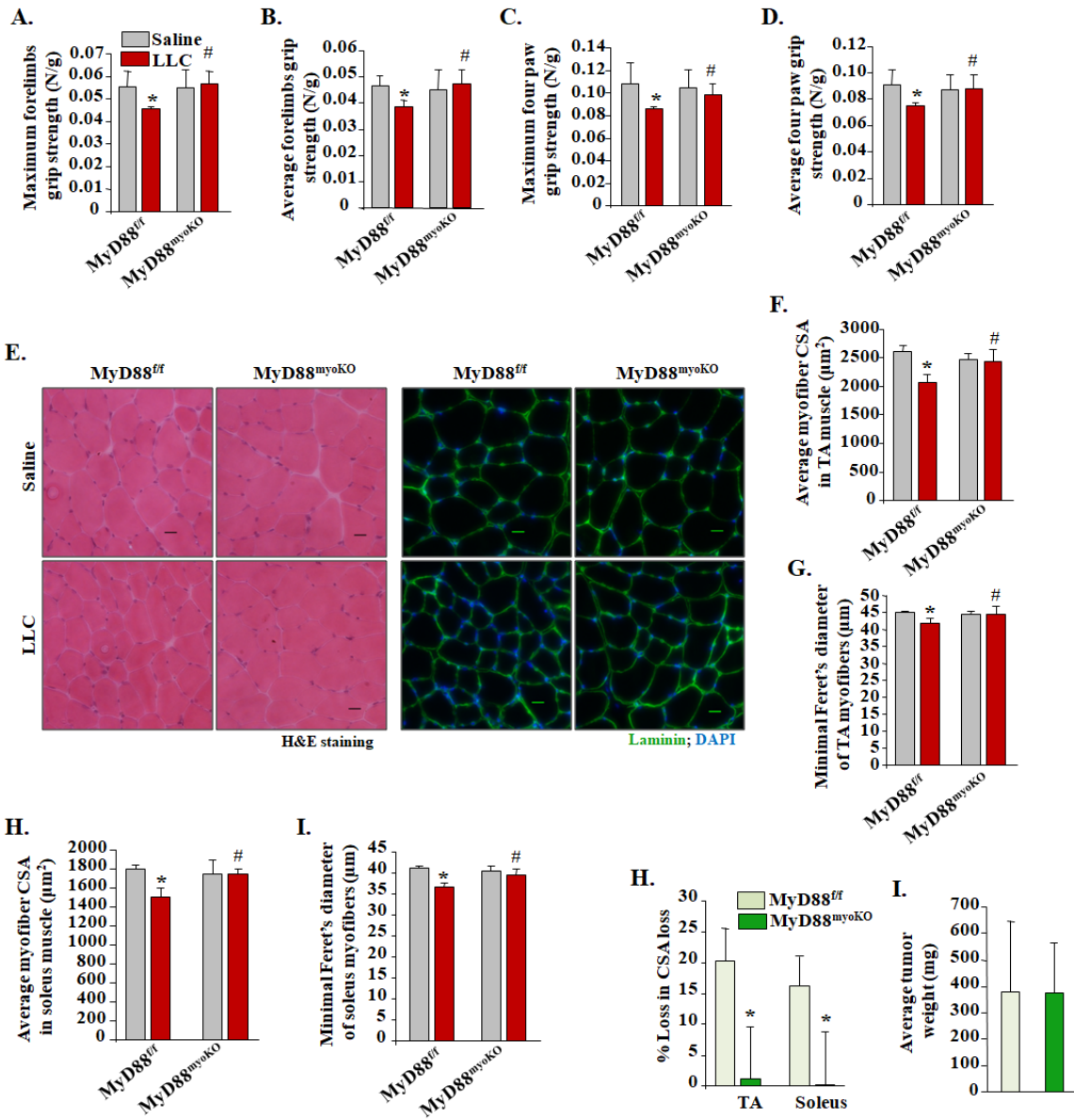


FIGURE 3.2: Targeted deletion of MyD88 prevents skeletal muscle atrophy in tumor-bearing mice. 3-month old MyD88^{ff} and MyD88^{myoKO} mice were inoculated with 2×10^6 LLC cells in the left flank and monitored for 20 days. Quantification of the (A) maximum, and (B) average forelimb strength of control and LLC-tumor bearing MyD88^{ff} and MyD88^{myoKO} mice normalized by body weight. Quantification of the (C) maximum and (D) average four-paw strength of control and tumor bearing MyD88^{ff} and MyD88^{myoKO} mice normalized by body weight. (E) Representative photomicrographs of H&E- and anti-Laminin-stained sections of the TA muscle of control and LLC tumor-bearing MyD88^{ff} and MyD88^{myoKO} mice. Scale 50 μ m. Quantification of average (F) cross-sectional area (CSA) and (G) minimal Feret's diameter of myofibers in TA muscle of control and tumor-bearing MyD88^{ff} and MyD88^{myoKO} mice. Quantification of average (H) CSA and (I) minimal Feret's diameter of myofibers in soleus muscle of control and tumor-bearing MyD88^{ff} and MyD88^{myoKO} mice. (H) Quantification of percentage loss in myofiber CSA after implantation of LLC tumor in TA and soleus muscle of MyD88^{ff} and MyD88^{myoKO} mice. (I) Average tumor wet weight in MyD88^{ff} and MyD88^{myoKO} mice after 21 days of injection of LLC cells. Error bars represent SD. N= 4-7/group. *p<0.05, values significantly different from MyD88^{ff} mice. #p<0.05, values significantly different from LLC tumor-bearing MyD88^{ff} mice.

FIGURE 3.3

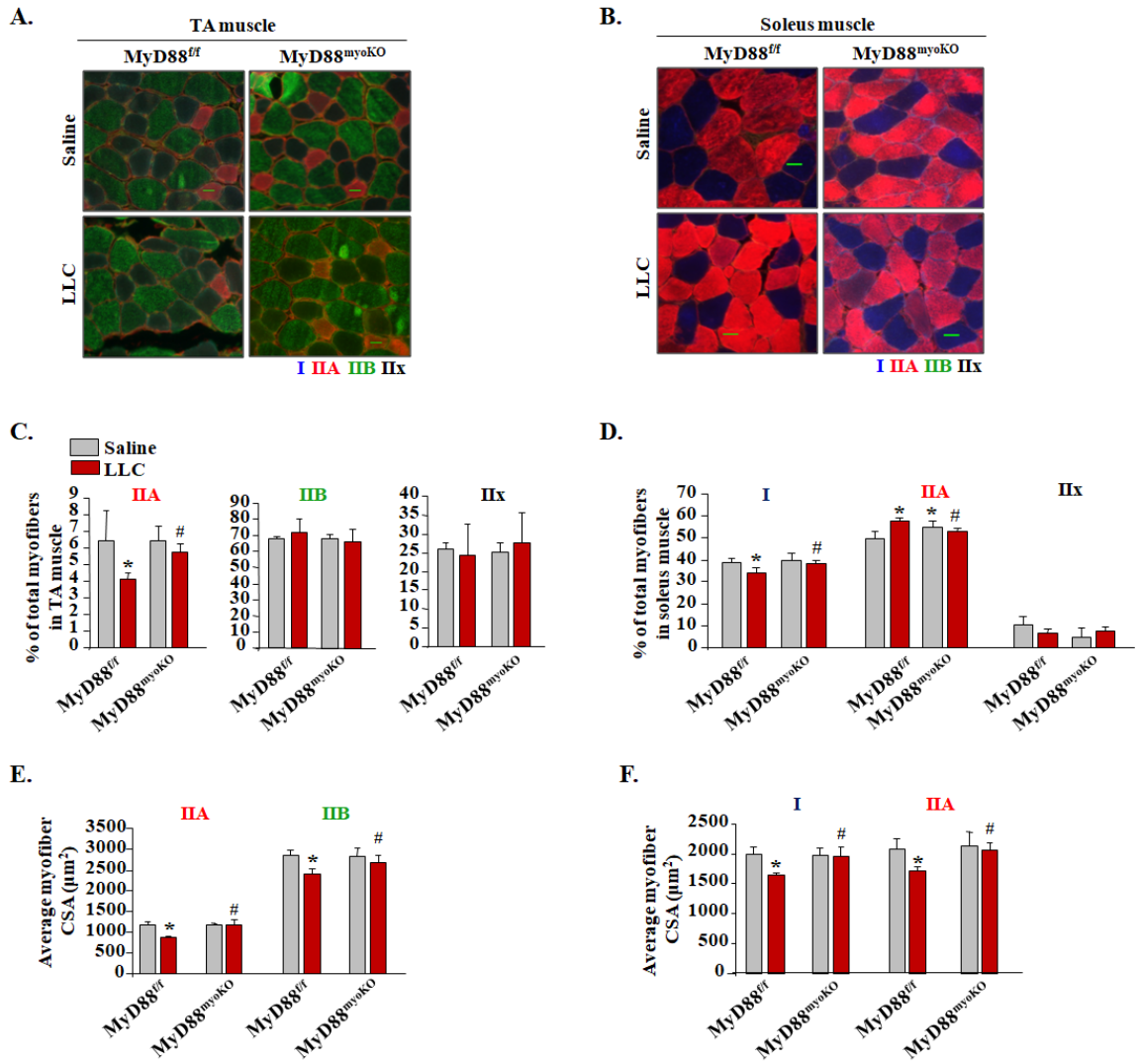


FIGURE 3.3: Ablation of MyD88 inhibits slow-to-fast fiber type transition in skeletal muscle during cachexia. TA and soleus muscle sections prepared from control and tumor-bearing MyD88^{ff} and MyD88^{myoKO} mice were subjected to triple immunostaining against MyHC I, IIA, and IIB antibodies. Representative photomicrographs of triple-stained sections of **(A)** TA, and **(B)** soleus muscle of control and LLC tumor-bearing MyD88^{ff} and MyD88^{myoKO} mice. Scale bar: 50 μ m. Quantification of percentage of **(C)** Type IIA, IIB, and IIX fibers in TA muscle and **(D)** Type I, IIA, and IIX in soleus muscle of control and LLC tumor-bearing MyD88^{ff} and MyD88^{myoKO} mice. Quantification of the average CSA of **(E)** Type IIA and IIB fibers in the TA muscle and **(F)** Type I and IIA in the soleus muscle in control and tumor-bearing MyD88^{ff} and MyD88^{myoKO} mice. N= 4/group. Error bars represent SD. *p<0.05, values significantly different from MyD88^{ff} mice. #p<0.05, values significantly different from LLC tumor-bearing MyD88^{ff} mice.

FIGURE 3.4

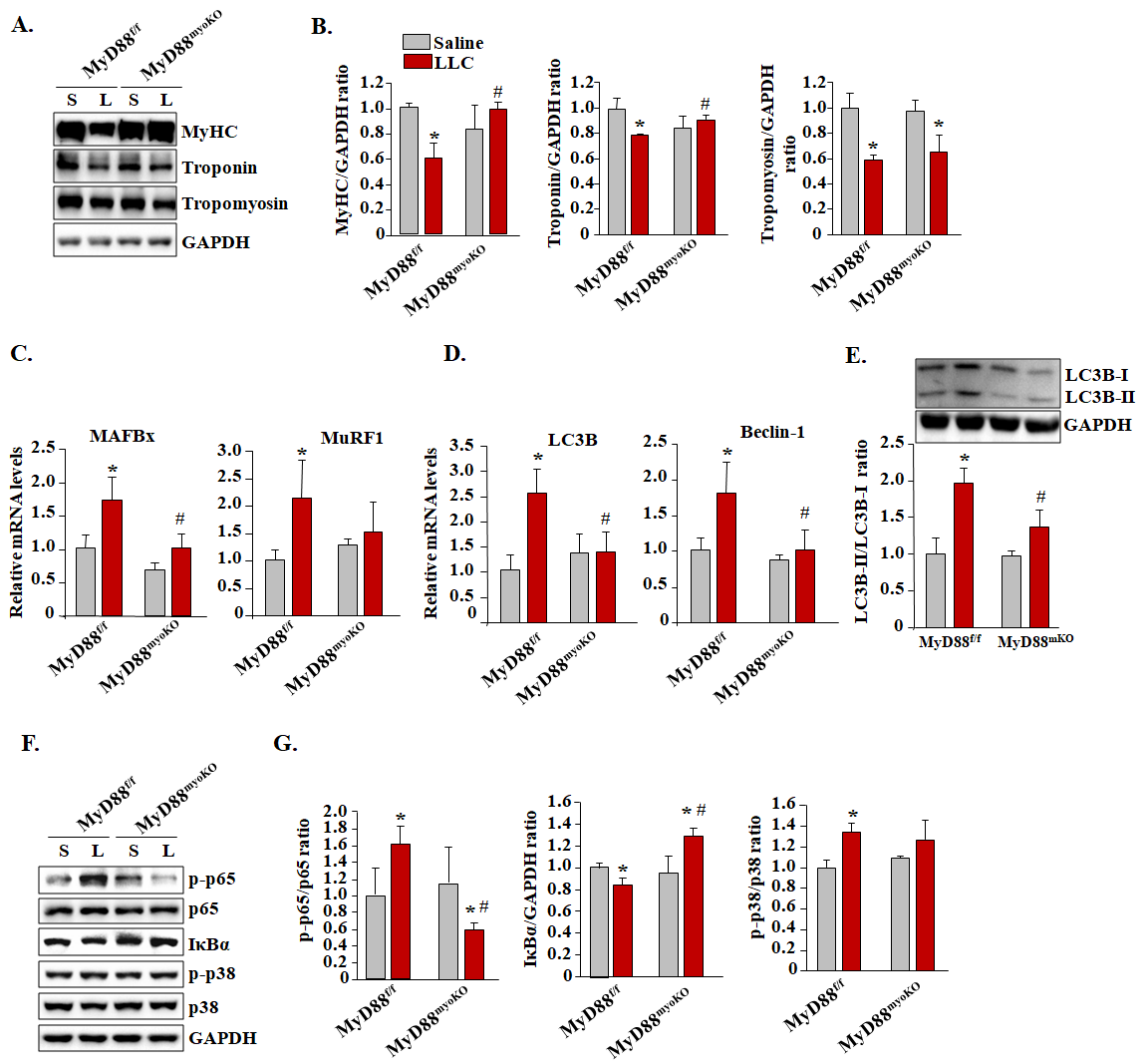


FIGURE 3.4: Ablation of MyD88 inhibits catabolic pathways in skeletal muscle during cancer cachexia. (A) Representative immunoblots demonstrating levels of MyHC, troponin, tropomyosin, and unrelated protein GAPDH in GA muscle of control and LLC tumor-bearing MyD88^{f/f} and MyD88^{mKO} mice. (B) Densitometry quantification of bands intensity of MyHC, Troponin, and Tropomyosin from multiple immunoblots. N= 4 in each group. (C) Relative mRNA levels of MAFBx and MuRF1 in GA muscle of control and LLC tumor-bearing MyD88^{f/f} and MyD88^{mKO} mice. (D) Relative mRNA levels of autophagy genes LC3B and Beclin-1 in GA muscle of control and LLC tumor bearing MyD88^{f/f} and MyD88^{mKO} mice. (E) Representative immunoblots and quantification of ratio of LC3BII and LC3BI in GA muscle. (F) Representative immunoblots demonstrating the levels of p-p65, IκBα, p-p38, total p38, and unrelated protein GAPDH in GA muscle of control and LLC tumor-bearing mice. (G) Densitometry analysis of ratio of p-p65/p6, p-p38/p38, IκBα/GAPDH from multiple immunoblots. N= 4/group. Error bars represent SD. *p<0.05, values significantly different from MyD88^{f/f} mice. #p<0.05, values significantly different from tumor-bearing MyD88^{f/f} mice.

FIGURE 3.5

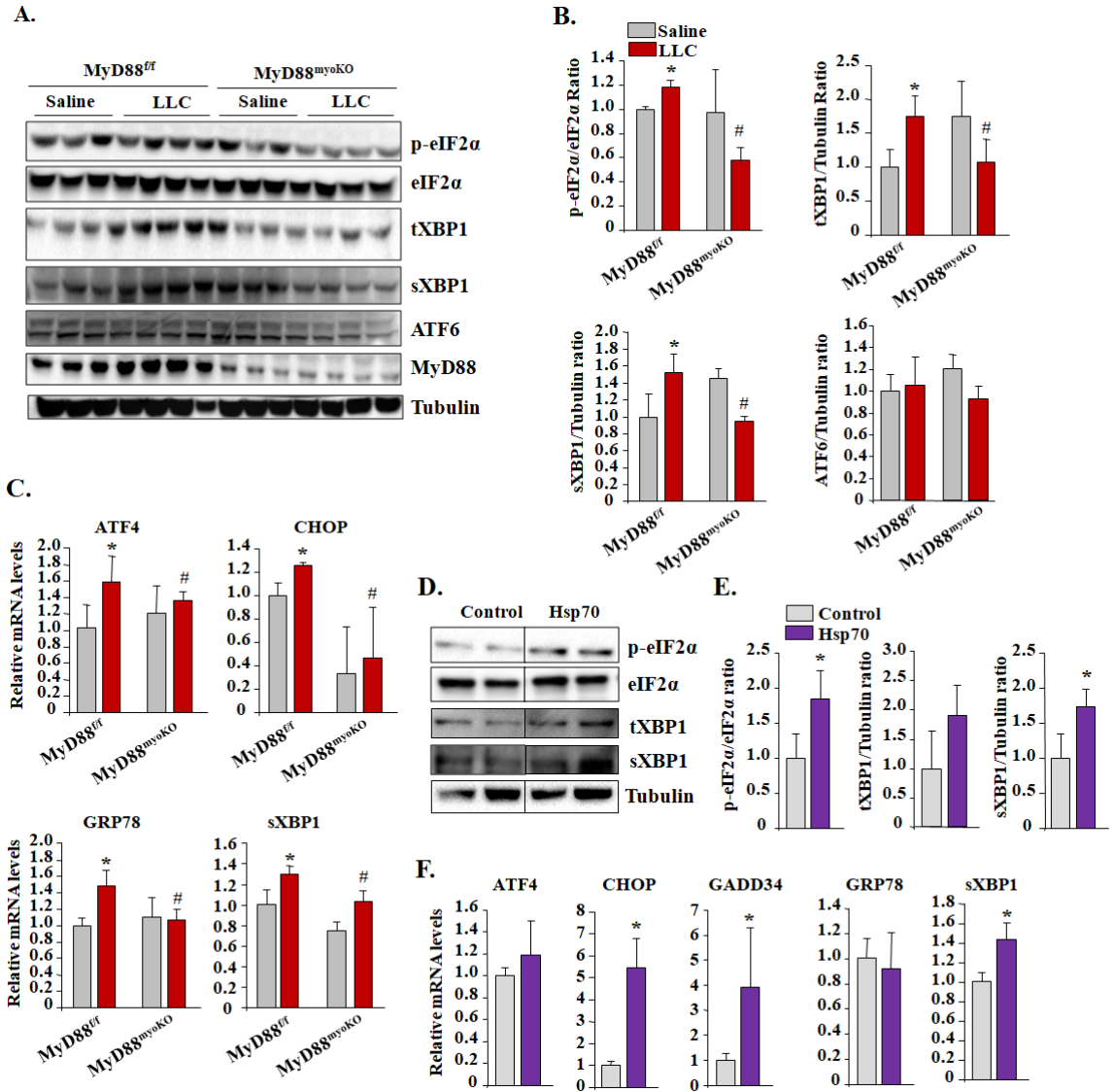


FIGURE 3.5: Genetic ablation of MyD88 in skeletal muscle hinders the activation of UPR pathways during cancer cachexia. (A) Immunoblots demonstrating levels of p-eIF2 α , eIF2 α , total XBP1 (tXBP1), spliced XBP1 (sXBP1), ATF6, MyD88, and unrelated protein tubulin in the GA muscle of control and LLC tumor-bearing MyD88^{ff} and MyD88^{myoKO} mice. **(B)** Densitometry quantification of bands in immunoblots. N=3 or 4 in each group. **(C)** Relative mRNA levels of ATF4, CHOP, GRP78, and sXBP1 in GA muscle of control and LLC tumor-bearing MyD88^{ff} and MyD88^{myoKO} mice. N= 4 in each group. C2C12 myotubes were treated with Hsp70 (100ng/ml) for 24h followed by performing biochemical analysis. **(D)** Representative immunoblots showing levels of p-eIF2 α , eIF2 α , tXBP1, sXBP1, and tubulin in control and Hsp70-treated myotubes. **(E)** Densitometry quantification of bands in immunoblots for p-eIF2 α , eIF2 α , tXBP1, and sXBP1 in control and Hsp70-treated C2C12 myotube cultures. **(F)** Relative mRNA levels of ATF4, CHOP, GADD34, GRP78, and sXBP1 in control and Hsp70-treated C2C12 myotubes. N= 3 in each group. Error bars represent SD. *p<0.05, values significantly different from MyD88^{ff} mice or control myotubes. #p<0.05, values significantly different from LLC tumor-bearing MyD88^{ff} mice.

FIGURE 3.6

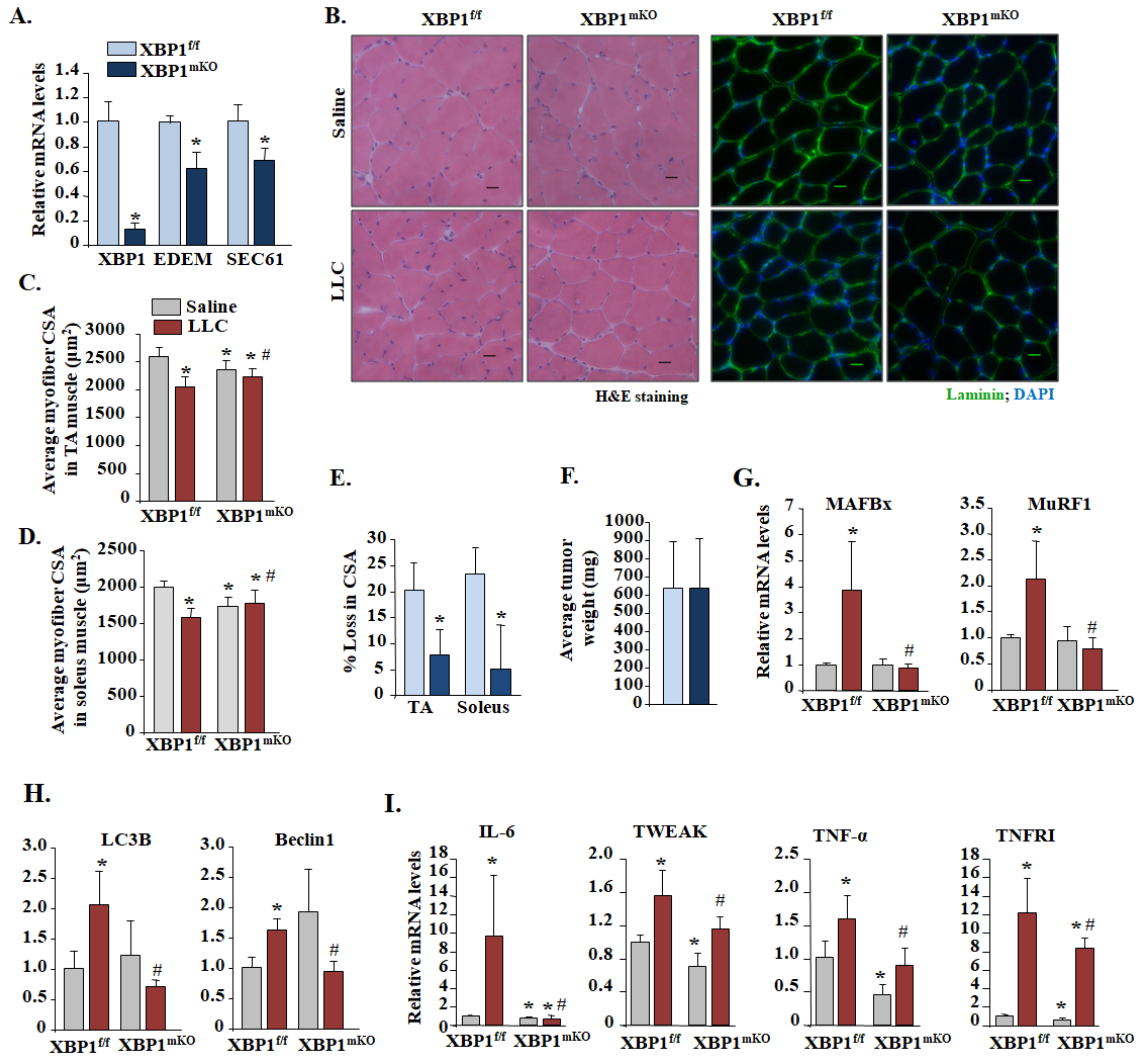


FIGURE 3.6: Targeted deletion of XBP1 inhibits skeletal muscle wasting in LLC tumor-bearing mice. (A) Relative mRNA levels of *XBP1*, *EDEM*, and *SEC61* in GA muscle of naïve $XBP1^{f/f}$ and $XBP1^{mKO}$ mice. N=4 in each group. 3-month old $XBP1^{f/f}$ and $XBP1^{mKO}$ mice were inoculated with 2×10^6 LLC cells in the left flank and monitored for 21 days. (B) Representative photomicrographs of H&E-stained and anti-Laminin-stained sections of TA muscle of control and LLC tumor-bearing $XBP1^{f/f}$ and $XBP1^{mKO}$ mice. Scale: 50 μ m. Quantification of average myofiber CSA in (C) TA and (D) soleus muscle of control and LLC tumor-bearing $XBP1^{f/f}$ and $XBP1^{mKO}$ mice. (E) Quantification of percentage loss in myofiber CSA in TA and soleus muscle of $XBP1^{f/f}$ and $XBP1^{mKO}$ mice after 21 days of inoculation with LLC cells. (F) Quantification of the average tumor wet weight in tumor bearing $XBP1^{f/f}$ and $XBP1^{mKO}$ mice. N=9-12 mice/group. Relative mRNA levels of (G) MAFBx and MuRF1, (H) LC3B and Beclin-1, and (I) IL-6, TWEAK, TNF- α , and TNFR1 in GA muscle of control and LLC-bearing $XBP1^{f/f}$ and $XBP1^{mKO}$ mice. N= 4 mice/ group. Error bars represent SD. * $p < 0.05$, values significantly different from $XBP1^{f/f}$ mice. # $p < 0.05$, values significantly different from LLC tumor-bearing $XBP1^{f/f}$ mice.

FIGURE 3.7

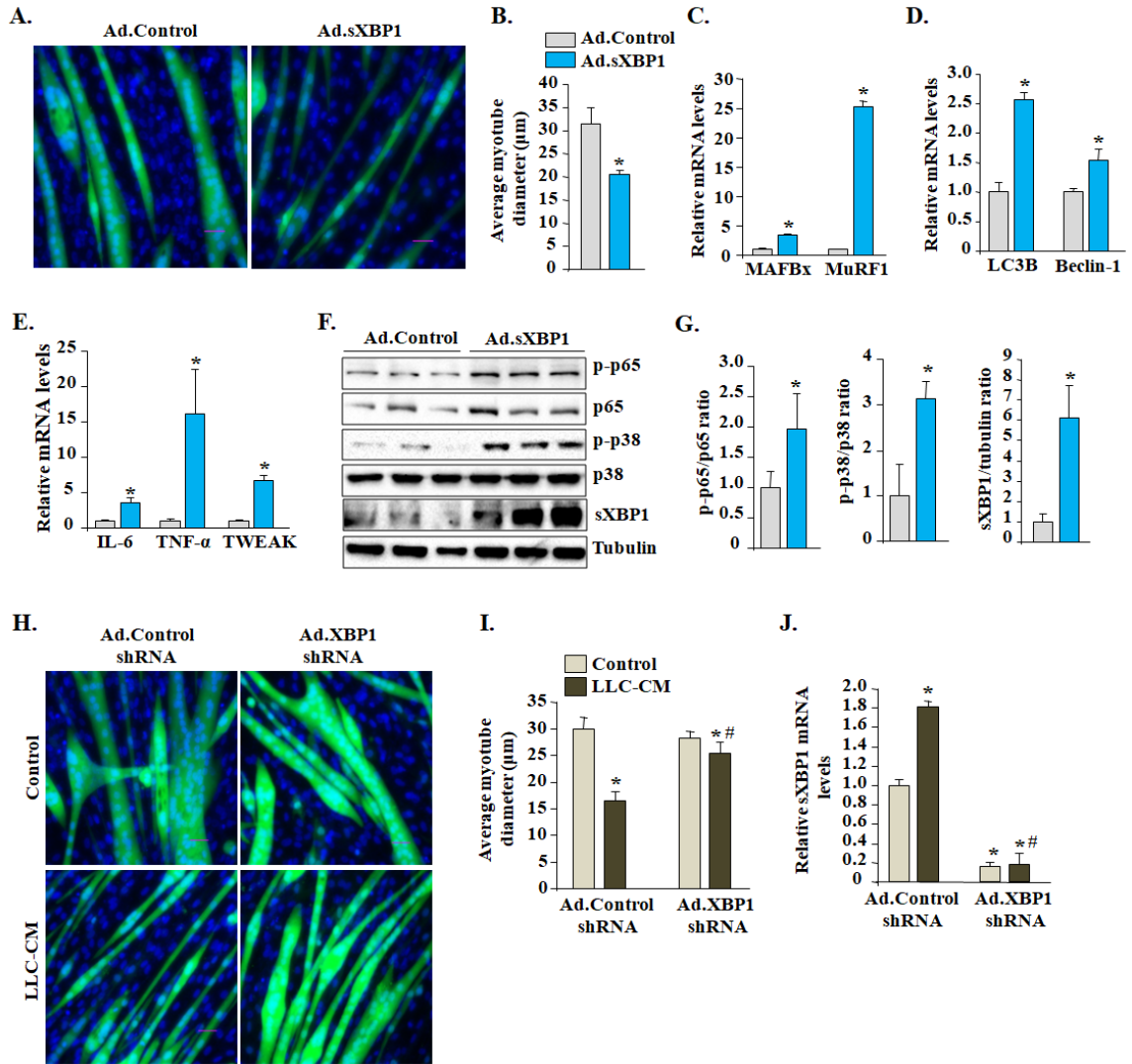


FIGURE 3.7: Activation of XBP1 causes atrophy in cultured myotubes. C2C12 myotubes were transduced with control adenovirus (Ad.Control) or sXBP1-expressing (Ad.sXBP1) for 24h. The cultures were incubated in differentiation medium for an additional 48h. **(A)** Representative images of control and sXBP1-overexpressing myotube cultures after staining with DAPI. **(B)** Quantification of average myotube diameter in control and sXBP1 overexpressing cultures. Relative mRNA levels of **(C)** *MAFBx* and *MuRF1*, **(D)** *LC3B* and *Beclin-1*, and **(E)** *IL-6*, *TNF α* , and *TWEAK* in control and sXBP1-overexpressing myotube cultures. **(F)** Representative immunoblots demonstrating levels of p-p65, p65, p-p38, p38, sXBP1, and tubulin proteins in control and sXBP1 overexpressing cultures. **(G)** Densitometry quantification of bands intensity in immunoblots. Ratio of p-p65/p65, p-p38/p38, and sXBP1/tubulin is presented here. N=4 in each group. *p<0.05, values significantly different from cultures transduced with Ad.Control. C2C12 myotubes were transduced with adenoviral vector expressing a scrambled shRNA (Ad.Control shRNA) or XBP1 shRNA (Ad.XBP1 shRNA) for 24h. The cells were washed and incubated with or without LLC-CM in 1:4 ratio for an additional 48h. **(H)** Representative images of myotube cultures after staining with DAPI. **(I)** Quantification of average myotube diameter in control and XBP1 knocked down myotube cultures. **(J)** Relative mRNA levels of XBP1 in myotube cultures transduced with Ad.Control shRNA or Ad.XBP1 shRNA incubated with or without LLC-CM. N=4 in each group. Error bars represent SD. *p<0.05, values significantly different from control cultures transduced with Ad.Control shRNA. #p<0.05, values significantly different from LLC-CM treated cultures transduced with Ad.Control shRNA.

CHAPTER 4

XBP1 PROMOTES SKELETAL MUSCLE REGENERATION AND GROWTH IN A CELL NON-AUTONOMOUS MANNER

4.1 Introduction

Skeletal muscle exhibits a remarkable capacity for regeneration following injury. Myofiber regeneration in adults is attributed mostly to the presence of a population of muscle precursor cells, termed satellite cells [25]. In the naive skeletal muscle, these mononucleated cells reside between the basement membrane and the sarcolemma in a relatively dormant state [16, 26]. Following injury to skeletal muscle, satellite cells become activated, undergo several rounds of cell division, and eventually differentiate into myocytes, which fuse either to form new muscle fibers or to repair damaged parts of existing myofibers. While the majority of activated satellite cells differentiate in the myogenic lineage and contribute to muscle repair, a fraction of them escape differentiation and restore the pool of quiescent satellite cells in regenerated or newly formed skeletal muscle [26]. Quiescent satellite cells express high levels of paired box 7 (Pax7) protein [25]. Following specification to the myogenic lineage, the levels of Pax7 are repressed and the levels of Myf5, MyoD, and myogenin are concomitantly increased, giving rise to proliferative myoblasts, which eventually fuse with injured myofibers to accomplish regeneration [25, 26, 172]. While satellite cells are the main cell type that

eventually contribute to the repair and nuclear accretion in myofibers, a number of other cell types, including inflammatory immune cells are also involved in the process of skeletal muscle regeneration. Inflammatory cells remove cellular debris and produce cytokines and growth factors, which support satellite cell proliferation, differentiation, and fusion in regenerating muscle.

It is also now evidenced that skeletal muscle regeneration involves coordinated activation of several intracellular signaling pathways that are activated in satellite cells, regenerating myofibers, as well as inflammatory immune cells. Skeletal muscle contains an extended network of endoplasmic reticulum (ER) that plays critical roles in protein folding and regulating calcium homeostasis in cell. Disruption in protein folding capacity or calcium levels leads to ER stress. The ER deals with this stress through initiating the unfolded protein response (UPR), mediated by inositol-requiring enzyme 1 (IRE1), RNA-dependent protein kinase-like ER eukaryotic translation initiation factor 2 alpha kinase (PERK), and activating transcription factor 6 (ATF6) [6, 7, 173]. In an unstressed cellular state, PERK, IRE1, and ATF6 are maintained in an inactive state by binding to BiP/glucose-regulating protein 78 (GRP78), an important ER chaperone. In response to stress in the ER, GRP78 disassociates from these proteins and preferentially binds to misfolded proteins in the ER lumen. This leads to PERK and IRE1 homodimerization and auto-phosphorylation leading to their activation. ATF6 moves to Golgi bodies where it undergoes cleavage by specific proteases leading to formation of a N-terminal ATF6 fragment which acts as a transcription factor [6]. Although the primary role of the UPR is to restore homeostasis, chronic stress in the ER can lead to the activation of other processes which leads to pathological changes in the tissue, including cell mortality [2].

Accumulating evidence suggests that the components of the UPR play important role in the satellite stem cell homeostasis and development and regeneration of myofiber upon injury. Previous studies have shown that the activation of the ATF6 arm of the UPR mediates apoptosis of a subpopulation of myoblasts that may be susceptible to cellular stresses, leading to a more efficient formation of myotubes [20, 21]. A recent study has shown that the PERK/eIF2 α arm of the UPR may be required for maintaining satellite cells in a quiescent state in adult skeletal muscle [28]. Additionally, we recently reported that PERK is important for satellite cell homeostasis and skeletal muscle regeneration upon injury. Inactivation of PERK leads to satellite cell mortality during myogenesis, potentially due to the precocious activation of p38 MAPK [27].

IRE1, which is activated in response to ER stress, has an endonuclease activity that mediates the unconventional splicing of XBP1 mRNA [7]. Spliced XBP1 (sXBP1) is a powerful transcription factor that induces gene expression of several UPR and other molecules in different cell types [5]. Previous studies have shown that the gene expression of *Xbp1* is regulated by MyoD and myogenin in myogenic cells [23]. Intriguingly, gene expression analysis has shown that XBP1 controls the expression of a large subset of molecules in myogenic cells including those involved in ER function, cellular growth, and DNA damage and repair processes [24]. Overexpression of sXBP1 inhibits myogenesis leading to the formation of tiny myotubes in C2C12 cultures after initiation of differentiation program. XBP1 augments the expression of transcription factor, Mist1, which negatively regulates MyoD activity [24]. Intriguingly, we found that inducible inactivation of XBP1 in satellite cells had no significant effect on skeletal muscle regeneration in adult mice [27]. By contrast, our studies in chapter 3 revealed that

average myofiber size was found to be reduced in skeletal muscle-specific XBP1-knockout (XBP1^{mKO}) mice suggesting that XBP1 may regulate development and growth myofibers in a cell-autonomous or cell non-autonomous manner.

In this study, we demonstrate that the levels of XBP1 are increased in regenerating skeletal muscle of adult mice. Similarly, XBP1 is upregulated in skeletal muscle during post-natal growth as well as during overload-induced skeletal muscle hypertrophy. We found that genetic deletion of XBP1 in myofibers inhibits their regeneration following muscle injury, potentially due to reduced proliferation and fusion of satellite cells. We also demonstrated that the targeted ablation of XBP1 reduces post-natal muscle growth and inhibits functional overload-induced myofiber hypertrophy in adult mice. XBP1 does not affect the rate of protein synthesis during muscle growth. Rather, XBP1 functions through inducing the proliferation and fusion of satellite cells with pre-existing myofibers in a cell non-autonomous manner.

4.2 Material and Methods

Animals. C57BL/6 mice were originally purchased from Jackson Laboratories (Bar Harbor, ME, USA). Skeletal muscle specific XBP1-knockout mice (XBP1^{mKO}) mice were generated by crossing MCK-Cre mice (Jax strain: B6.FVB(129S4)-Tg (Ckmm-cre)5Khn/J) with floxed XBP1 mice (MGI strain: Xbp1^{tm2Glm})[7] mice, respectively. All mice were in the C57BL/6 background and their genotype was determined by PCR from tail DNA.

Skeletal muscle injury and in vivo fusion assay. At 10 weeks of age, 100 μ l of 1.2% BaCl₂ (Sigma Chemical Co.) was injected into the TA muscle of male mice to induce necrotic injury as described [174, 175]. At various time points, mice were euthanized, TA muscle was isolated, and processed for biochemical and histological analysis. To study myoblast fusion in vivo, XBP1^{ff} and XBP1^{mk0} mice were given an intraperitoneal injection of EdU (4 μ g per gram body weight) at day 2 following TA muscle injury by intramuscular injection of BaCl₂ solution. After 11 days of EdU injection, the TA muscle was isolated and sectioned in a microtome cryostat. For studying myoblast fusion during post-natal growth period, mice were injected with EdU at day 5 post birth (P5) and analyzed at the age of 2 weeks (confirm). Transverse muscle sections made were immunostained with anti-laminin and processed for detection of EdU and nuclei. The number of intrafiber EdU⁺ myonuclei/myofiber was quantified using National Institutes of Health (NIH) ImageJ software.

Synergistic ablation surgery. The mice were subjected to bilateral synergistic ablation surgery to induce myofiber hypertrophy of the plantaris muscle following a method as described [154]. In brief, mice were anesthetized using tribromoethanol and the soleus and ~60% of the gastrocnemius muscles were surgically excised while ensuring that the neural and vascular supply remained intact and undamaged for the remaining plantaris muscle. A sham surgery was performed for controls following exactly the same procedures except that gastrocnemius and soleus muscles were not excised. After 7 or 14 days, plantaris muscle was isolated and processed for histomorphometric and biochemical analysis. To study the contribution of myoblast fusion in overload-induced

hypertrophy, 2 days after performing synergistic ablation surgery, XBP1^{ff} and XBP1^{mk0} mice were given an intraperitoneal injection of EdU (4 µg/g body weight). After 12 days of EdU injection, the plantaris muscle was isolated and transverse muscle sections made were immunostained with anti-laminin and processed for detection of EdU and nuclei. The number of intrafiber EdU⁺ myonuclei/myofiber was quantified using NIH ImageJ software. Samples were blinded for analysis.

Histology and morphometric analysis. Individual TA and soleus muscles were isolated from mice, snap frozen in liquid nitrogen, and sectioned with a microtome cryostat. For the assessment of muscle morphology and to quantify fiber cross-sectional area (CSA), 10-µm-thick transverse sections of TA and plantaris muscle were stained with hematoxylin and eosin (H&E). The sections were examined under an Eclipse TE 2000-U microscope (Nikon, Tokyo, Japan). Fiber cross-sectional area (CSA) was analyzed in H&E-stained or Dystrophin-stained muscle sections using ImageJ software (NIH). For each muscle, CSA was calculated by analyzing 75 fibers per each 20 X image. 5 images randomly were taken for each mouse, allowing for 375 fibers measured per mouse.

Immunohistochemistry. For immunohistochemistry studies, frozen TA or soleus muscle sections were fixed in acetone, blocked in 2% bovine serum albumin in PBS for 1 h and subsequently incubated with anti-Pax7 (1:5-1:10, DSHB Cat# pax7, RRID:AB_528428), anti-Dystrophin (1:100, Sigma Chemical Co.), anti-eMyHC (1:200, DSHB Cat# F1.652, RRID:AB_447163), or anti-Laminin (1:150, Cell Signaling Technology Cat# L9393, RRID:AB_477163) in blocking solution at 4°C overnight under

humidified conditions. The sections were washed briefly with PBS before incubation with Alexa Fluor® 488 (1:2000, Thermo Fisher Scientific Cat# A-11034, RRID:AB_2534095) and Alexa Fluor® 594 (1:2000, Thermo Fisher Scientific Cat# A-11037, RRID:AB_2534095) secondary antibody for one hour at room temperature and then washed three times for five minutes with PBS. Nuclei were visualized by counterstaining with DAPI for five minutes.

To determine the composition of different types of fibers in the TA and soleus muscle of mice, transverse cross sections were made and blocked in 5% goat serum and 2% bovine serum albumin (BSA) for 30 min, followed by incubation for 1 h with monoclonal antibodies against type I, IIA, and IIB MyHC isoforms using clone BA-D5, SC-7, and BF-F3, respectively (Developmental Studies Hybridoma Bank, Iowa City, IA, USA). Secondary antibody used was goat anti-mouse IgG2b conjugated with Alexa-350, goat anti-mouse IgG1 conjugate with Alexa-568, and goat anti-mouse IgM conjugated with Alexa-488. Finally, the fluorescence was captured with an Eclipse TE 2000-Umicroscope (Nikon), the images were merged, and the percentage of each type of fibers in whole muscle section was recorded. Fiber CSA of each fiber type was analyzed using NIH ImageJ software. For each muscle, CSA was calculated for approximately 100 Type I and Type IIA fiber and 300 Type IIB fibers for each mouse.

Primary myoblast cultures. Primary myoblasts were isolated from the hind limbs of 8-week-old male or female mice as described [175]. Briefly, hind limb muscles of C57BL6 mice were isolated and excess connective tissues and fat were cleaned in sterile PBS. Muscle tissues were then minced into coarse slurry and enzymatically digested at 37 °C

for 1 h by adding 400 IU/ml collagenase II (Worthington). The digested slurry was spun, pelleted, and triturated multiple times, and then sequentially passed through a 70- μ m and then 30- μ m cell strainer (BD Falcon). The filtrate was spun at $1000 \times g$ and suspended in myoblast growth medium (Ham's F-10 medium with 20% FBS supplemented with 10 ng/ml of basic fibroblast growth factor). Cells were first re-fed after 3 days of initial plating. Cells were pre-plated for 15–30 min for the first few passages to select for a pure myoblast population (cells in suspension). Upon selection of each cell type, the cells were cultured in their corresponding culturing medium till reaching 80% confluence. To induce differentiation, the cells were incubated in differentiation medium (DM; 2% horse serum in DMEM).

Total RNA extraction and QRT-PCR assay. RNA isolation and QRT-PCR were performed using a published method [58, 59]. In brief, total RNA was extracted from gastrocnemius (GA) and TA muscles of mice or cultured C2C12 myotubes isolated with TRIzol reagent (Thermo Fisher Scientific Life Sciences) and an RNeasy Mini Kit (Qiagen, Valencia, CA, USA) according to the manufacturers' protocols. First-strand cDNA for PCR analyses was made with a commercially available kit (Thermo Fisher Scientific Life Sciences). The quantification of mRNA expression was performed using the SYBR Green dye (Thermo Fisher Scientific Life Sciences) method on a sequence detection system (model 7300; Thermo Fisher Scientific Life Sciences). Primers were designed with Vector NTI software (Thermo Fisher Scientific Life Sciences). Primer sequences are shown in Appendix 1. Data normalization was accomplished with the

endogenous control (β -actin), and the normalized values were subjected to a 2DDCt formula to calculate the fold change between control and experimental groups.

Western blot analysis. Relative levels of various proteins were quantitated by performing Western blot analysis. TA or GA muscle of mice or primary myotubes were washed with sterile PBS and homogenized in lysis buffer: 50 mM Tris-Cl (pH 8.0), 200 mM NaCl, 50 mM NaF, 1 mM dithiothreitol, 1 mM sodium orthovanadate, 0.3% IGEPAL, and protease inhibitors. Approximately 100 mg protein was resolved in each lane on 10% SDS-polyacrylamide gels, electrotransferred onto nitrocellulose membranes, and probed with the following antibodies: anti-sXBP-1 (1:1000; Cell Signaling Technology), anti-phospho-Akt (Ser473) (1:500; Cell Signaling Technology), anti-Akt(1:500; Cell Signaling Technology), anti-phospho-mTOR (1:500; Cell Signaling Technology), anti-mTOR (1:500; Cell Signaling Technology), anti-phospho-ribosomal protein (rp)S6 (1:500; Cell Signaling Technology), anti-rpS6 (1:000; Cell Signaling Technology), anti- α -tubulin (1:1000; Cell Signaling Technology), and anti-GAPDH (1:2000; Cell Signaling Technology). Antibodies were detected by chemi-luminescence. Quantitative estimation of the bands' intensity was performed with ImageJ software (NIH).

SUnSET assay. In vivo, the mice were anesthetized and given i.p. injection of 0.04 μ M of puromycin per gram of body weight. The mice were euthanized exactly 30 minutes after injection of puromycin, and hind limb muscle was isolated and snap-frozen. For cultured myotubes, 1 μ M puromycin was added in the culture medium for 30 minutes.

Finally, protein extracts were made from muscles or cultured myotubes, and newly synthesized protein was detected by performing immunoblotting using primary antibody anti-puromycin (1:1,000; catalog MABE343, MilliporeSigma).

Statistical analysis. Results are expressed as mean \pm standard deviation (SD). For statistical analyses, we used unpaired two-tailed Student's t-test. A value of $P < 0.05$ was considered statistically significant, unless otherwise specified.

4.3 Results

4.3.1 Myofiber-specific deletion of XBP1 inhibits skeletal muscle regeneration in adult mice. We first investigated how the protein expression of spliced and total XBP1 is affected in injured skeletal muscle of adult mice. Tibialis anterior (TA) muscle of C57BL/6J mice was injected with 1.2% BaCl₂ solution, a widely used myotoxin for experimental muscle injury in mice, as previously described [175, 176]. The contralateral TA muscle was injected with saline only and served as control. After 5 or 14 days, the TA muscles were isolated and the levels of spliced XBP1 (sXBP1) and total XBP1 (tXBP1) were measured by performing Western blot. Results showed that levels of sXBP1 were significantly increased in injured TA muscle compared to contralateral uninjured muscle. Moreover, we observed that tXBP1 levels were significantly decreased in injured TA muscle as compared to control (**Figure 4.1A, B**).

To investigate the role of XBP1 in skeletal muscle regeneration after injury, we generated muscle-specific XBP1-KO mice (henceforth XBP1^{mKO}) by crossing floxed XBP1 (XBP1^{f/f}) mice with MCK-Cre mice. At 10 weeks of age, the TA muscle of

littermate XBP1^{f/f} and XBP1^{mKO} mice was injected with 100 μ l of 1.2% BaCl₂ solution to induce necrotic muscle injury. Muscle regeneration was evaluated at day 5 and 14 post-BaCl₂ injection. There was no overt difference in TA muscle regeneration between XBP1^{f/f} and XBP1^{mKO} mice at day 5 post-injury (**Figure 4.1C**). However, average cross-sectional area (CSA) and minimal Feret's diameter of regenerating myofibers was significantly reduced in TA muscle of XBP1^{mKO} mice compared to XBP1^{f/f} mice both at 5d and 14d post-injury (**Figure 4.1D-G**). Moreover, the percentage of myofibers containing two or more centrally located nuclei was significantly reduced in 5d-injured TA muscles of XBP1^{mKO} mice as compared to XBP1^{f/f} mice (**Figure 4.1H**). Collectively, these results suggest that myofiber-specific inhibition of XBP1 diminishes skeletal muscle regeneration after acute injury.

4.3.2 Ablation of XBP1 inhibits the expression of myogenic markers during skeletal muscle regeneration in mice. Embryonic isoform of myosin heavy chain (eMyHC) is highly expressed in newly regenerating myofibers. To further confirm the role of XBP1 in skeletal muscle regeneration, we examined the number of myofibers expressing eMyHC. After 5 days of injury, the TA muscle was isolated and analyzed by performing immunostaining for eMyHC and Laminin. Nuclei were stained with DAPI (**Figure 4.2A**). This analysis showed that the number of eMyHC⁺ myofibers within Laminin staining was significantly reduced in 5d-injured TA muscle of XBP1^{mKO} mice compared to XBP1^{f/f} mice (**Figure 4.2B**). Moreover, the average CSA of eMyHC⁺ myofibers was significantly reduced in TA muscle of XBP1^{mKO} mice as compared to corresponding injured TA muscle of XBP1^{f/f} mice (**Figure 4.2C**). We also found that mRNA levels of

eMyHC (gene name: *Myh3*) were significantly reduced in 5d-injured TA muscle of XBP1^{mKO} mice compared to corresponding muscle of littermate XBP1^{ff} mice (**Figure 4.2D**). Skeletal muscle regeneration involves sequential expression of essential myogenic regulatory factors: Myf5, MyoD, and myogenin [25, 26]. Interestingly, we found that mRNA levels of MyoD and myogenin were significantly reduced in 5d-injured TA muscle of XBP1^{mKO} mice compared with XBP1^{ff} mice (**Figure 4.2E**). Collectively, these results suggest that the XBP1 transcription factor plays an important role in skeletal muscle regeneration in adult mice.

4.3.3 Targeted deletion of XBP1 reduces the number of satellite cells in regenerating skeletal muscle. To understand the cellular mechanisms through which XBP1 regulates muscle regeneration, we next investigated whether the deletion of XBP1 in myofibers affects the abundance of satellite cells in regenerating muscle. Transcription factor Pax7 is commonly used as a marker to label both quiescent and activated satellite cells [25]. TA muscle sections from XBP1^{ff} and XBP1^{mKO} mice were immunostained for Pax7 to detect satellite cells. The sections were also immunostained for Laminin to mark the boundary of the myofibers and counterstained with DAPI to identify nuclei. There was no significant difference in the number of Pax7⁺ cells in uninjured TA muscle of XBP1^{ff} and XBP1^{mKO} mice (**data not shown**). Intriguingly, we found that the number of Pax7⁺ cells was significantly reduced in 5d-injured TA muscle of XBP1^{mKO} mice compared to littermate XBP1^{ff} mice (**Figure 4.3 A,B**). Furthermore, mRNA levels of Pax7 were also significantly reduced in 5d-injured TA muscle of XBP1^{mKO} mice as compared to XBP1^{ff}

mice (**Figure 4.3C**). These results suggest that myofiber-specific deletion of XBP1 reduces the number of satellite cell in regenerating skeletal muscle of adult mice.

We next investigated the role of XBP1 in the proliferation and fusion of satellite cells. TA muscle of XBP1^{f/f} and XBP1^{mKO} mice were injured by intramuscular injection of 1.2% BaCl₂ solution. After 48h, the mice were given an intraperitoneal (i.p.) injection of EdU and the number of EdU⁺ nuclei in the TA muscle was determined 12 days later. A significant reduction in EdU⁺ nuclei was observed in TA muscle of XBP1^{mKO} mice compared with XBP1^{f/f} mice (**Figure 4.3D, E**). Moreover, we found mRNA levels of Myomaker, an essential fusion molecule, were also significantly reduced in 5d-injured TA muscle of XBP1^{mKO} mice compared with XBP1^{f/f} mice (**Figure 4.3F**). Taken together, these results suggest that XBP1-mediated signaling in myofibers promotes the proliferation and fusion of satellite cells with injured myofibers to promote muscle regeneration.

4.3.4 XBP1 mediates post-natal skeletal muscle growth. We also investigated how the levels of XBP1 are regulated in skeletal muscle of young and adult mice. Our analysis showed that the protein levels of sXBP1 were significantly higher in skeletal muscle of 2-week mice compared to adult 12-week old mice (**Figure 4.4 A,B**). To understand what role XBP1 has in post-natal skeletal muscle development, we euthanized littermate XBP1^{f/f} and XBP1^{mKO} mice at 2 weeks of age and performed histological and biochemical analysis. Initially, TA muscle transverse sections were generated and stained with H&E to assess skeletal muscle morphology (**Figure 4.4C**). Interestingly, the average myofiber CSA of TA muscle was significantly reduced in XBP1^{mKO} mice compared to

XBP1^{f/f} mice (**Figure 4.4D**). One possible explanation for the decrease in average myofiber CSA is a possible change in muscle fiber type after the deletion of XBP1. Skeletal muscle is made up of 3 distinct types of fibers. Type I fibers are considered as slow-type fiber due to its composition of large amounts of mitochondria, resistance to fatigue, and smaller CSA. In contrast, Type IIA and IIB fibers are considered fast type fibers, contain fewer amounts of mitochondria, and are more fatigable. Type IIB fibers are mostly glycolytic and correspond to the largest CSA [125]. To investigate whether deletion of XBP1 affects the composition of slow- and fast-type fibers in skeletal muscle, we prepared transverse sections of the TA muscles and stained them with anti-myosin heavy chain (MyHC) types I, IIA, and IIB. Representative images of TA sections are presented in **Figure 4.4E**. Interestingly, a significant increase in Type I and IIA fibers and a significant decrease in Type IIB was noticeable in TA muscle of 2-week old XBP1^{mKO} mice compared with XBP1^{f/f} mice (**Figure 4.4F**). This was further confirmed by QRT-PCR analysis where we demonstrate a significant increase in mRNA levels of MyHC I and MyHC IIA and significant decrease in MyHC IIB in TA muscle of XBP1^{mKO} mice compared to XBP1^{f/f} (**Figure 4.4G**). Moreover, analysis of each fiber type average CSA suggested a decrease in myofiber size of type I, IIA, and IIB in XBP1^{mko} mice as compared to XBP1^{f/f} (**Figure 4.4H**).

Skeletal muscle growth during post-natal development also involves myonuclear accretion, which occurs due to the proliferation of satellite cells and fusion of myoblasts with mature myofibers (18, 24, 43, 44). We next evaluated the effect of myofiber-specific deletion of XBP1 on satellite cell proliferation and fusion. TA muscle sections from 2-week old XBP1^{f/f} and XBP1^{mKO} mice were immunostained for Pax7, Laminin, and DAPI

to identify satellite cells. Interestingly, we found that the number of Pax7⁺ cells was significantly reduced in 2-week TA muscle of XBP1^{mKO} mice compared to littermate control mice (**Figure 4.5 A,B**). However, our results did not indicate any significant difference in the mRNA levels of Pax7, whereas they did reveal a significant increase in myogenic markers eMyHC and MyoD (**Figure 4.5 C**).

We next evaluated the role of XBP1 in myonuclear accretion at 2-weeks of age by measuring the amount of DAPI labeled nuclei within the anti-Dystrophin-stained sarcolemma (**Figure 4.5D**). Interestingly, the number of myonuclei residing within the dystrophin-stained sarcolemma of the TA muscle was significantly reduced in 2-week old XBP1^{mKO} mice as compared to XBP1^{f/f} mice (**Figure 4.5E**). Lastly, we analyzed the proliferation of satellite cells during skeletal muscle growth post-birth. At post-natal day 7, the mice were given an i.p. injection of EdU and the number of EdU⁺ nuclei in the TA muscle was determined 14 days later. Interestingly, a significant reduction in EdU⁺ nuclei was observed in TA muscle of XBP1^{mKO} mice compared with XBP1^{f/f} mice at post-natal day 21 (**Figure 4.5 F,J**). Collectively, these results suggest that targeted deletion of XBP1 prevents post-natal muscle growth, potentially through inhibiting satellite cell proliferation and their fusion to myofibers.

4.3.5 XBP1 mediates myofiber hypertrophy in response to functional overload.

During exercise, skeletal muscle experiences skeletal muscle injury before undergoing hypertrophy [177]. We next investigated whether the levels of XBP1 change during skeletal muscle growth in response to functional overload. After 5 days of synergistic ablation (SA) surgery, the mice were euthanized and plantaris muscle was isolated and

analyzed for biochemistry. Representative immunoblots (**Figure 4.6A**) and densitometry quantification of bands in immunoblots (**Figure 4.6B**) showed that the protein levels of sXBP1 were significantly increased in plantaris muscle after 5d of performing SA surgery. Moreover, semi-quantitative RT-PCR analysis revealed an increase in the *sXBP1* mRNA levels in 5d-loaded plantaris muscle compared with corresponding control muscle (**Figure 4.6C**).

To investigate the role of XBP1 in overload-induced skeletal muscle growth, 10-week old XBP1^{f/f} and XBP1^{mKO} mice were subjected to sham or SA surgery. After 7 or 14 days, the mice were euthanized and the plantaris muscle was isolated and analyzed. Results showed that the wet weight of the plantaris muscle was significantly decreased in XBP1^{mKO} mice compared to XBP1^{f/f} mice (**Figure 4.6D**). Next, we generated transverse sections of plantaris muscle followed by performing H&E staining and morphological analysis (**Figure 4.6E**). Interestingly, average myofiber CSA was significantly reduced in plantaris muscle of XBP1^{mKO} mice compared to littermate XBP1^{f/f} mice at day 14 post-SA surgery (**Figure 4.6F**). Moreover, the percentage increase in myofiber CSA after SA surgery was significantly less in plantaris of XBP1^{mKO} mice compared to XBP1^{f/f} mice (**Figure 4.6G**). Altogether, these results suggest that XBP1 promotes overload-induced myofiber hypertrophy in adult mice.

4.3.6 Genetic ablation of XBP1 inhibits satellite cell proliferation during overload-induced myofiber hypertrophy. To understand the mechanisms through which XBP1 promotes muscle hypertrophy in adult mice, we investigated the role of XBP1 in satellite cell proliferation and fusion during overload-induced myofiber hypertrophy. At day 14

after SA surgery, plantaris muscle was isolated and transverse sections immunostained for Pax7, Laminin, and DAPI to identify satellite cells. Interestingly, the number of Pax7⁺ cells was significantly reduced in 14d-loaded plantaris muscle of XBP1^{mKO} mice compared to littermate XBP1^{f/f} mice (**Figure 4.7A,B**). Next, we investigated whether the deletion of XBP1 had any effect on myonuclear accretion 14 days after SA surgery. Interestingly, the number of myonuclei residing within the Dystrophin-stained sarcolemma of the plantaris muscle was significantly reduced in XBP1^{mKO} mice compared to XBP1^{f/f} mice (**Figure 4.7C,D**). Finally, we investigated whether the deletion of XBP1 in myofibers affects fusion of muscle progenitor cells with myofibers during overload-induced muscle hypertrophy. For this experiment, XBP1^{f/f} and XBP1^{mKO} mice were given an i.p. injection of EdU at day 2 post-SA surgery and 12 days later, plantaris muscle was isolated and analyzed. Interestingly, a significant reduction in EdU⁺ nuclei was observed in overloaded plantaris muscle of XBP1^{mKO} mice compared with XBP1^{f/f} mice (**Figure 4.7E,F**).

Skeletal muscle growth in response to functional overload involves an increase in the rate of protein synthesis, which is mediated primarily through the activation of Akt/mTOR/p70S6K signaling pathway [137, 178, 179]. We next investigated the rate of protein synthesis and the activation of the components of the Akt/mTOR/p70S6K pathway in skeletal muscle of 7d-loaded plantaris muscle. We performed SuNSET assay to measure the rate of protein synthesis. An increase in protein synthesis (i.e. puromycin-tagged proteins) was clearly visible in plantaris muscle 7 days after SA surgery (**Figure 4.6G**). However, there was no significant difference in the amounts of puromycin-tagged proteins in TA muscle of 7d-overloaded plantaris muscle of XBP1^{f/f} and XBP1^{mKO} mice.

As expected, we observed a considerable increase in the levels of p-Akt, p-p70S6K, and p-mTOR in plantaris muscle at day 7 after performing SA surgery (**Figure 4.7G**).

However, there was no significant difference in the levels of p-Akt, p-p70S6K, or p-mTOR in 7d-loaded plantaris muscle of XBP1^{ff} and XBP1^{mKO} mice (**Figure 4.7H**).

Taken together, these results suggest that XBP1 promotes overload-induced myofiber hypertrophy through augmenting satellite cell proliferation and fusion, but without affecting on the rate of protein synthesis.

4.3.7 XBP1 is essential for myoblast fusion *in vitro*. We next investigated the effects of knockdown of XBP1 on myoblast differentiation and fusion *in vitro*. Primary myoblasts were incubated in differentiation medium (DM) for 24 hours followed by transducing with adenoviral vector for a scrambled shRNA or XBP1 shRNA. The cultures were incubated in DM for an additional 48h, followed by analysis for myotube formation and expression of fusion-related molecules. Interestingly, we found that the knockdown of XBP1 caused a significant reduction in myotube diameter (**Figure 4.8A,B**). Furthermore, the knockdown of XBP1 caused a significant increase in the number of myotubes containing less than 2 nuclei and a significant decrease in myotubes containing more than 5 nuclei (**Figure 4.8C**). Our QRT-PCR analysis revealed a drastic reduction in mRNA levels of XBP1 in cultures transduced with Ad.XBP1 shRNA (**Figure 4.8D**). We also measured gene expression of a few molecules that are known to promote myoblast fusion during myogenesis. Our analysis showed that knockdown of XBP1 significantly reduced mRNA levels of Myomaker and TWEAK, while having no effect on mRNA levels of N-cadherin and Nephronectin (**Figure 4.8D**).

4.3.8 Forced expression of XBP1 reduces myoblast fusion *in vitro*. Since knockdown of XBP1 inhibits myoblast fusion, we next sought to determine whether overexpression of XBP1 can induce fusion of cultured myoblasts. Primary myoblasts were incubated in DM for 24h followed by transduction with adenoviral vector expressing control or sXBP1 cDNA. The cells were then incubated in DM for an additional 48h (**Figure 4.9A**). Interestingly, we found that overexpression of sXBP1 also reduced myotube diameter (**Figure 4.9B**). Overexpression of XBP1 resulted in a significant increase in the number of myotubes containing less than 2 nuclei and a significant decrease in myotubes containing more than 5 nuclei (**Figure 4.9C**). However, there were no significant effects on the gene expression of myoblasts fusion molecules: Myomaker, N-cadherin, and Nephronectin. Interestingly, we found a significant increase in mRNA levels of TWEAK (**Figure 4.9D**). Collectively, these results suggest that while XBP1 is essential for myoblast differentiation and fusion, supra-physiological activation of XBP1 inhibits myotube formation in myogenic cultures.

4.4 Discussion

Myofibers grow in size due to the increased rate of protein synthesis as well as nuclear accretion, which occurs due to the activation and fusion of muscle progenitor cells to myofibers [180, 181]. Recent studies have demonstrated that the markers of ER stress/UPR are increased in skeletal muscle in response to endurance exercise and in other conditions of skeletal muscle growth [60, 62, 63, 70, 182]. The importance of the UPR pathways in development and homeostasis is evidenced by the finding that genetic

deletion of PERK, IRE, or ATF6 α/β causes growth retardation, pancreatic dysfunction, and embryonic lethality in mice [12, 131-133, 183]. Moreover, XBP1, a direct target of IRE1, is essential for the functioning of intestinal epithelial cells, immune cells, hepatocytes [184], and adipocytes [185], as well as for the development of professional secretory cells, such as: B cells, hepatocytes, and pancreatic β cells [186, 187]. However, the role of XBP1 in the regulation of skeletal muscle growth or regeneration remained unknown. The results of the present study suggest that the transcription factor XBP1 is an essential regulator of skeletal muscle growth and regeneration following injury.

In this study, we have discovered that the levels of sXBP1 are increased in skeletal muscle during regeneration (**Figure 4.1A**), post-natal growth (**Figure 4.4A**), and in a model of overload-induced hypertrophy (**Figure 4.6A**). Our results further demonstrate that the myofiber-specific deletion of XBP1 inhibits skeletal muscle regeneration and overload-induced muscle hypertrophy in adult mice. Similarly, we found that the myofiber-specific deletion of XBP1 inhibits skeletal muscle growth post-birth. Satellite cells are essential for skeletal muscle regeneration [188, 189], development [190], and myofiber hypertrophy [191]. We have recently reported that the inducible deletion of XBP1 in satellite cells does not affect their function during regenerative myogenesis in adult mice [27]. It is now increasingly clear that satellite cell function can be influenced by a variety of factors that are produced by other cell types and are present in the injured muscle microenvironment. Indeed, we have previously demonstrated that the deletion of TNF receptor-associated factor 6 (TRAF6) in myofiber and satellite cells produce opposite effects on skeletal muscle regeneration [174, 175]. Intriguingly, we found that the myofiber-specific deletion of XBP1 significantly reduced

the number of satellite cells in skeletal muscle in the “settings” of muscle regeneration, and overload-induced myofiber hypertrophy implying that XBP1 regulates satellite cell proliferation and function in a cell non-autonomous manner.

Myofiber formation follows the coordinated activation of Myf5, MyoD, and myogenin [26, 192]. Specifically, inducible expression of Myf5 and MyoD is necessary for the activation and proliferation of satellite cells [192]. Interestingly, genetic ablation of XBP1 resulted in a significant reduction in the levels of MyoD and myogenin in regenerating skeletal muscle of adult mice (**Figure 4.2E**). Moreover, the number of eMyHC⁺ myofibers and mRNA levels of eMyHC were significantly diminished in regenerating muscle of XBP1^{mKO} mice compared with XBP1^{f/f} mice further confirming that deletion of MyD88 inhibits regenerative myogenesis (**Figure 4.2**). Interestingly, mRNA levels of eMyHC were found to be significantly increased in 2-week old XBP1^{mKO} mice (**Figure 4.5C**), potentially due to a delay in skeletal muscle development. A more comprehensive examination of these markers during the post-natal period would be essential to understand whether deletion of XBP1 inhibits muscle growth or myogenic differentiation.

The proliferation of satellite cells is a necessary step prior to the ultimate addition of myonuclei to growing myofibers [193]. Myonuclear accretion involves the fusion of myoblasts with mature myofibers and is known to be paramount for skeletal muscle development and growth (18, 24, 43, 44). Interestingly, we found that the myofiber-specific deletion of XBP1 attenuates myonuclear accretion by inhibiting myoblast fusion during post-natal growth (**Figure 4.5 F, G**) and overload-induced hypertrophy (**Figure 4.7C-F**). Therefore, increased activation of the transcription factor XBP1 appears to be

an important mechanism to promote myonuclear accretion under multiple physiological conditions.

In addition to myoblast fusion, skeletal muscle increases its size through increasing the rate of protein synthesis in myofibers [44, 194]. Indeed, we have recently reported that pan-inhibition of ER stress using the pharmacological agent, 4-PBA, inhibits the rate of protein synthesis in cultured myotubes [159]. Moreover, there is also the possibility that the inhibition of IRE1/XBP1 can lead to the activation of the other arms of the UPR. Indeed, it is well established that activation of the PERK arm of the UPR inhibits protein synthesis through phosphorylation of eIF2 α [6, 157]. Interestingly, deletion of XBP1 did not have any significant impact on the rate of protein synthesis or activation of Akt/mTOR pathway in skeletal muscle in response functional overload **(Figure 4.7G, H)**.

Our results indicate that XBP1 regulates satellite cell proliferation and fusion in a cell non-autonomous manner as evidenced by the findings that the number of EdU⁺ nuclei within the sarcolemma was significantly reduced in skeletal muscle of XBP1^{mKO} mice compared to XBP1^{f/f} mice during muscle regeneration **(Figure 4.3D)**, post-natal development **(Figure 4.5A, B)**, or overload-induced muscle hypertrophy **(Figure 4.7E)**. Moreover, the deletion of XBP1 led to reduced number of myofibers containing 2 or more nuclei after skeletal muscle injury **(Figure 4.1H)**. Furthermore, shRNA-mediated knockdown of XBP1 inhibited the formation of multinucleated myotubes in primary myoblast cultures **(Figure 4.8A-C)**. It is now established that myoblast fusion involves the increased expression of a number of cell adhesion and transmembrane molecules that accumulate at contact sites between the two myogenic cells during myogenesis [26, 195].

Our results demonstrate that gene expression of Myomaker, a critical protein for myoblast fusion, is inhibited in regenerating skeletal muscle of XBP1^{mkO} mice compared to littermate control mice (**Figure 4.3F**). Similarly, knockdown of XBP1 also reduced the gene expression of Myomaker in cultured myotubes (**Figure 4.8D**). However, it remains to be investigated whether XBP1 directly induces gene expression of Myomaker or it is a result of inhibition of myogenic differentiation.

Recently, XBP1 was shown to regulate the expression of several cytokines/myokines, such as IL-6 and TNF- α , which have previously been shown to induce satellite cell proliferation and fusion during skeletal muscle hypertrophy [156, 181]. It has been suggested that toll-like receptors (TLRs) through activation of myeloid differentiation primary response gene 88 (MyD88) signaling leads to the activation of XBP1, which then induces the gene expression of IL-6 and TNF- α [156]. Indeed, we recently reported that MyD88 promotes myoblast fusion independent of TLRs [154]. Thus, it remains possible that XBP1 is essential for the regulation of important myokines, such as IL-6 and TNF- α , and activation of these myokines in turn stimulates proliferation and fusion of satellite cells. However, a direct link between XBP1 and these myokines is lacking in skeletal muscle.

Recently, Enwere *et al.* have shown that low concentrations of TWEAK cytokine augment the fusion of cultured primary myoblasts, primarily through activating the non-canonical NF- κ B pathway [196]. This is further demonstrated by studies showing that the TWEAK receptor, Fn14, is essential for myotube formation in cultures and for the regeneration of adult skeletal muscle in response to injury [197, 198]. Interestingly, we found that knockdown of XBP1 also inhibits the gene expression of TWEAK in cultured

myoblasts (**Figure 4.8D**). Although not statistically significant, overexpression of sXBP1 showed a trend towards an increase in the mRNA levels of TWEAK in cultured myoblasts (**Figure 4.9D**) suggesting that XBP1 promotes myoblast fusion, at least in part, through increasing the levels of TWEAK.

In summary, the results of the present chapter suggest that XBP1-mediated signaling in myofibers promote satellite cell proliferation and fusion in a non-cell autonomous manner. XBP1 may be important for increased production of myokines responsible for the proliferation and fusion of satellite cells. More investigations are needed to further understand the mechanisms especially gene network that XBP1 regulates during skeletal muscle formation and growth.

FIGURE 4.1

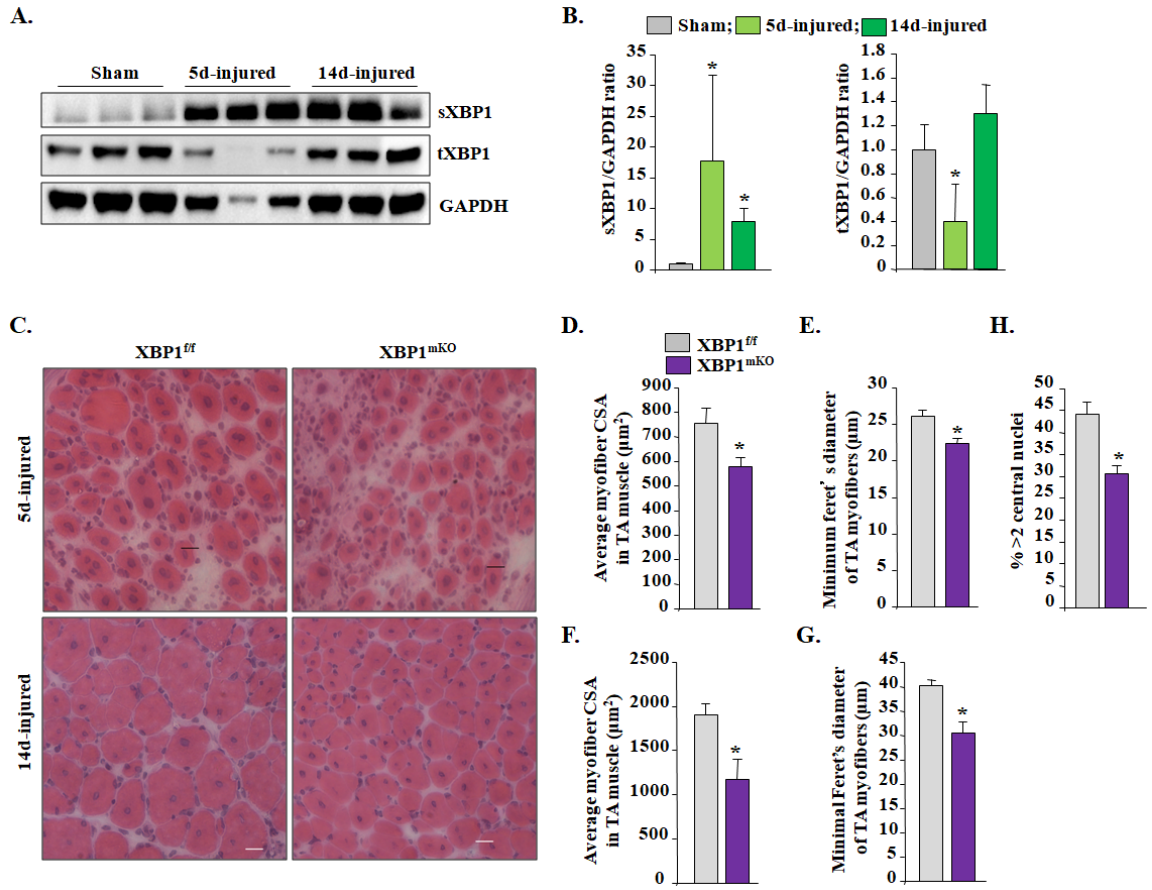


FIGURE 4.1: XBP1 is required for skeletal muscle regeneration. TA muscle of 3-month old mice C57BL/6J mice was injured by intramuscular injection of 1.2% BaCl₂ solution. The muscle was isolated at day 5 or 14 and analysed by performing Western blot. **(A)** Immunoblots and **(B)** densitometry quantification of sXBP1, tXBP1, and GAPDH in control and injured TA muscle. N=3/group. 3-month old XBP1^{ff} and XBP1^{mKO} mice were injected with 1.2% BaCl₂ in TA muscle and muscle regeneration was studied at day 5 or 14 post-injury. **(C)** Representative photomicrographs of H&E-stained TA muscle sections are presented here. Scale 50µm. Quantification of average **(D)** myofiber CSA, and **(E)** minimal Feret's diameter in 5d-injured TA muscle sections of XBP1^{ff} and XBP1^{mKO} mice. Quantification of average **(F)** myofiber CSA and **(G)** minimal Feret's diameter of TA muscle sections of XBP1^{ff} and XBP1^{mKO} mice at day 14 post-BaCl₂-mediated injury. **(H)** Percentage of myofibers containing 2 or more central nuclei. Error bars represent SD. *p<0.05, values significantly different from corresponding muscle of XBP1^{ff} mice.

FIGURE 4.2

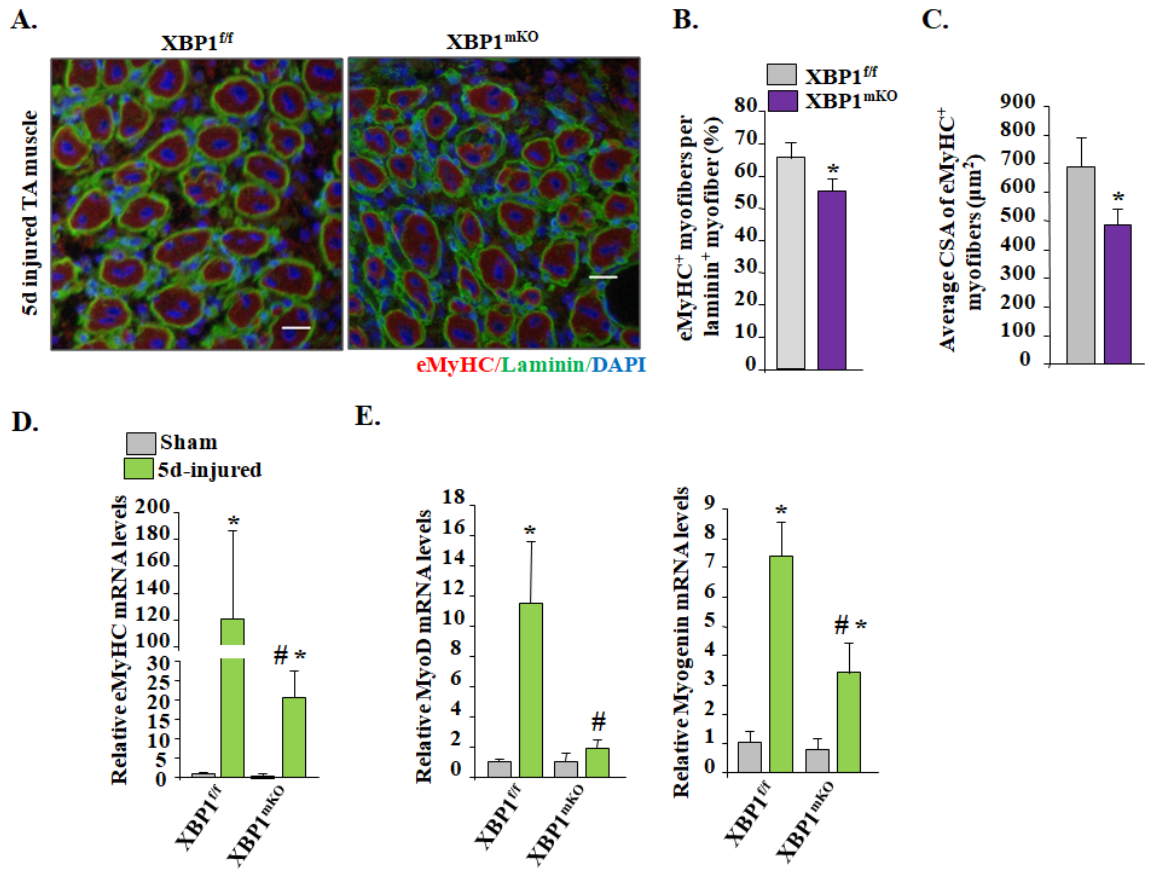


FIGURE 4.2: Genetic deletion of XBP1 reduces levels of eMyHC and myogenic regulatory factors. (A) Representative photomicrographs showing eMyHC⁺ myofibers in 5d-injured TA muscle of XBP1^{ff} and XBP1^{mKO} mice. Scale 50µm. **(B)** Percentage of eMyHC⁺ cells in 5d-injured TA muscle of XBP1^{ff} and XBP1^{mKO} mice. **(C)** Quantification of average CSA of eMyHC⁺ myofibers. Relative mRNA levels of **(D)** eMyHC (i.e. *Myh3*), and **(E)** MyoD and myogenin in control and 5d-injured TA muscle of XBP1^{ff} and XBP1^{mKO} mice. n= 4-6 per group. Error bars represent SD. *p<0.05, values significantly different from XBP1^{ff} mice. #p<0.05, values significantly different from injured XBP1^{ff} mice.

FIGURE 4.3

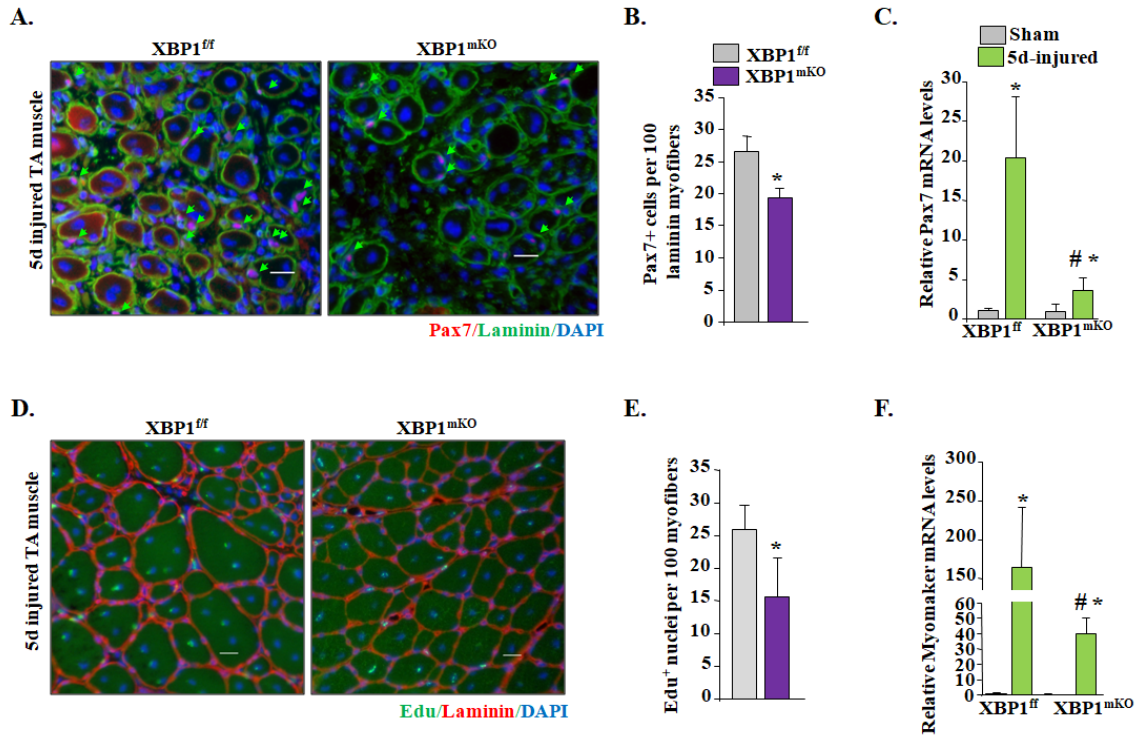


FIGURE 4.3: Myofiber-specific ablation of XBP1 inhibits proliferation and fusion of satellite cells. (A) Representative photomicrographs of Pax7/Laminin/DAPI-stained TA muscle sections of XBP1^{ff} and XBP1^{mKO} mice at day 5 post BaCl₂-mediated injury. **(B)** Quantification of number of Pax7⁺ cells in 5d-injured TA muscle of XBP1^{ff} and XBP1^{mKO} mice. Scale 50μm. **(C)** Relative mRNA levels of Pax7 in control and 5d-injured TA muscle of XBP1^{ff} and XBP1^{mKO} mice. Two days after BaCl₂-mediated TA muscle injury, the mice were given an intraperitoneal injection of EdU and analyzed 12 days later. **(D)** Representative photomicrographs of Edu/ Laminin/DAPI staining of TA muscle sections at day 14 post-injury. Scale 50μm. **(E)** Quantification of number of EdU⁺ nuclei in 14d-injured TA muscle sections of XBP1^{ff} and XBP1^{mKO} mice. **(F)** Relative mRNA levels of Myomaker in control and 5d-injured TA muscle of XBP1^{ff} and XBP1^{mKO} mice. N= 4-6/group. Error bars represent SD. *p<0.05, values significantly different from XBP1^{ff} mice. #p<0.05, values significantly different from injured XBP1^{ff} mice.

FIGURE 4.4

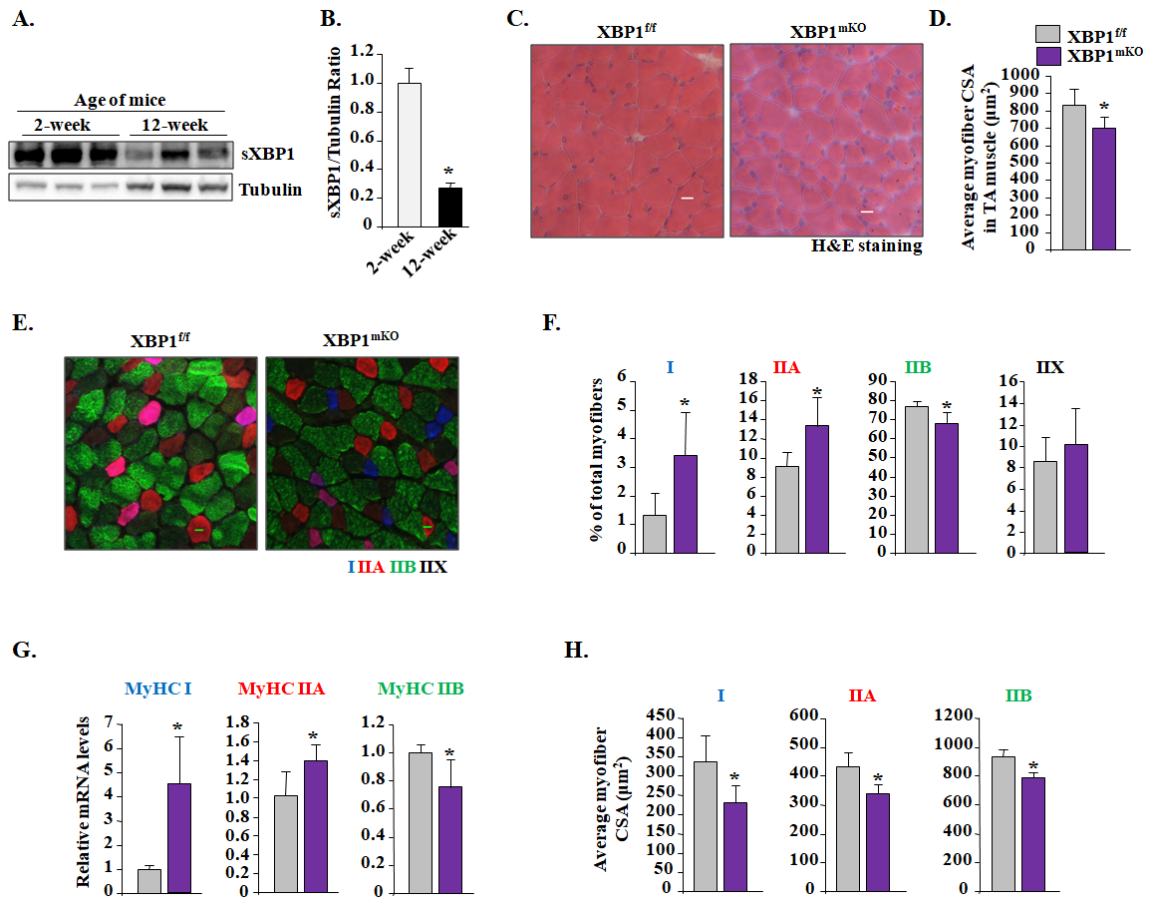


FIGURE 4.4: Genetic deletion of XBP1 inhibits post-natal skeletal muscle growth.

GA muscle of 2-week or 12-week old mice was isolated and processed to measure the levels of sXBP1. **(A)** Representative immunoblot, and **(B)** densitometry quantification of sXBP1 and an unrelated protein, tubulin in GA muscle. N = 3 /group **(C)** Representative photomicrographs of H&E-stained TA muscle sections of 2-week old XBP1^{ff} and XBP1^{mKO} mice. Scale 50µm. **(D)** Quantification of average myofiber CSA in TA muscle of 2-week old XBP1^{ff} and XBP1^{mKO} mice. TA muscle sections prepared from 2-week old XBP1^{ff} and XBP1^{mKO} mice were subjected to triple immunostaining for MyHC I, IIA, and IIB protein. **(E)** Representative photomicrographs of triple-stained whole sections of TA muscle. Scale bar, 50 µm. **(F)** Quantification of the percentage of each fiber type in different groups. **(G)** Relative mRNA levels of MyHC I, MyHC IIA, and MyHC IIB in TA muscle of 2-week old XBP1^{ff} and XBP1^{mKO} mice. **(H)** Average CSA of Type IIA and IIB fibers in the TA muscle of mice in each group. N=5-7/group. Error bars represent SD. *p<0.05, values significantly different from XBP1^{ff} mice.

FIGURE 4.5

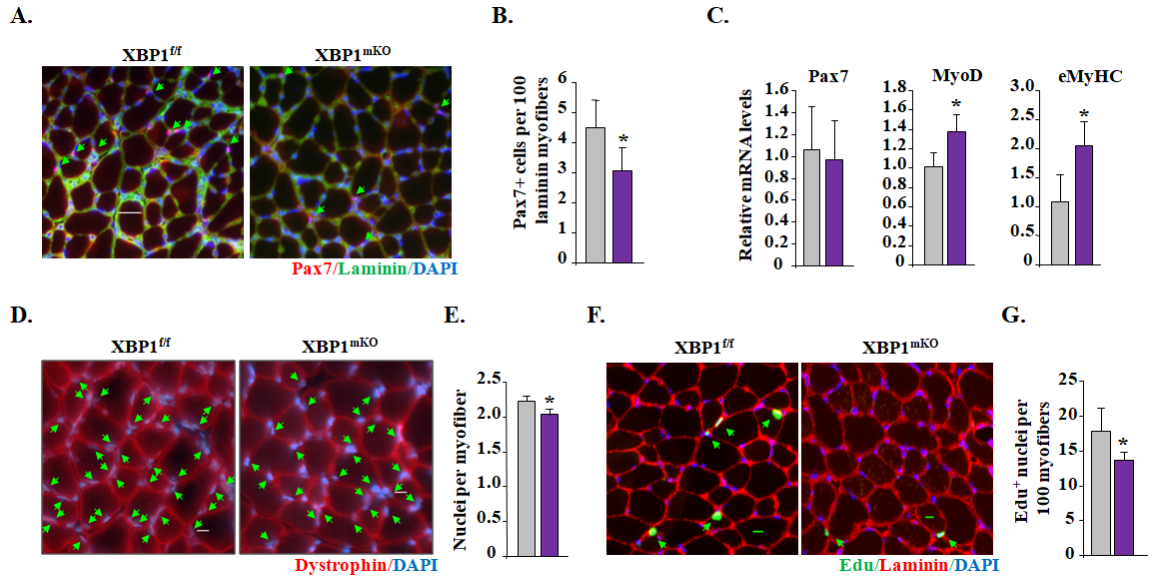


FIGURE 4.5. Genetic deletion of XBP1 reduces proliferation and fusion of satellite cells in 2-week old mice. (A) Representative photomicrographs of TA muscle of XBP1^{f/f} and XBP1^{mKO} mice after staining with anti-Pax7, anti-Laminin, and DAPI. (B) Quantification of number of Pax7⁺ cells in TA muscle of XBP1^{f/f} and XBP1^{mKO} mice. Scale 50µm. (C) Relative mRNA levels of Pax7, MyoD, and eMyHC in skeletal muscle of 2-week old XBP1^{f/f} and XBP1^{mKO} mice (D) Representative photomicrographs of TA muscle sections after staining with anti-dystrophin and DAPI. (E) Quantification of average number of nuclei within the dystrophin-stained myofiber. Scale 50µm. One week old XBP1^{f/f} and XBP1^{mKO} mice were injected with EdU and euthanized at the age of 3 weeks. (F) Representative photomicrographs, and (G) quantification of average number of EdU⁺ nuclei in TA muscle of XBP1^{f/f} and XBP1^{mKO} mice. Scale bar: 50µm. N= 5-7/group. Error bars represent SD. *p<0.05, values significantly different from XBP1^{f/f} mice.

FIGURE 4.6

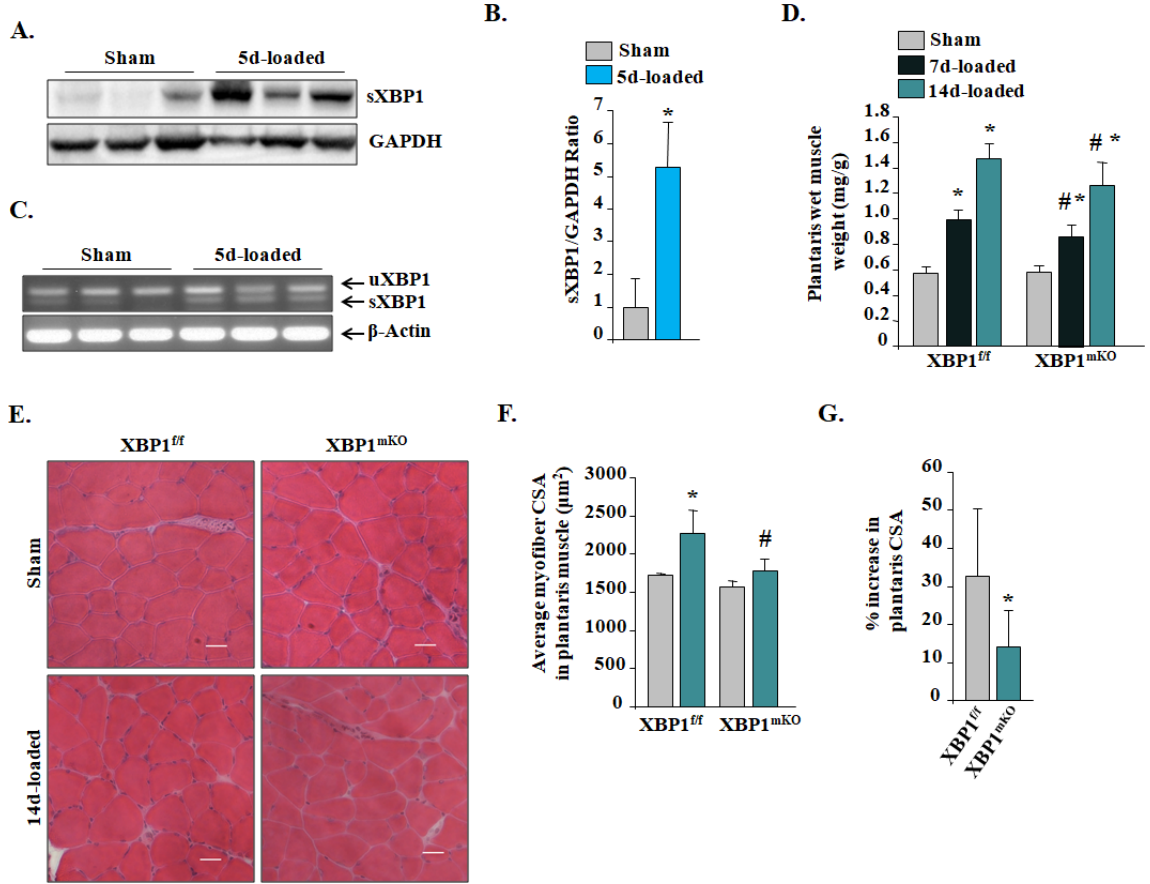


FIGURE 4.6: Targeted ablation of XBP1 inhibits overload-induced muscle

hypertrophy in adult mice. 10-week old C57BL6 mice were subjected to synergistic

ablation (SA) surgery of the GA and soleus muscle. After 5 days, plantaris muscle was

isolated and analysed by performing Western blot. **(A)** Representative immunoblot, and

(B) densitometry quantification of sXBP1 and GAPDH ratio in sham- and 5d-loaded

plantaris muscle. **(C)** Representative agarose gel of semi-quantitative RT-PCR showing

relative amounts of spliced XBP1 (sXBP1) and unspliced XBP1 (uXBP1) and an

unrelated gene β -Actin in sham and 5d-loaded plantaris muscle. N=3/group. **(D)** Wet

weight of plantaris muscle normalized to body weight of XBP1^{ff} and XBP1^{mKO} mice at

7d and 14d after performing SA surgery. **(E)** Representative photomicrographs of H&E-

stained sections of sham- and 7d-loaded plantaris muscle of XBP1^{ff} and XBP1^{mKO} mice.

Scale, 50 μ m. **(F)** Quantification of average fiber CSA in plantaris muscle of XBP1^{ff} and

XBP1^{mKO} mice after 2 weeks of performing SA surgery. **(G)** Quantification of percentage

increase in myofiber CSA after 2 weeks of functional overload in XBP1^{ff} and XBP1^{mKO}

mice. N= 8-10/group. Error bars represent SD. *p<0.05, values significantly different

from XBP1^{ff} mice. #p<0.05, values significantly different from loaded muscle of XBP1^{ff}

mice.

FIGURE 4.7

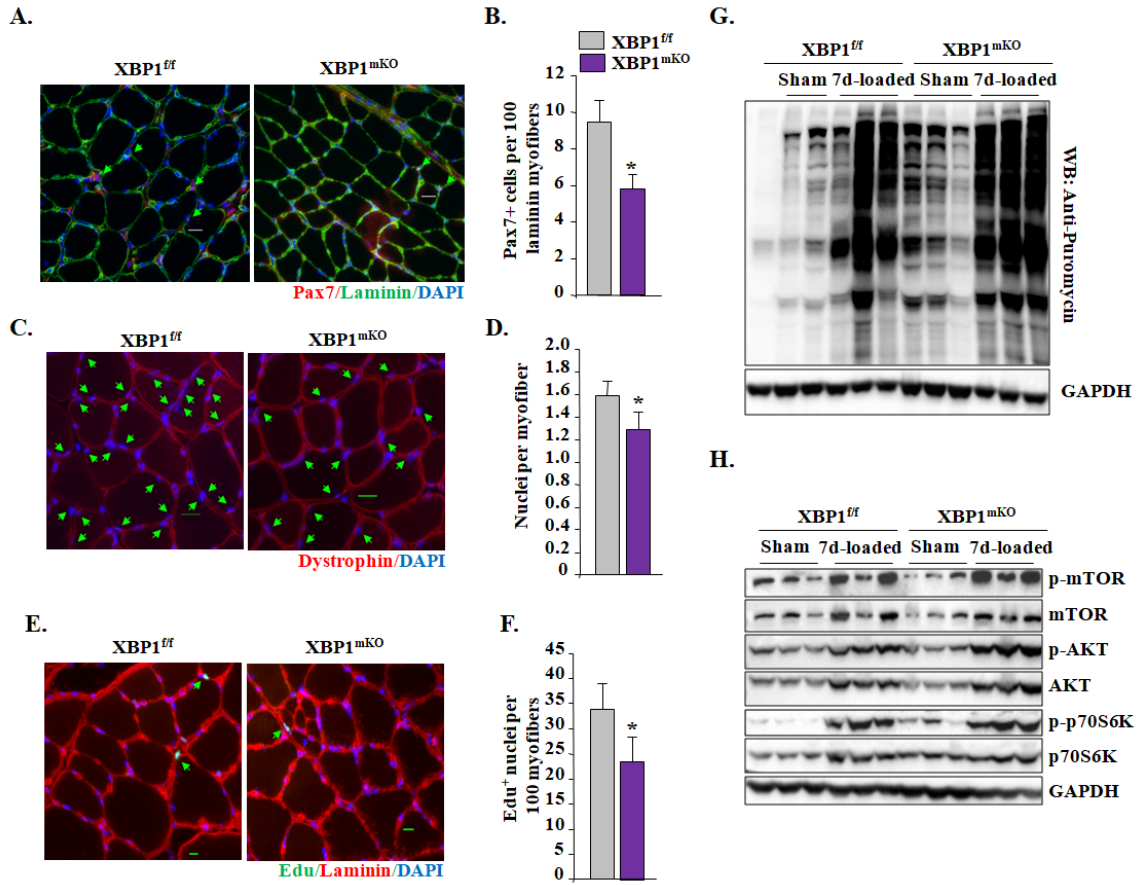


FIGURE 4.7: Myofiber-specific deletion of XBP1 inhibits satellite cell proliferation and fusion during functional overload. (A) Representative photomicrographs of 14d-loaded plantaris muscle sections of XBP1^{f/f} and XBP1^{mKO} mice after staining with anti-Pax7, anti-laminin, and DAPI. **(B)** Quantification of number of Pax7⁺ cells in 14d-loaded plantaris muscle of XBP1^{f/f} and XBP1^{mKO} mice. Scale 50μm. **(C)** Representative photomicrographs of 14d-loaded plantaris muscle sections after staining with anti-dystrophin and DAPI. **(D)** Quantification of average number of nuclei within anti-dystrophin-stained myofibers in plantaris muscle of XBP1^{f/f} and XBP1^{mKO} mice. Scale bar, 50μm. 10-week old XBP1^{f/f} and XBP1^{mKO} mice were subjected to synergistic ablation surgery. After 2d, the mice were given i.p. injection of EdU and number of EdU⁺ nuclei was measured 12d later. **(E)** Representative photomicrographs of 14d-loaded plantaris muscle sections after staining for EdU, anti-laminin, and DAPI. Scale bar: 50μm. **(F)** Quantification of number of EdU⁺ nuclei in 14d-loaded plantaris muscle of XBP1^{f/f} and XBP1^{mKO} mice. N=5-7/group. **(G)** Western Blot analysis demonstrate the levels of puromycin-tagged protein in sham (S) or 14d-overloaded (O) plantaris muscle of XBP1^{f/f} and XBP1^{mKO} mice. **(H)** Western Blot analysis of p-mTOR, mTOR, p-AKT, AKT, p-p70S6K, p70S6K, and unrelated protein GAPDH in sham (S) or 14d-overloaded (O) plantaris muscle of XBP1^{f/f} and XBP1^{mKO} mice. N= 3-4/group. Error bars represent SD. *p<0.05, values significantly different from XBP1^{f/f} mice.

FIGURE 4.8

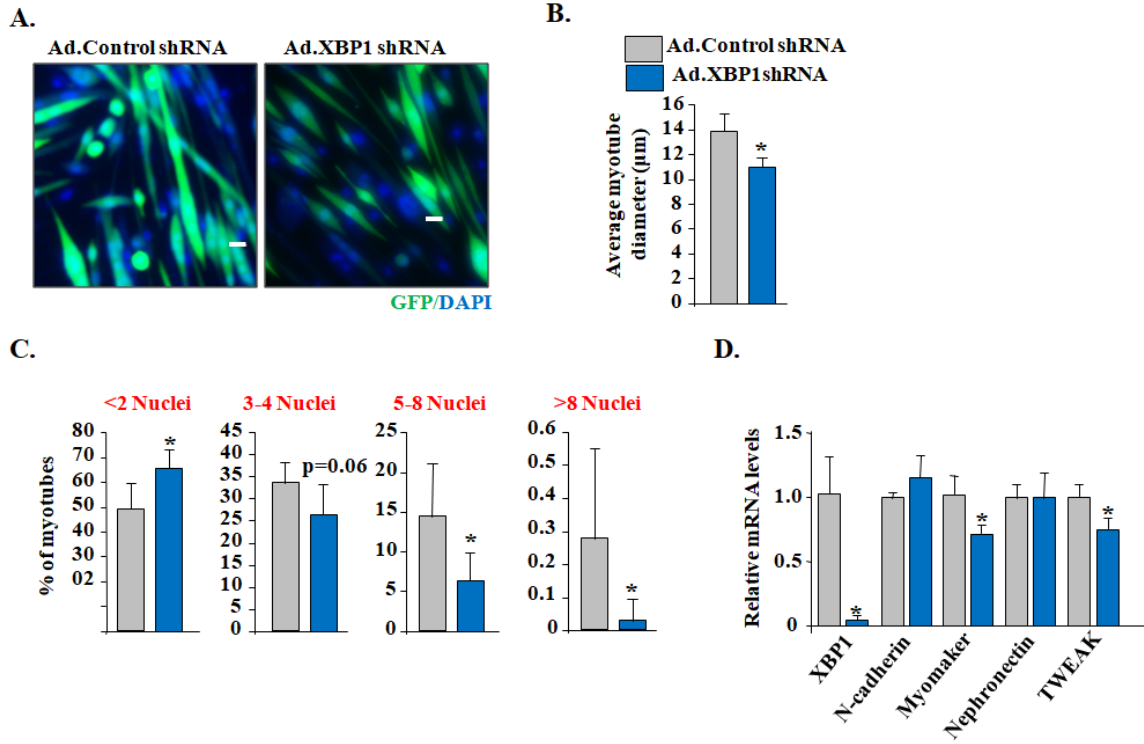


FIGURE 4.8: Knockdown of XBP1 inhibits myotube formation in cultured myoblasts. Primary myoblasts were incubated in differentiation medium (DM) for 24h. The cells were then transduced with adenoviral vectors expressing scrambled (i.e. control) or XBP1 shRNA and incubated in DM for additional 48h. **(A)** Representative photomicrographs adenoviral transduced (i.e. GFP⁺) myotubes after staining with DAPI. Scale bar: 50µm. **(B)** Average myotube diameter in control and XBP1 shRNA-expressing cultures. **(C)** Percentage of myotubes containing indicated number of nuclei in control and XBP1 shRNA-expressing cultures. **(D)** Relative mRNA levels of XBP1, N-cadherin, Myomaker, Nephronectin, and TWEAK in control and XBP1 shRNA-expressing cultures. N= 4-6/group. Error bars represent SD. *p<0.05, values significantly different from scrambled shRNA-expressing myotubes.

FIGURE 4.9

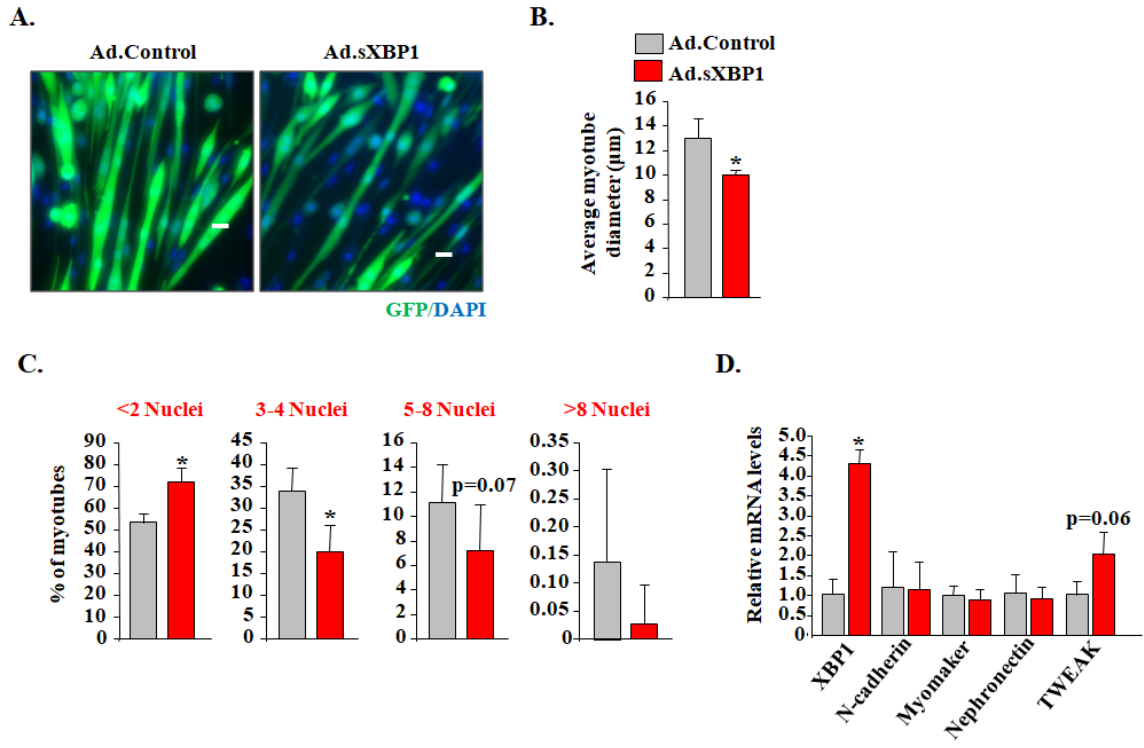


FIGURE 4.9: Overexpression of XBP1 inhibits fusion of cultured myoblasts. Primary myoblasts were incubated in DM for 24h followed by addition of adenoviral vectors expressing GFP only or GFP along with sXBP1 cDNA. The cells were then incubated in DM for an additional 48 h. **(A)** Representative photomicrographs of GFP-expressing myotubes co-stained with DAPI. Scale bar: 50 μ m. **(B)** Average myotube diameter of control and sXBP1-overexpressing cultures. **(C)** Percentage of myotubes containing various amounts of nuclei in control and sXBP1-overexpressing myogenic cultures. **(D)** Relative mRNA levels of XBP1, N-cadherin, Myomaker, Nephronectin, and TWEAK in control and sXBP1-overexpressing cultures. N= 4-6/group. Error bars represent SD. *p<0.05, values significantly different from cultures transduced with Ad.Control vector.

CHAPTER 5

CONCLUSIONS AND FUTURE WORK

This chapter summarizes the work presented in this dissertation and discusses its implications in understanding the role of ER stress and the Unfolded Protein Response (UPR) in the regulation of skeletal muscle physiology and pathophysiology. It also highlights the significance of the findings obtained throughout this dissertation while acknowledging the limitations in implementing such findings in future research.

5.1 Review of Dissertation. Skeletal muscle is a highly plastic tissue that can be adaptable to a number of different cellular stresses. The endoplasmic reticulum (ER) is an organelle that is essential for the folding and trafficking of various proteins in the mammalian cell. In conditions of increased load of unfolded/misfolded proteins, the ER initiates the UPR to aid in the proper folding and/or removal of the misfolded proteins. However, under conditions of unmitigated ER stress, the activation of the UPR can lead to inflammation and cell death. Prior to the work in this dissertation, there were only few reports which suggested that the UPR get activated in specific physiological and pathological conditions. There was also some studies which implicated the role of ER stress and UPR pathways in the regulation of skeletal myogenesis (reviewed in chapter 1). However, the role of individual arms of the UPR in the regulation of skeletal muscle

mass and function was largely unknown. We were the first to report activation of all the three arms of the UPR in skeletal muscle of mice during cancer-induced cachexia. To obtain insights into the role of ER stress and UPR pathways, we first used a pharmacological approach followed by generation and use of genetic mouse models. This dissertation highlights the importance of physiological levels of ER stress and the role of the IRE1 α /XBP1 pathway in skeletal muscle homeostasis. Our investigations revealed a dual role of the IRE1 α /XBP1 arm of the UPR in the regulation of skeletal muscle mass in cancer-induced cachexia and skeletal muscle regeneration and overload-induced myofiber growth. It also suggests that distinct arms of the UPR may play different roles in the regulation of skeletal mass and that the function of each arm may depend on the underlying condition and duration of activation (i.e. transient vs chronic).

Recent studies have demonstrated that the markers of ER stress are activated in skeletal muscle in multiple catabolic states, including starvation and cancer cachexia. As discussed in Chapter 2, the original goal of these investigations was to determine the role of ER stress-induced UPR pathways in skeletal muscle mass, specifically cancer-induced cachexia. Because unmitigated ER stress leads to inflammation and cell death, the original hypothesis was that the activation of UPR is detrimental to skeletal muscle health and contributes to loss of muscle mass in tumor-bearing mice. Specifically, it was hypothesized that inhibition of ER stress via chemical chaperone 4-PBA would attenuate skeletal muscle wasting during cancer cachexia. Contrary to our hypothesis, our results demonstrated that pan-inhibition of the UPR through chronic administration of 4-PBA resulted in a loss of skeletal muscle mass and strength both in naïve and tumor-bearing mice. Our findings revealed that inhibition of the ER stress/UPR in naïve mice resulted in

the activation of both ubiquitin-proteasome system and autophagy. Intriguingly, these proteolytic mechanisms were inhibited in tumor-bearing mice after treatment with 4-PBA but still there was loss of muscle mass. Our findings reveal that several other mechanisms such as activation of AMPK and repression of Akt/mTOR signaling may be responsible for the loss of muscle mass in naïve as well as LLC tumor-bearing mice upon pan-inhibition of ER stress using 4-PBA. While these results suggested that certain levels of activation of the UPR is essential for maintaining skeletal muscle health in naïve as well as catabolic states, they also raised the possibility that different arms of the UPR may have distinct roles in the regulation of skeletal muscle mass. It is possible that specific arms of the UPR may be promoting muscle wasting, whereas others may be antagonizing the loss of muscle mass in catabolic states.

A pitfall of the experiments in Chapter 2 is that we used 4-PBA, a pharmacological agent that is known to inhibit ER stress and hence the inhibition of all the three arms of the UPR. Furthermore, since 4-PBA is known to modulate the activation of several other unrelated pathways, there is always a possibility that 4-PBA induces the loss of skeletal muscle mass through some other mechanisms independent of inhibition of ER stress. Additional experimentation that involves other pharmacological inhibitors of ER stress, such as Taurine-conjugated ursodeoxycholic acid (TUDCA), would further help understanding the role of ER stress in the regulation of skeletal muscle mass. Moreover, pharmacological compounds targeting specific arms of the UPR have been identified. Future studies will investigate the effects of such compounds in the animal models of skeletal muscle atrophy and hypertrophy.

The findings of Chapter 2 also highlighted the need to use genetic mouse models to tease out the roles of individual arms of the UPR. Thus, in Chapter 3, we investigated the role of IRE1/XBP1 arm of the UPR in the regulation of skeletal mass in tumor-bearing mice. Since TLRs and MyD88-mediated signaling contributes to the loss of skeletal muscle mass during cancer-induced cachexia, it was investigated whether UPR pathways are activated through the TLR/MyD88 signaling axis. Indeed, our findings suggested that ablation of MyD88 inhibits the activation of the UPR in skeletal muscle of LLC tumor-bearing mice. Since the XBP1 transcription factor is involved in gene expression of many inflammatory cytokines, which are known to cause muscle wasting, we focused our next work on studying the role of IRE1/XBP1 arm of the UPR in regulation of skeletal muscle mass in LLC tumor-induced cachexia. Specifically, it was hypothesized that genetic deletion of MyD88 would attenuate skeletal muscle wasting during cancer-bearing mice through inhibiting the IRE1/XBP1 signaling axis. Indeed, results showed that deletion of MyD88 in skeletal muscle prevented the loss of skeletal muscle mass in LLC tumor-bearing mice. Our investigations further showed that genetic ablation of XBP1, specifically in differentiated skeletal muscle, rescues the loss of myofiber diameter during cancer-induced cachexia in adult mice. Additionally, our findings revealed that deletion of XBP1 in skeletal muscle reduces the gene expression of classical pro-inflammatory cytokines IL-6, TNF- α , and TWEAK and several components of ubiquitin-proteasome system and autophagy. Finally, the experimentation in chapter 3 revealed that the forced expression of sXBP1 alone is sufficient to induce atrophy and stimulate gene expression of pro-inflammatory cytokines in cultured myotubes.

Conversely, shRNA-mediated knockdown of XBP1 prevents myotube atrophy in response to LLC tumor-derived factors.

Although the findings of Chapter 3 suggested a role for the IRE1 α /XBP1 pathway, it does not provide detailed mechanisms of action of XBP1 in skeletal muscle wasting. Although not in skeletal muscle, recent findings have demonstrated that XBP1 binds to the promoter regions of the pro-inflammatory cytokines IL-6 and TNF- α in macrophages. Therefore, it is possible that activation of XBP1 directly induces the gene expression of pro-inflammatory cytokines which in turn increases the activity of various proteolytic pathways through activation of catabolic signaling pathways, including the p38 MAPK and NF- κ B. It is notable that during cancer-induced skeletal muscle wasting, UPR pathways are stimulated through the TLR/MyD88 axis and potentially independent of the classical ER stress response. Thus, the conclusions of Chapter 2 that ER stress and its activation of the UPR is necessary to maintain skeletal muscle homeostasis could still be accurate. This is further supported by our unpublished results demonstrating that targeted inducible ablation of PERK leads to skeletal muscle atrophy in adult mice.

For all our studies, we used lower extremity musculature when examining skeletal muscle atrophy during cancer-induced cachexia. However, in addition to extremity muscles, cachexia also has a robust effect on other muscles, including diaphragm and cardiac muscle, leading respiratory and cardiac failure in cancer patients. Considering the MCK promoter is expressed in all skeletal muscle and some cardiac muscle, a more comprehensive evaluation of all muscle types is needed in future experiments. It is also known that different fiber types show differential sensitivity to specific pathophysiologic atrophy signals. Specifically, type I fibers are more sensitive to inactivity, microgravity,

and denervation-induced atrophy, whereas type II fibers are more vulnerable in conditions of cancer cachexia, diabetes, chronic heart failure, and aging. Importantly, our experiments suggest that inhibition of MyD88 or XBP1 attenuates tumor-induced atrophy in both oxidative and glycolytic fibers.

A potential limitation to our experiments in chapter 3 is not having non-cachectic tumor as a control. Specifically, as a control for LLC tumor-bearing mice, the mice were injected with saline alone. This may not be the best control as the engraftment of cells by themselves can cause systematic effect other than cachexia. A more suitable control would have been to implant tumor cells that do not cause muscle wasting. However, it is important to note that the loss of muscle mass in LLC tumor-bearing mice does not occur until up to two weeks of implantation of LLC cells. Therefore, any acute effect (if any) of the injection of cells would be considered minor.

While the findings in Chapter 3 suggested that the IRE1 α /XBP1 arm of the UPR mediates muscle loss during cancer-induced cachexia, it did not address the potential physiological role of XBP1 in regulation of muscle growth and regeneration. Therefore, the focus of Chapter 4 was to further investigate the role of XBP1 in the regulation of skeletal muscle development during post-natal period and myofiber regeneration and overload-induced hypertrophy in adult mice. The findings of this chapter revealed that XBP1 promotes skeletal muscle regeneration and growth. Indeed, this investigation determined that myofiber-specific deletion of XBP1 attenuates the proliferation and fusion of activated satellite cells in a cell non-autonomous manner to myofibers during muscle regeneration, post-natal development, and overload-induced myofiber growth. Intriguingly, skeletal muscle-specific deletion of XBP1 had no effect on the rate of

protein synthesis during overload-induced hypertrophy. Our findings further revealed that knockdown of XBP1 in vitro inhibits myoblast fusion potentially through reducing the gene expression of some profusion molecules, such as Myomaker and TWEAK. Our results also showed that the targeted deletion of XBP1 did not affect the total number of fibers at 2-week and 12-week of age mice suggesting that while XBP1 promotes satellite cell proliferation and fusion, it does not regulate the number of myofibers in skeletal muscle.

Chapter 3 suggests that in physiological conditions XBP1 promotes skeletal muscle growth through augmenting the proliferation and fusion of satellite cells. Since XBP1 was ablated in myofiber only but it reduced the abundance of satellite cells in skeletal muscle, XBP1 appears to promote skeletal muscle growth in a non-cell autonomous manner. However, the XBP1-induced molecules in myofibers that augment the proliferation of satellite cells in a paracrine manner remain to be identified. Insulin-like growth factor-1 (IGF-1), hepatocyte growth factor (HGF), nitric oxide (NO), fibroblast growth factors (FGFs), and some inflammatory cytokines including TWEAK are some of the candidates which may be regulated through XBP1-dependent manner and responsible for the increased proliferation of satellite cells in skeletal muscle. Future studies will tease out these potential mechanisms.

It is still not clear whether the activation of XBP1 during skeletal muscle growth and regeneration is through classical ER stress or due to the activation of other pathways, such as TLR-mediated signaling. Skeletal muscle growth involves a robust increase in the rate of protein synthesis. Thus it could be deduced that this increase in protein synthesis leads to the accumulation of misfolded proteins and causes ER stress. Indeed, ER stress-

induced UPR pathways have been implicated in proliferation and differentiation of multiple cell types in various organs. Thus, the activation of the IRE1/XBP1 arm of the UPR during skeletal muscle growth appears to be a result of ER stress, not due to potential non-canonical pathways.

Collectively, the results of this dissertation reveal that the UPR pathways have an important role in the regulation of muscle mass in both physiological and pathophysiological conditions. Specifically, ER stress and the classical UPR pathways are important to maintain skeletal muscle homeostasis and complete inhibition of the UPR is deleterious to skeletal muscle health both in naïve conditions and during cancer-induced cachexia. The dissertation also revealed some of the arms of the UPR can be activated independent of ER stress in models of cancer cachexia. We provided initial evidence that TLR/MyD88 signaling mediates the activation of the IRE1/XBP1 pathway in LLC-tumor bearing mice. Moreover, hyper-activation of the IRE1/XBP1 pathway leads to muscle wasting potentially through increasing the inflammatory milieu. In contrast, during muscle development and growth, XBP1 is activated potentially by ER stress to augment the proliferation and fusion of muscle progenitor cells to myofibers. Thus, depending on the stimuli and underlying condition, XBP1 can act as a friend or foe for skeletal muscle.

5.2 Scientific contribution and future implementation. The research within this dissertation provides initial evidence about the role of ER stress and the IRE1/XBP1 arm of the UPR in the regulation of skeletal muscle mass in conditions of skeletal muscle growth and atrophy. While skeletal muscle is not a major secretory organ where ER

stress is quite common, the findings in the dissertation highlight that the UPR is induced in skeletal muscle in multiple physiological and pathophysiological conditions. The dissertation also provides the potential signaling mechanisms and cross-talk through which the UPR regulates skeletal muscle mass. It is interesting to note that targeted deletion of XBP1 inhibits skeletal muscle wasting during cancer cachexia, whereas pan-inhibition of the UPR via 4-PBA promotes skeletal muscle atrophy. These findings highlight that other arms of the UPR may have an opposite effect than the IRE1/XBP1 arm during cancer-induced cachexia. Specifically, it is possible that the inhibition of ATF6 or PERK arm of the UPR may cause skeletal muscle wasting similar to that observed using 4-PBA. Future studies examining the roles of PERK and ATF6 and other components of the UPR is necessary to further our understanding of involvement and mechanisms of action of the UPR in skeletal muscle homeostasis.

The results in Chapter 3 indicate that XBP1 promotes the gene expression of pro-inflammatory cytokines and the components of the UPR. However, a direct link between XBP1 and gene expression was not deduced. Further investigations including chromatin immunoprecipitation (ChIP) assay would be necessary to determine if sXBP1 can directly bind to the promoter region of the affected genes in catabolic conditions. Since XBP1 appears to promote gene expression of inflammatory molecules in chronic disease states, such as cancer, it is possible that activation of XBP1 is a mechanism for inflammatory immune response in other skeletal muscle disorders. For example, Duchenne muscular dystrophy (DMD) is a disease in which the dystrophin protein is non-functional in skeletal muscle leading to multiple rounds of degeneration and regeneration. Levels of various pro-inflammatory cytokines are increased and contribute

to dystrophinopathy. On the contrary, XBP1 is also essential for skeletal muscle regeneration and its inhibition may block the regeneration of myofibers in dystrophic muscle. Specific experiments are required to understand whether muscle-specific inhibition of XBP1 improves or worsen dystrophic phenotype. Deletion of XBP1 in myofibers of the mdx mouse model of DMD would facilitate better understanding of the role of XBP1 in the regulation of inflammatory signaling and myofiber regeneration.

The findings of Chapter 3 highlight that deletion of XBP1 prevents the loss of muscle mass in LLC tumor-bearing mice potentially through activation of the TLR/MyD88 signaling axis. Furthermore, Chapter 3 reveals that treatment of C2C12 myotubes with known tumor-secreted molecule, Hsp70, can induce activation of the UPR. However, it is not known whether the UPR are activated in other models of skeletal muscle atrophy not induced by tumor-secreted molecules. Further investigations are needed to determine whether deletion of XBP1, or other molecules of the UPR, can inhibit skeletal muscle loss during conditions such as denervation and starvation are necessary.

Lastly, work has unveiled MyD88 as a potential upstream activator of XBP1 in skeletal muscle during cancer-induced cachexia. However, it remains unclear whether the activation of XBP1 during skeletal muscle growth and regeneration is also driven by common molecular regulators or is mediated through distinct signaling events. Precise delineation of such mechanisms represents an area of forthcoming investigations.

5.3 Limitations of future implementation. This dissertation concludes in identifying a role of ER stress and the UPR in skeletal muscle homeostasis. Specifically, MyD88

mediates the activation of the IRE1/XBP1 to promote skeletal muscle wasting during cancer-induced cachexia. Moreover, possibly when activated by ER stress, IRE1/XBP1 signaling is important for proliferation and fusion of satellite cells during skeletal muscle regeneration, development, and growth. While muscle-specific XBP1-knockout mice were used to understand the role of XBP1 in skeletal muscle, some of the effects could be attributed to the potential role of XBP1 in skeletal muscle development. Specifically, the muscle creatine kinase (MCK)-Cre line was used to delete XBP1 in skeletal muscle. Since MCK is expressed early on in development, prolonged deletion of XBP1 could have a compensatory effect on other signaling mechanisms. Thus, use of an inducible muscle-specific Cre line, such as the HSA-MCM, would allow for a more accurate understanding of role of XBP1 in adult skeletal muscle. Additionally, the use of genetic manipulation through mice may have relatively low translational relevance. Therefore, investigating the effects of pharmacological inhibition of the splicing of XBP1 might ultimately be essential to developing XBP1-based novel therapies to prevent skeletal muscle wasting. However, the clinical significance of inhibition or deletion of XBP1 on skeletal muscle homeostasis remains enigmatic. ER stress and the UPR were initially viewed as a pathological events that occurred downstream of primary etiology. However, studies using genetically modified animals and small molecules that selectively target specific mediators have revealed that the UPR can have distinct outcomes in different diseases and when different physiological components are manipulated. Moreover, the UPR can have opposite effects depending on the disease stage. Initially, the UPR may work as a pro-survival factor to sustain proteostasis, but its chronic activation can lead to cell damage during late symptomatic phases. The results of the present study also

suggests that while the inhibition of XBP1 may be beneficial in patients with cachexia, it could also become detrimental to them during recovery if the tumor is resolved.

In addition, it is important to investigate whether the inhibition of IRE1/XBP1 arm of the UPR can also ameliorate skeletal muscle wasting in other conditions such as disuse, aging, diabetes, chronic heart failure or does it only promote atrophy when stimulated by molecules secreted from tumors. Moreover, while the dissertation focused on XBP1, it remains to be determined whether skeletal muscle-specific inhibition of IRE1 would produce similar effects on skeletal muscle mass in catabolic conditions and in response to injury. Addressing such questions would elevate the significance of the findings acquired throughout this dissertation.

While our studies provided initial evidence that ER stress and the UPR regulate skeletal muscle mass, there are also several outstanding questions. For example, it is of critical importance to examine the role of other arms of the UPR in skeletal muscle physiology and various disease conditions using genetic mouse models. Similarly, the role of the downstream effectors of the UPR in skeletal muscle needs to be investigated using molecular and genetic approaches. It is also increasingly evidenced that some of the components of UPR can be activated independent of ER stress and modulate the activity of other signaling pathways. Therefore, signaling cross-talk of UPR with other intracellular pathways that are involved in regulation of skeletal muscle mass, needs to be further investigated. Finally, the role of UPR in metabolic perturbations in skeletal muscle including oxidative phosphorylation should be investigated using molecular, genetic, and proteomics approaches. Nevertheless, this dissertation and available literature provides strong evidence that ER stress and the UPR pathways regulate skeletal

muscle health and disease. With the availability of genetic mouse models and specific inhibitors and activators of various components of the UPR, there is a renewed interest towards understanding the role and mechanisms of action of the UPR in skeletal muscle biology.

REFERENCES

1. Bohnert KR, McMillan JD, Kumar A: **Emerging roles of ER stress and unfolded protein response pathways in skeletal muscle health and disease.** *J Cell Physiol* 2017.
2. Welihinda AA, Tirasophon W, Kaufman RJ: **The cellular response to protein misfolding in the endoplasmic reticulum.** *Gene Expr* 1999, **7**(4-6):293-300.
3. Isler JA, Maguire TG, Alwine JC: **Production of infectious human cytomegalovirus virions is inhibited by drugs that disrupt calcium homeostasis in the endoplasmic reticulum.** *J Virol* 2005, **79**(24):15388-15397.
4. Pyrko P, Kardosh A, Liu YT, Soriano N, Xiong W, Chow RH, Uddin J, Petasis NA, Mircheff AK, Farley RA *et al*: **Calcium-activated endoplasmic reticulum stress as a major component of tumor cell death induced by 2,5-dimethyl-celecoxib, a non-coxib analogue of celecoxib.** *Mol Cancer Ther* 2007, **6**(4):1262-1275.
5. Wang M, Kaufman RJ: **The impact of the endoplasmic reticulum protein-folding environment on cancer development.** *Nat Rev Cancer* 2014, **14**(9):581-597.
6. Wu J, Kaufman RJ: **From acute ER stress to physiological roles of the Unfolded Protein Response.** *Cell Death Differ* 2006, **13**(3):374-384.
7. Hetz C: **The unfolded protein response: controlling cell fate decisions under ER stress and beyond.** *Nat Rev Mol Cell Biol* 2012, **13**(2):89-102.
8. Harding HP, Zhang Y, Ron D: **Protein translation and folding are coupled by an endoplasmic-reticulum-resident kinase.** *Nature* 1999, **397**(6716):271-274.
9. Ma Y, Brewer JW, Diehl JA, Hendershot LM: **Two distinct stress signaling pathways converge upon the CHOP promoter during the mammalian unfolded protein response.** *J Mol Biol* 2002, **318**(5):1351-1365.
10. Ron D, Walter P: **Signal integration in the endoplasmic reticulum unfolded protein response.** *Nat Rev Mol Cell Biol* 2007, **8**(7):519-529.

11. Flamment M, Hajduch E, Ferre P, Fougelle F: **New insights into ER stress-induced insulin resistance.** *Trends Endocrinol Metab* 2012, **23**(8):381-390.
12. Tirasophon W, Welihinda AA, Kaufman RJ: **A stress response pathway from the endoplasmic reticulum to the nucleus requires a novel bifunctional protein kinase/endoribonuclease (Ire1p) in mammalian cells.** *Genes Dev* 1998, **12**(12):1812-1824.
13. Haze K, Yoshida H, Yanagi H, Yura T, Mori K: **Mammalian transcription factor ATF6 is synthesized as a transmembrane protein and activated by proteolysis in response to endoplasmic reticulum stress.** *Mol Biol Cell* 1999, **10**(11):3787-3799.
14. Mollereau B, Manie S, Napoletano F: **Getting the better of ER stress.** *J Cell Commun Signal* 2014, **8**(4):311-321.
15. van Galen P, Kreso A, Mbong N, Kent DG, Fitzmaurice T, Chambers JE, Xie S, Laurenti E, Hermans K, Eppert K *et al*: **The unfolded protein response governs integrity of the haematopoietic stem-cell pool during stress.** *Nature* 2014, **510**(7504):268-272.
16. Bentzinger CF, Wang YX, Rudnicki MA: **Building muscle: molecular regulation of myogenesis.** *Cold Spring Harb Perspect Biol* 2012, **4**(2).
17. Buckingham M, Bajard L, Chang T, Daubas P, Hadchouel J, Meilhac S, Montarras D, Rocancourt D, Relaix F: **The formation of skeletal muscle: from somite to limb.** *J Anat* 2003, **202**(1):59-68.
18. Olson EN: **Interplay between proliferation and differentiation within the myogenic lineage.** *Dev Biol* 1992, **154**(2):261-272.
19. Fidzianska A, Goebel HH: **Human ontogenesis. 3. Cell death in fetal muscle.** *Acta Neuropathol* 1991, **81**(5):572-577.
20. Nakanishi K, Sudo T, Morishima N: **Endoplasmic reticulum stress signaling transmitted by ATF6 mediates apoptosis during muscle development.** *J Cell Biol* 2005, **169**(4):555-560.
21. Nakanishi K, Dohmae N, Morishima N: **Endoplasmic reticulum stress increases myofiber formation in vitro.** *FASEB J* 2007, **21**(11):2994-3003.
22. Alter J, Bengal E: **Stress-induced C/EBP homology protein (CHOP) represses MyoD transcription to delay myoblast differentiation.** *PLoS One* 2011, **6**(12):e29498.

23. Blais A, Tsikitis M, Acosta-Alvear D, Sharan R, Kluger Y, Dynlacht BD: **An initial blueprint for myogenic differentiation.** *Genes Dev* 2005, **19**(5):553-569.
24. Acosta-Alvear D, Zhou Y, Blais A, Tsikitis M, Lents NH, Arias C, Lennon CJ, Kluger Y, Dynlacht BD: **XBP1 controls diverse cell type- and condition-specific transcriptional regulatory networks.** *Mol Cell* 2007, **27**(1):53-66.
25. Relaix F, Zammit PS: **Satellite cells are essential for skeletal muscle regeneration: the cell on the edge returns centre stage.** *Development* 2012, **139**(16):2845-2856.
26. Yin H, Price F, Rudnicki MA: **Satellite cells and the muscle stem cell niche.** *Physiological reviews* 2013, **93**(1):23-67.
27. Xiong G, Hindi SM, Mann AK, Gallot YS, Bohnert KR, Cavener DR, Whittimore SR, Kumar A: **The PERK arm of the unfolded protein response regulates satellite cell-mediated skeletal muscle regeneration.** *Elife* 2017, **6**.
28. Zismanov V, Chichkov V, Colangelo V, Jamet S, Wang S, Syme A, Koromilas AE, Crist C: **Phosphorylation of eIF2alpha Is a Translational Control Mechanism Regulating Muscle Stem Cell Quiescence and Self-Renewal.** *Cell Stem Cell* 2016, **18**(1):79-90.
29. Kilberg MS, Shan J, Su N: **ATF4-dependent transcription mediates signaling of amino acid limitation.** *Trends Endocrinol Metab* 2009, **20**(9):436-443.
30. Avivar-Valderas A, Salas E, Bobrovnikova-Marjon E, Diehl JA, Nagi C, Debnath J, Aguirre-Ghiso JA: **PERK integrates autophagy and oxidative stress responses to promote survival during extracellular matrix detachment.** *Mol Cell Biol* 2011, **31**(17):3616-3629.
31. Lu PD, Jousse C, Marciniak SJ, Zhang Y, Novoa I, Scheuner D, Kaufman RJ, Ron D, Harding HP: **Cytoprotection by pre-emptive conditional phosphorylation of translation initiation factor 2.** *EMBO J* 2004, **23**(1):169-179.
32. Cavener DR, Gupta S, McGrath BC: **PERK in beta cell biology and insulin biogenesis.** *Trends Endocrinol Metab* 2010, **21**(12):714-721.
33. Bonaldo P, Sandri M: **Cellular and molecular mechanisms of muscle atrophy.** *Dis Model Mech* 2013, **6**(1):25-39.
34. Du J, Wang X, Miereles C, Bailey JL, Debigare R, Zheng B, Price SR, Mitch WE: **Activation of caspase-3 is an initial step triggering accelerated muscle proteolysis in catabolic conditions.** *J Clin Invest* 2004, **113**(1):115-123.

35. Cohen S, Brault JJ, Gygi SP, Glass DJ, Valenzuela DM, Gartner C, Latres E, Goldberg AL: **During muscle atrophy, thick, but not thin, filament components are degraded by MuRF1-dependent ubiquitylation.** *J Cell Biol* 2009, **185**(6):1083-1095.
36. Bodine SC, Baehr LM: **Skeletal muscle atrophy and the E3 ubiquitin ligases MuRF1 and MAFbx/atrogen-1.** *Am J Physiol Endocrinol Metab* 2014, **307**(6):E469-484.
37. Sandri M: **Autophagy in skeletal muscle.** *FEBS Lett* 2010, **584**(7):1411-1416.
38. Carnio S, LoVerso F, Baraibar MA, Longa E, Khan MM, Maffei M, Reischl M, Canepari M, Loeffler S, Kern H *et al*: **Autophagy impairment in muscle induces neuromuscular junction degeneration and precocious aging.** *Cell reports* 2014, **8**(5):1509-1521.
39. Masiero E, Agatea L, Mammucari C, Blaauw B, Loro E, Komatsu M, Metzger D, Reggiani C, Schiaffino S, Sandri M: **Autophagy is required to maintain muscle mass.** *Cell Metab* 2009, **10**(6):507-515.
40. Sandri M: **Signaling in muscle atrophy and hypertrophy.** *Physiology (Bethesda)* 2008, **23**:160-170.
41. Sandri M, Sandri C, Gilbert A, Skurk C, Calabria E, Picard A, Walsh K, Schiaffino S, Lecker SH, Goldberg AL: **Foxo transcription factors induce the atrophy-related ubiquitin ligase atrogen-1 and cause skeletal muscle atrophy.** *Cell* 2004, **117**(3):399-412.
42. Penna F, Costamagna D, Pin F, Camperi A, Fanzani A, Chiarpotto EM, Cavallini G, Bonelli G, Baccino FM, Costelli P: **Autophagic degradation contributes to muscle wasting in cancer cachexia.** *Am J Pathol* 2013, **182**(4):1367-1378.
43. Li H, Malhotra S, Kumar A: **Nuclear factor-kappa B signaling in skeletal muscle atrophy.** *J Mol Med (Berl)* 2008, **86**(10):1113-1126.
44. Egerman MA, Glass DJ: **Signaling pathways controlling skeletal muscle mass.** *Crit Rev Biochem Mol Biol* 2014, **49**(1):59-68.
45. Romanello V, Guadagnin E, Gomes L, Roder I, Sandri C, Petersen Y, Milan G, Masiero E, Del Piccolo P, Foretz M *et al*: **Mitochondrial fission and remodelling contributes to muscle atrophy.** *EMBO J* 2010, **29**(10):1774-1785.
46. Miyake M, Nomura A, Ogura A, Takehana K, Kitahara Y, Takahara K, Tsugawa K, Miyamoto C, Miura N, Sato R *et al*: **Skeletal muscle-specific eukaryotic translation initiation factor 2alpha phosphorylation controls amino acid**

metabolism and fibroblast growth factor 21-mediated non-cell-autonomous energy metabolism. *FASEB J* 2016, **30**(2):798-812.

47. Hunter RB, Mitchell-Felton H, Essig DA, Kandarian SC: **Expression of endoplasmic reticulum stress proteins during skeletal muscle disuse atrophy.** *Am J Physiol Cell Physiol* 2001, **281**(4):C1285-1290.
48. Baehr LM, West DW, Marcotte G, Marshall AG, De Sousa LG, Baar K, Bodine SC: **Age-related deficits in skeletal muscle recovery following disuse are associated with neuromuscular junction instability and ER stress, not impaired protein synthesis.** *Aging (Albany NY)* 2016, **8**(1):127-146.
49. Yu Z, Wang AM, Adachi H, Katsuno M, Sobue G, Yue Z, Robins DM, Lieberman AP: **Macroautophagy is regulated by the UPR-mediator CHOP and accentuates the phenotype of SBMA mice.** *PLoS Genet* 2011, **7**(10):e1002321.
50. Chen D, Wang Y, Chin ER: **Activation of the endoplasmic reticulum stress response in skeletal muscle of G93A*SOD1 amyotrophic lateral sclerosis mice.** *Front Cell Neurosci* 2015, **9**:170.
51. Hetz C, Thielen P, Matus S, Nassif M, Court F, Kiffin R, Martinez G, Cuervo AM, Brown RH, Glimcher LH: **XBP-1 deficiency in the nervous system protects against amyotrophic lateral sclerosis by increasing autophagy.** *Genes Dev* 2009, **23**(19):2294-2306.
52. Chalil S, Pierre N, Bakker AD, Manders RJ, Pletsers A, Francaux M, Klein-Nulend J, Jaspers RT, Deldicque L: **Aging related ER stress is not responsible for anabolic resistance in mouse skeletal muscle.** *Biochem Biophys Res Commun* 2015.
53. Deldicque L: **Endoplasmic reticulum stress in human skeletal muscle: any contribution to sarcopenia?** *Front Physiol* 2013, **4**:236.
54. Ogata T, Machida S, Oishi Y, Higuchi M, Muraoka I: **Differential cell death regulation between adult-unloaded and aged rat soleus muscle.** *Mech Ageing Dev* 2009, **130**(5):328-336.
55. O'Leary MF, Vainshtein A, Iqbal S, Ostojic O, Hood DA: **Adaptive plasticity of autophagic proteins to denervation in aging skeletal muscle.** *Am J Physiol Cell Physiol* 2013, **304**(5):C422-430.
56. Jiao G, Hao L, Wang M, Zhong B, Yu M, Zhao S, Wang P, Feng R, Tan S, Chen L: **Upregulation of endoplasmic reticulum stress is associated with diaphragm contractile dysfunction in a rat model of sepsis.** *Mol Med Rep* 2017, **15**(1):366-374.

57. Madaro L, Marrocco V, Carnio S, Sandri M, Bouche M: **Intracellular signaling in ER stress-induced autophagy in skeletal muscle cells.** *FASEB J* 2013, **27**(5):1990-2000.
58. Paul PK, Bhatnagar S, Mishra V, Srivastava S, Darnay BG, Choi Y, Kumar A: **The E3 ubiquitin ligase TRAF6 intercedes in starvation-induced skeletal muscle atrophy through multiple mechanisms.** *Mol Cell Biol* 2012, **32**(7):1248-1259.
59. Paul PK, Gupta SK, Bhatnagar S, Panguluri SK, Darnay BG, Choi Y, Kumar A: **Targeted ablation of TRAF6 inhibits skeletal muscle wasting in mice.** *J Cell Biol* 2010, **191**(7):1395-1411.
60. Wu J, Ruas JL, Estall JL, Rasbach KA, Choi JH, Ye L, Bostrom P, Tyra HM, Crawford RW, Campbell KP *et al*: **The unfolded protein response mediates adaptation to exercise in skeletal muscle through a PGC-1alpha/ATF6alpha complex.** *Cell Metab* 2011, **13**(2):160-169.
61. Pereira BC, da Rocha AL, Pinto AP, Pauli JR, de Souza CT, Cintra DE, Ropelle ER, de Freitas EC, Zagatto AM, da Silva AS: **Excessive eccentric exercise-induced overtraining model leads to endoplasmic reticulum stress in mice skeletal muscles.** *Life Sci* 2016, **145**:144-151.
62. Memme JM, Oliveira AN, Hood DA: **Chronology of UPR activation in skeletal muscle adaptations to chronic contractile activity.** *Am J Physiol Cell Physiol* 2016, **310**(11):C1024-1036.
63. Kim HJ, Jamart C, Deldicque L, An GL, Lee YH, Kim CK, Raymackers JM, Francaux M: **Endoplasmic reticulum stress markers and ubiquitin-proteasome pathway activity in response to a 200-km run.** *Med Sci Sports Exerc* 2011, **43**(1):18-25.
64. Handschin C, Chin S, Li P, Liu F, Maratos-Flier E, Lebrasseur NK, Yan Z, Spiegelman BM: **Skeletal muscle fiber-type switching, exercise intolerance, and myopathy in PGC-1alpha muscle-specific knock-out animals.** *J Biol Chem* 2007, **282**(41):30014-30021.
65. Lin J, Wu H, Tarr PT, Zhang CY, Wu Z, Boss O, Michael LF, Puigserver P, Isotani E, Olson EN *et al*: **Transcriptional co-activator PGC-1 alpha drives the formation of slow-twitch muscle fibres.** *Nature* 2002, **418**(6899):797-801.
66. Baar K, Wende AR, Jones TE, Marison M, Nolte LA, Chen M, Kelly DP, Holloszy JO: **Adaptations of skeletal muscle to exercise: rapid increase in the transcriptional coactivator PGC-1.** *FASEB J* 2002, **16**(14):1879-1886.

67. Russell AP, Feilchenfeldt J, Schreiber S, Praz M, Crettenand A, Gobelet C, Meier CA, Bell DR, Kralli A, Giacobino JP *et al*: **Endurance training in humans leads to fiber type-specific increases in levels of peroxisome proliferator-activated receptor-gamma coactivator-1 and peroxisome proliferator-activated receptor-alpha in skeletal muscle.** *Diabetes* 2003, **52**(12):2874-2881.
68. Calvo JA, Daniels TG, Wang X, Paul A, Lin J, Spiegelman BM, Stevenson SC, Rangwala SM: **Muscle-specific expression of PPARgamma coactivator-1alpha improves exercise performance and increases peak oxygen uptake.** *J Appl Physiol (1985)* 2008, **104**(5):1304-1312.
69. Hamilton DL, Philp A, MacKenzie MG, Patton A, Towler MC, Gallagher IJ, Bodine SC, Baar K: **Molecular brakes regulating mTORC1 activation in skeletal muscle following synergist ablation.** *Am J Physiol Endocrinol Metab* 2014, **307**(4):E365-373.
70. Ogborn DI, McKay BR, Crane JD, Parise G, Tarnopolsky MA: **The unfolded protein response is triggered following a single, unaccustomed resistance-exercise bout.** *Am J Physiol Regul Integr Comp Physiol* 2014, **307**(6):R664-669.
71. Lundberg IE: **Idiopathic inflammatory myopathies: why do the muscles become weak?** *Curr Opin Rheumatol* 2001, **13**(6):457-460.
72. Vitadello M, Doria A, Tarricone E, Ghirardello A, Gorza L: **Myofiber stress-response in myositis: parallel investigations on patients and experimental animal models of muscle regeneration and systemic inflammation.** *Arthritis Res Ther* 2010, **12**(2):R52.
73. Nagaraju K, Casciola-Rosen L, Lundberg I, Rawat R, Cutting S, Thapliyal R, Chang J, Dwivedi S, Mitsak M, Chen YW *et al*: **Activation of the endoplasmic reticulum stress response in autoimmune myositis: potential role in muscle fiber damage and dysfunction.** *Arthritis Rheum* 2005, **52**(6):1824-1835.
74. Li CK, Knopp P, Moncrieffe H, Singh B, Shah S, Nagaraju K, Varsani H, Gao B, Wedderburn LR: **Overexpression of MHC class I heavy chain protein in young skeletal muscle leads to severe myositis: implications for juvenile myositis.** *Am J Pathol* 2009, **175**(3):1030-1040.
75. DeVere R, Bradley WG: **Polymyositis: its presentation, morbidity and mortality.** *Brain* 1975, **98**(4):637-666.
76. Freret M, Drouot L, Obry A, Ahmed-Lacheheb S, Daully C, Adriouch S, Cosette P, Authier FJ, Boyer O: **Overexpression of MHC class I in muscle of lymphocyte-deficient mice causes a severe myopathy with induction of the unfolded protein response.** *Am J Pathol* 2013, **183**(3):893-904.

77. Askanas V, Engel WK: **Inclusion-body myositis and myopathies: different etiologies, possibly similar pathogenic mechanisms.** *Curr Opin Neurol* 2002, **15**(5):525-531.
78. Askanas V, Engel WK: **Inclusion-body myositis: newest concepts of pathogenesis and relation to aging and Alzheimer disease.** *J Neuropathol Exp Neurol* 2001, **60**(1):1-14.
79. Vattemi G, Engel WK, McFerrin J, Askanas V: **Endoplasmic reticulum stress and unfolded protein response in inclusion body myositis muscle.** *Am J Pathol* 2004, **164**(1):1-7.
80. Nogalska A, D'Agostino C, Engel WK, Cacciottolo M, Asada S, Mori K, Askanas V: **Activation of the Unfolded Protein Response in Sporadic Inclusion-Body Myositis but Not in Hereditary GNE Inclusion-Body Myopathy.** *J Neuropathol Exp Neurol* 2015, **74**(6):538-546.
81. Xiao F, Tan JZ, Xu XY, Wang XF: **Increased levels of HSPA5 in the serum of patients with inflammatory myopathies--preliminary findings.** *Clin Rheumatol* 2015, **34**(4):715-720.
82. Lightfoot AP, Nagaraju K, McArdle A, Cooper RG: **Understanding the origin of non-immune cell-mediated weakness in the idiopathic inflammatory myopathies - potential role of ER stress pathways.** *Curr Opin Rheumatol* 2015, **27**(6):580-585.
83. Meriggioli MN, Sanders DB: **Autoimmune myasthenia gravis: emerging clinical and biological heterogeneity.** *Lancet Neurol* 2009, **8**(5):475-490.
84. Iwasa K, Nambu Y, Motozaki Y, Furukawa Y, Yoshikawa H, Yamada M: **Increased skeletal muscle expression of the endoplasmic reticulum chaperone GRP78 in patients with myasthenia gravis.** *J Neuroimmunol* 2014, **273**(1-2):72-76.
85. Suzuki S, Utsugisawa K, Iwasa K, Satoh T, Nagane Y, Yoshikawa H, Kuwana M, Suzuki N: **Autoimmunity to endoplasmic reticulum chaperone GRP94 in myasthenia gravis.** *J Neuroimmunol* 2011, **237**(1-2):87-92.
86. Du A, Huang S, Zhao X, Zhang Y, Zhu L, Ding J, Xu C: **Endoplasmic reticulum stress contributes to acetylcholine receptor degradation by promoting endocytosis in skeletal muscle cells.** *J Neuroimmunol* 2016, **290**:109-114.
87. Shin J, Tajrishi MM, Ogura Y, Kumar A: **Wasting mechanisms in muscular dystrophy.** *Int J Biochem Cell Biol* 2013, **45**(10):2266-2279.
88. Emery AE: **The muscular dystrophies.** *Lancet* 2002, **359**(9307):687-695.

89. Bohnert KR, McMillan JD, Kumar A: **Emerging roles of ER stress and unfolded protein response pathways in skeletal muscle health and disease.** *J Cell Physiol* 2018, **233**(1):67-78.
90. Hulmi JJ, Hentila J, DeRuisseau KC, Oliveira BM, Papaioannou KG, Autio R, Kujala UM, Ritvos O, Kainulainen H, Korkmaz A *et al*: **Effects of muscular dystrophy, exercise and blocking activin receptor IIB ligands on the unfolded protein response and oxidative stress.** *Free Radic Biol Med* 2016, **99**:308-322.
91. Moorwood C, Barton ER: **Caspase-12 ablation preserves muscle function in the mdx mouse.** *Hum Mol Genet* 2014, **23**(20):5325-5341.
92. Pauly M, Angebault-Prouteau C, Dridi H, Notarnicola C, Scheuermann V, Lacampagne A, Matecki S, Fauconnier J: **ER stress disturbs SR/ER-mitochondria Ca²⁺ transfer: Implications in Duchenne muscular dystrophy.** *Biochim Biophys Acta* 2017, **1863**(9):2229-2239.
93. Ikezoe K, Nakamori M, Furuya H, Arahata H, Kanemoto S, Kimura T, Imaizumi K, Takahashi MP, Sakoda S, Fujii N *et al*: **Endoplasmic reticulum stress in myotonic dystrophy type 1 muscle.** *Acta Neuropathol* 2007, **114**(5):527-535.
94. Fujita E, Kouroku Y, Isoai A, Kumagai H, Misutani A, Matsuda C, Hayashi YK, Momoi T: **Two endoplasmic reticulum-associated degradation (ERAD) systems for the novel variant of the mutant dysferlin: ubiquitin/proteasome ERAD(I) and autophagy/lysosome ERAD(II).** *Hum Mol Genet* 2007, **16**(6):618-629.
95. Ikezoe K, Furuya H, Ohyagi Y, Osoegawa M, Nishino I, Nonaka I, Kira J: **Dysferlin expression in tubular aggregates: their possible relationship to endoplasmic reticulum stress.** *Acta Neuropathol* 2003, **105**(6):603-609.
96. De Palma S, Capitanio D, Vasso M, Braghetta P, Scotton C, Bonaldo P, Lochmuller H, Muntoni F, Ferlini A, Gelfi C: **Muscle proteomics reveals novel insights into the pathophysiological mechanisms of collagen VI myopathies.** *J Proteome Res* 2014, **13**(11):5022-5030.
97. Udd B: **Limb-girdle type muscular dystrophy in a large family with distal myopathy: homozygous manifestation of a dominant gene?** *J Med Genet* 1992, **29**(6):383-389.
98. Screen M, Raheem O, Holmlund-Hampf J, Jonson PH, Huovinen S, Hackman P, Udd B: **Gene expression profiling in tibial muscular dystrophy reveals unfolded protein response and altered autophagy.** *PLoS One* 2014, **9**(3):e90819.

99. Fearon K, Strasser F, Anker SD, Bosaeus I, Bruera E, Fainsinger RL, Jatoi A, Loprinzi C, MacDonald N, Mantovani G *et al*: **Definition and classification of cancer cachexia: an international consensus**. *Lancet Oncol* 2011, **12**(5):489-495.
100. Fearon KC, Glass DJ, Guttridge DC: **Cancer cachexia: mediators, signaling, and metabolic pathways**. *Cell Metab* 2012, **16**(2):153-166.
101. Johns N, Stephens NA, Fearon KC: **Muscle wasting in cancer**. *Int J Biochem Cell Biol* 2013, **45**(10):2215-2229.
102. He WA, Berardi E, Cardillo VM, Acharyya S, Aulino P, Thomas-Ahner J, Wang J, Bloomston M, Muscarella P, Nau P *et al*: **NF-kappaB-mediated Pax7 dysregulation in the muscle microenvironment promotes cancer cachexia**. *J Clin Invest* 2013, **123**(11):4821-4835.
103. Sandri M: **Protein breakdown in cancer cachexia**. *Semin Cell Dev Biol* 2015.
104. Zhang G, Jin B, Li YP: **C/EBPbeta mediates tumour-induced ubiquitin ligase atrogen1/MAFbx upregulation and muscle wasting**. *EMBO J* 2011, **30**(20):4323-4335.
105. Zhang G, Lin RK, Kwon YT, Li YP: **Signaling mechanism of tumor cell-induced up-regulation of E3 ubiquitin ligase UBR2**. *FASEB J* 2013, **27**(7):2893-2901.
106. Mizushima N, Yamamoto A, Matsui M, Yoshimori T, Ohsumi Y: **In vivo analysis of autophagy in response to nutrient starvation using transgenic mice expressing a fluorescent autophagosome marker**. *Mol Biol Cell* 2004, **15**(3):1101-1111.
107. Schwartz AL, Ciechanover A: **The ubiquitin-proteasome pathway and pathogenesis of human diseases**. *Annu Rev Med* 1999, **50**:57-74.
108. Cai D, Frantz JD, Tawa NE, Jr., Melendez PA, Oh BC, Lidov HG, Hasselgren PO, Frontera WR, Lee J, Glass DJ *et al*: **IKKbeta/NF-kappaB activation causes severe muscle wasting in mice**. *Cell* 2004, **119**(2):285-298.
109. Tian M, Nishijima Y, Asp ML, Stout MB, Reiser PJ, Belury MA: **Cardiac alterations in cancer-induced cachexia in mice**. *Int J Oncol* 2010, **37**(2):347-353.
110. Yu AP, Pei XM, Sin TK, Yip SP, Yung BY, Chan LW, Wong CS, Siu PM: **Acylated and unacylated ghrelin inhibit doxorubicin-induced apoptosis in skeletal muscle**. *Acta Physiol (Oxf)* 2014, **211**(1):201-213.

111. Roxburgh CS, McMillan DC: **Role of systemic inflammatory response in predicting survival in patients with primary operable cancer.** *Future Oncol* 2010, **6**(1):149-163.
112. Kuga A, Ohsawa Y, Okada T, Kanda F, Kanagawa M, Toda T, Sunada Y: **Endoplasmic reticulum stress response in P104L mutant caveolin-3 transgenic mice.** *Hum Mol Genet* 2011, **20**(15):2975-2983.
113. Ozcan U, Yilmaz E, Ozcan L, Furuhashi M, Vaillancourt E, Smith RO, Gorgun CZ, Hotamisligil GS: **Chemical chaperones reduce ER stress and restore glucose homeostasis in a mouse model of type 2 diabetes.** *Science* 2006, **313**(5790):1137-1140.
114. Zode GS, Kuehn MH, Nishimura DY, Searby CC, Mohan K, Grozdanic SD, Bugge K, Anderson MG, Clark AF, Stone EM *et al*: **Reduction of ER stress via a chemical chaperone prevents disease phenotypes in a mouse model of primary open angle glaucoma.** *J Clin Invest* 2015, **125**(8):3303.
115. Hindi SM, Mishra V, Bhatnagar S, Tajrishi MM, Ogura Y, Yan Z, Burkly LC, Zheng TS, Kumar A: **Regulatory circuitry of TWEAK-Fn14 system and PGC-1alpha in skeletal muscle atrophy program.** *FASEB J* 2014, **28**(3):1398-1411.
116. Goodman CA, Hornberger TA: **Measuring protein synthesis with SUNSET: a valid alternative to traditional techniques?** *Exerc Sport Sci Rev* 2013, **41**(2):107-115.
117. Mittal A, Bhatnagar S, Kumar A, Lach-Trifilieff E, Wauters S, Li H, Makonchuk DY, Glass DJ, Kumar A: **The TWEAK-Fn14 system is a critical regulator of denervation-induced skeletal muscle atrophy in mice.** *J Cell Biol* 2010, **188**(6):833-849.
118. Sato S, Ogura Y, Tajrishi MM, Kumar A: **Elevated levels of TWEAK in skeletal muscle promote visceral obesity, insulin resistance, and metabolic dysfunction.** *FASEB J* 2015, **29**(3):988-1002.
119. Baltgalvis KA, Berger FG, Pena MM, Davis JM, Muga SJ, Carson JA: **Interleukin-6 and cachexia in ApcMin/+ mice.** *Am J Physiol Regul Integr Comp Physiol* 2008, **294**(2):R393-401.
120. Zhao J, Brault JJ, Schild A, Cao P, Sandri M, Schiaffino S, Lecker SH, Goldberg AL: **FoxO3 coordinately activates protein degradation by the autophagic/lysosomal and proteasomal pathways in atrophying muscle cells.** *Cell Metab* 2007, **6**(6):472-483.

121. Yoshida H, Matsui T, Yamamoto A, Okada T, Mori K: **XBP1 mRNA is induced by ATF6 and spliced by IRE1 in response to ER stress to produce a highly active transcription factor.** *Cell* 2001, **107**(7):881-891.
122. Acharyya S, Ladner KJ, Nelsen LL, Damrauer J, Reiser PJ, Swoap S, Guttridge DC: **Cancer cachexia is regulated by selective targeting of skeletal muscle gene products.** *J Clin Invest* 2004, **114**(3):370-378.
123. Ebert SM, Monteys AM, Fox DK, Bongers KS, Shields BE, Malmberg SE, Davidson BL, Suneja M, Adams CM: **The transcription factor ATF4 promotes skeletal myofiber atrophy during fasting.** *Mol Endocrinol* 2010, **24**(4):790-799.
124. Caiozzo VJ, Haddad F, Baker MJ, Herrick RE, Prietto N, Baldwin KM: **Microgravity-induced transformations of myosin isoforms and contractile properties of skeletal muscle.** *J Appl Physiol (1985)* 1996, **81**(1):123-132.
125. Wang Y, Pessin JE: **Mechanisms for fiber-type specificity of skeletal muscle atrophy.** *Curr Opin Clin Nutr Metab Care* 2013, **16**(3):243-250.
126. Diffie GM, Kalfas K, Al-Majid S, McCarthy DO: **Altered expression of skeletal muscle myosin isoforms in cancer cachexia.** *Am J Physiol Cell Physiol* 2002, **283**(5):C1376-1382.
127. Bodine SC, Latres E, Baumhueter S, Lai VK, Nunez L, Clarke BA, Poueymirou WT, Panaro FJ, Na E, Dharmarajan K *et al*: **Identification of ubiquitin ligases required for skeletal muscle atrophy.** *Science* 2001, **294**(5547):1704-1708.
128. Sartori R, Schirwis E, Blaauw B, Bortolanza S, Zhao J, Enzo E, Stantzou A, Mouisel E, Toniolo L, Ferry A *et al*: **BMP signaling controls muscle mass.** *Nat Genet* 2013, **45**(11):1309-1318.
129. Gao S, Carson JA: **Lewis lung carcinoma regulation of mechanical stretch-induced protein synthesis in cultured myotubes.** *Am J Physiol Cell Physiol* 2016, **310**(1):C66-79.
130. Rayavarapu S, Coley W, Nagaraju K: **Endoplasmic reticulum stress in skeletal muscle homeostasis and disease.** *Curr Rheumatol Rep* 2012, **14**(3):238-243.
131. Zhang P, McGrath B, Li S, Frank A, Zambito F, Reinert J, Gannon M, Ma K, McNaughton K, Cavener DR: **The PERK eukaryotic initiation factor 2 alpha kinase is required for the development of the skeletal system, postnatal growth, and the function and viability of the pancreas.** *Mol Cell Biol* 2002, **22**(11):3864-3874.
132. Wu J, Rutkowski DT, Dubois M, Swathirajan J, Saunders T, Wang J, Song B, Yau GD, Kaufman RJ: **ATF6alpha optimizes long-term endoplasmic**

- reticulum function to protect cells from chronic stress.** *Dev Cell* 2007, **13**(3):351-364.
133. Yamamoto K, Sato T, Matsui T, Sato M, Okada T, Yoshida H, Harada A, Mori K: **Transcriptional induction of mammalian ER quality control proteins is mediated by single or combined action of ATF6alpha and XBP1.** *Dev Cell* 2007, **13**(3):365-376.
134. Salvado L, Coll T, Gomez-Foix AM, Salmeron E, Barroso E, Palomer X, Vazquez-Carrera M: **Oleate prevents saturated-fatty-acid-induced ER stress, inflammation and insulin resistance in skeletal muscle cells through an AMPK-dependent mechanism.** *Diabetologia* 2013, **56**(6):1372-1382.
135. Gomes AV, Waddell DS, Siu R, Stein M, Dewey S, Furlow JD, Bodine SC: **Upregulation of proteasome activity in muscle RING finger 1-null mice following denervation.** *FASEB J* 2012, **26**(7):2986-2999.
136. Hwee DT, Baehr LM, Philp A, Baar K, Bodine SC: **Maintenance of muscle mass and load-induced growth in Muscle RING Finger 1 null mice with age.** *Aging Cell* 2014, **13**(1):92-101.
137. Bodine SC, Stitt TN, Gonzalez M, Kline WO, Stover GL, Bauerlein R, Zlotchenko E, Scrimgeour A, Lawrence JC, Glass DJ *et al*: **Akt/mTOR pathway is a crucial regulator of skeletal muscle hypertrophy and can prevent muscle atrophy in vivo.** *Nat Cell Biol* 2001, **3**(11):1014-1019.
138. Judge SM, Wu CL, Beharry AW, Roberts BM, Ferreira LF, Kandarian SC, Judge AR: **Genome-wide identification of FoxO-dependent gene networks in skeletal muscle during C26 cancer cachexia.** *BMC Cancer* 2014, **14**:997.
139. Mounier R, Theret M, Lantier L, Foretz M, Viollet B: **Expanding roles for AMPK in skeletal muscle plasticity.** *Trends Endocrinol Metab* 2015, **26**(6):275-286.
140. Miller AC, Cohen S, Stewart M, Rivas R, Lison P: **Radioprotection by the histone deacetylase inhibitor phenylbutyrate.** *Radiation and Environmental Biophysics* 2011, **50**(4):585.
141. Hu H, Li L, Wang C, He H, Mao K, Ma X, Shi R, Oh Y, Zhang F, Lu Y *et al*: **4-Phenylbutyric acid increases GLUT4 gene expression through suppression of HDAC5 but not endoplasmic reticulum stress.** *Cell Physiol Biochem* 2014, **33**(6):1899-1910.
142. Chueh AC, Tse JWT, Tögel L, Mariadason JM: **Mechanisms of Histone Deacetylase Inhibitor-Regulated Gene Expression in Cancer Cells.** *Antioxid Redox Signal* 2015, **23**(1):66-84.

143. Walsh ME, Van Remmen H: **Emerging roles for histone deacetylases in age-related muscle atrophy.** *Nutr Healthy Aging*, **4**(1):17-30.
144. Argiles JM, Busquets S, Stemmler B, Lopez-Soriano FJ: **Cancer cachexia: understanding the molecular basis.** *Nat Rev Cancer* 2014, **14**(11):754-762.
145. Smith KL, Tisdale MJ: **Mechanism of muscle protein degradation in cancer cachexia.** *Br J Cancer* 1993, **68**(2):314-318.
146. Andreyev HJ, Norman AR, Oates J, Cunningham D: **Why do patients with weight loss have a worse outcome when undergoing chemotherapy for gastrointestinal malignancies?** *Eur J Cancer* 1998, **34**(4):503-509.
147. Kandarian SC, Stevenson EJ: **Molecular events in skeletal muscle during disuse atrophy.** *Exerc Sport Sci Rev* 2002, **30**(3):111-116.
148. Zhang G, Liu Z, Ding H, Zhou Y, Doan HA, Sin KWT, Zhu ZJ, Flores R, Wen Y, Gong X *et al*: **Tumor induces muscle wasting in mice through releasing extracellular Hsp70 and Hsp90.** *Nat Commun* 2017, **8**(1):589.
149. Zhang G, Liu Z, Ding H, Miao H, Garcia JM, Li YP: **Toll-like receptor 4 mediates Lewis lung carcinoma-induced muscle wasting via coordinate activation of protein degradation pathways.** *Sci Rep* 2017, **7**(1):2273.
150. Doyle A, Zhang G, Abdel Fattah EA, Eissa NT, Li YP: **Toll-like receptor 4 mediates lipopolysaccharide-induced muscle catabolism via coordinate activation of ubiquitin-proteasome and autophagy-lysosome pathways.** *FASEB J* 2011, **25**(1):99-110.
151. Takeuchi O, Akira S: **Pattern recognition receptors and inflammation.** *Cell* 2010, **140**(6):805-820.
152. Akira S, Takeda K: **Toll-like receptor signalling.** *Nat Rev Immunol* 2004, **4**(7):499-511.
153. Janeway CA, Jr., Medzhitov R: **Innate immune recognition.** *Annu Rev Immunol* 2002, **20**:197-216.
154. Hindi SM, Shin J, Gallot YS, Straughn AR, Simionescu-Bankston A, Hindi L, Xiong G, Friedland RP, Kumar A: **MyD88 promotes myoblast fusion in a cell-autonomous manner.** *Nat Commun* 2017, **8**(1):1624.
155. Hindi SM, Kumar A: **Toll-like receptor signalling in regenerative myogenesis: friend and foe.** *J Pathol* 2016, **239**(2):125-128.

156. Martinon F, Chen X, Lee AH, Glimcher LH: **TLR activation of the transcription factor XBP1 regulates innate immune responses in macrophages.** *Nat Immunol* 2010, **11**(5):411-418.
157. Afroze D, Kumar A: **ER stress in skeletal muscle remodeling and myopathies.** *FEBS J* 2017.
158. Bohnert KR, Gallot YS, Sato S, Xiong G, Hindi SM, Kumar A: **Inhibition of ER stress and unfolding protein response pathways causes skeletal muscle wasting during cancer cachexia.** *FASEB J* 2016, **30**(9):3053-3068.
159. Bohnert KR, Gallot YS, Sato S, Xiong G, Hindi SM, Kumar A: **Inhibition of ER stress and unfolding protein response pathways causes skeletal muscle wasting during cancer cachexia.** *FASEB J* 2016.
160. Bhatnagar S, Kumar A, Makonchuk DY, Li H, Kumar A: **Transforming growth factor-beta-activated kinase 1 is an essential regulator of myogenic differentiation.** *J Biol Chem* 2010, **285**(9):6401-6411.
161. Hindi SM, Sato S, Xiong G, Bohnert KR, Gibb AA, Gallot YS, McMillan JD, Hill BG, Uchida S, Kumar A: **TAK1 regulates skeletal muscle mass and mitochondrial function.** *JCI Insight* 2018, **3**(3).
162. Sandri M: **Protein breakdown in muscle wasting: role of autophagy-lysosome and ubiquitin-proteasome.** *Int J Biochem Cell Biol* 2013, **45**(10):2121-2129.
163. Seto DN, Kandarian SC, Jackman RW: **A Key Role for Leukemia Inhibitory Factor in C26 Cancer Cachexia.** *J Biol Chem* 2015, **290**(32):19976-19986.
164. Braun TP, Grossberg AJ, Krasnow SM, Levasseur PR, Szumowski M, Zhu XX, Maxson JE, Knoll JG, Barnes AP, Marks DL: **Cancer- and endotoxin-induced cachexia require intact glucocorticoid signaling in skeletal muscle.** *FASEB J* 2013, **27**(9):3572-3582.
165. He WA, Calore F, Londhe P, Canella A, Guttridge DC, Croce CM: **Microvesicles containing miRNAs promote muscle cell death in cancer cachexia via TLR7.** *Proc Natl Acad Sci U S A* 2014, **111**(12):4525-4529.
166. Miyake M, Kuroda M, Kiyonari H, Takehana K, Hisanaga S, Morimoto M, Zhang J, Oyadomari M, Sakaue H, Oyadomari S: **Ligand-induced rapid skeletal muscle atrophy in HSA-Fv2E-PERK transgenic mice.** *PLoS One* 2017, **12**(6):e0179955.
167. Fox DK, Ebert SM, Bongers KS, Dyle MC, Bullard SA, Dierdorff JM, Kunkel SD, Adams CM: **p53 and ATF4 mediate distinct and additive pathways to**

- skeletal muscle atrophy during limb immobilization.** *Am J Physiol Endocrinol Metab* 2014, **307**(3):E245-261.
168. Ebert SM, Dyle MC, Bullard SA, Dierdorff JM, Murry DJ, Fox DK, Bongers KS, Lira VA, Meyerholz DK, Talley JJ *et al*: **Identification and Small Molecule Inhibition of an Activating Transcription Factor 4 (ATF4)-dependent Pathway to Age-related Skeletal Muscle Weakness and Atrophy.** *J Biol Chem* 2015, **290**(42):25497-25511.
169. Bonetto A, Aydogdu T, Jin X, Zhang Z, Zhan R, Puzis L, Koniaris LG, Zimmers TA: **JAK/STAT3 pathway inhibition blocks skeletal muscle wasting downstream of IL-6 and in experimental cancer cachexia.** *Am J Physiol Endocrinol Metab* 2012, **303**(3):E410-421.
170. Puppa MJ, White JP, Velazquez KT, Baltgalvis KA, Sato S, Baynes JW, Carson JA: **The effect of exercise on IL-6-induced cachexia in the Apc (Min/+) mouse.** *J Cachexia Sarcopenia Muscle* 2012, **3**(2):117-137.
171. White JP, Puppa MJ, Sato S, Gao S, Price RL, Baynes JW, Kostek MC, Matesic LE, Carson JA: **IL-6 regulation on skeletal muscle mitochondrial remodeling during cancer cachexia in the ApcMin/+ mouse.** *Skelet Muscle* 2012, **2**:14.
172. Kuang S, Rudnicki MA: **The emerging biology of satellite cells and their therapeutic potential.** *Trends Mol Med* 2008, **14**(2):82-91.
173. Henriques-Pons A, Yu Q, Rayavarapu S, Cohen TV, Ampong B, Cha HJ, Jahnke V, Van der Meulen J, Wang D, Jiang W *et al*: **Role of Toll-like receptors in the pathogenesis of dystrophin-deficient skeletal and heart muscle.** *Human molecular genetics* 2014, **23**(10):2604-2617.
174. Hindi SM, Paul PK, Dahiya S, Mishra V, Bhatnagar S, Kuang S, Choi Y, Kumar A: **Reciprocal interaction between TRAF6 and notch signaling regulates adult myofiber regeneration upon injury.** *Mol Cell Biol* 2012, **32**(23):4833-4845.
175. Hindi SM, Kumar A: **TRAF6 regulates satellite stem cell self-renewal and function during regenerative myogenesis.** *J Clin Invest* 2016, **126**(1):151-168.
176. Ogura Y, Hindi SM, Sato S, Xiong G, Akira S, Kumar A: **TAK1 modulates satellite stem cell homeostasis and skeletal muscle repair.** *Nat Commun* 2015, **6**:10123.
177. Paulsen G, Mikkelsen UR, Raastad T, Peake JM: **Leucocytes, cytokines and satellite cells: what role do they play in muscle damage and regeneration following eccentric exercise?** *Exerc Immunol Rev* 2012, **18**:42-97.

178. Latres E, Amini AR, Amini AA, Griffiths J, Martin FJ, Wei Y, Lin HC, Yancopoulos GD, Glass DJ: **Insulin-like growth factor-1 (IGF-1) inversely regulates atrophy-induced genes via the phosphatidylinositol 3-kinase/Akt/mammalian target of rapamycin (PI3K/Akt/mTOR) pathway.** *J Biol Chem* 2005, **280**(4):2737-2744.
179. Rommel C, Bodine SC, Clarke BA, Rossman R, Nunez L, Stitt TN, Yancopoulos GD, Glass DJ: **Mediation of IGF-1-induced skeletal myotube hypertrophy by PI(3)K/Akt/mTOR and PI(3)K/Akt/GSK3 pathways.** *Nat Cell Biol* 2001, **3**(11):1009-1013.
180. Hindi SM, Tajrishi MM, Kumar A: **Signaling mechanisms in mammalian myoblast fusion.** *Science signaling* 2013, **6**(272):re2.
181. Serrano AL, Baeza-Raja B, Perdiguero E, Jardí M, Muñoz-Cánoves P: **Interleukin-6 Is an Essential Regulator of Satellite Cell-Mediated Skeletal Muscle Hypertrophy.** *Cell Metabolism*, **7**(1):33-44.
182. Kim K, Kim YH, Lee SH, Jeon MJ, Park SY, Doh KO: **Effect of exercise intensity on unfolded protein response in skeletal muscle of rat.** *Korean J Physiol Pharmacol* 2014, **18**(3):211-216.
183. Urano F, Wang X, Bertolotti A, Zhang Y, Chung P, Harding HP, Ron D: **Coupling of stress in the ER to activation of JNK protein kinases by transmembrane protein kinase IRE1.** *Science* 2000, **287**(5453):664-666.
184. Glimcher LH: **XBP1: the last two decades.** *Ann Rheum Dis* 2010, **69** Suppl 1:i67-71.
185. Gregor Margaret F, Misch Emily S, Yang L, Hummasti S, Inouye Karen E, Lee A-H, Bierie B, Hotamisligil Gökhan S: **The Role of Adipocyte XBP1 in Metabolic Regulation during Lactation.** *Cell reports*, **3**(5):1430-1439.
186. Lee AH, Chu GC, Iwakoshi NN, Glimcher LH: **XBP-1 is required for biogenesis of cellular secretory machinery of exocrine glands.** *EMBO J* 2005, **24**(24):4368-4380.
187. Lee AH, Heidtman K, Hotamisligil GS, Glimcher LH: **Dual and opposing roles of the unfolded protein response regulated by IRE1alpha and XBP1 in proinsulin processing and insulin secretion.** *Proceedings of the National Academy of Sciences of the United States of America* 2011, **108**(21):8885-8890.
188. Seale P, Sabourin LA, Girgis-Gabardo A, Mansouri A, Gruss P, Rudnicki MA: **Pax7 is required for the specification of myogenic satellite cells.** *Cell* 2000, **102**(6):777-786.

189. von Maltzahn J, Jones AE, Parks RJ, Rudnicki MA: **Pax7 is critical for the normal function of satellite cells in adult skeletal muscle.** *Proceedings of the National Academy of Sciences of the United States of America* 2013, **110**(41):16474-16479.
190. Lepper C, Conway SJ, Fan CM: **Adult satellite cells and embryonic muscle progenitors have distinct genetic requirements.** *Nature* 2009, **460**(7255):627-631.
191. Fry CS, Lee JD, Jackson JR, Kirby TJ, Stasko SA, Liu H, Dupont-Versteegden EE, McCarthy JJ, Peterson CA: **Regulation of the muscle fiber microenvironment by activated satellite cells during hypertrophy.** *FASEB J* 2014, **28**(4):1654-1665.
192. Dumont NA, Wang YX, Rudnicki MA: **Intrinsic and extrinsic mechanisms regulating satellite cell function.** *Development* 2015, **142**(9):1572-1581.
193. Rosenblatt JD, Parry DJ: **Adaptation of rat extensor digitorum longus muscle to gamma irradiation and overload.** *Pflugers Arch* 1993, **423**(3-4):255-264.
194. Glass DJ: **Skeletal muscle hypertrophy and atrophy signaling pathways.** *Int J Biochem Cell Biol* 2005, **37**(10):1974-1984.
195. Pavlath GK: **Spatial and functional restriction of regulatory molecules during mammalian myoblast fusion.** *Exp Cell Res* 2010, **316**(18):3067-3072.
196. Enwere EK, Holbrook J, Lejmi-Mrad R, Vineham J, Timusk K, Sivaraj B, Isaac M, Uehling D, Al-awar R, LaCasse E *et al*: **TWEAK and cIAP1 regulate myoblast fusion through the noncanonical NF-kappaB signaling pathway.** *Sci Signal* 2012, **5**(246):ra75.
197. Girgenrath M, Weng S, Kostek CA, Browning B, Wang M, Brown SA, Winkles JA, Michaelson JS, Allaire N, Schneider P *et al*: **TWEAK, via its receptor Fn14, is a novel regulator of mesenchymal progenitor cells and skeletal muscle regeneration.** *EMBO J* 2006, **25**(24):5826-5839.
198. Dogra C, Hall SL, Wedhas N, Linkhart TA, Kumar A: **Fibroblast growth factor inducible 14 (Fn14) is required for the expression of myogenic regulatory factors and differentiation of myoblasts into myotubes. Evidence for TWEAK-independent functions of Fn14 during myogenesis.** *J Biol Chem* 2007, **282**(20):15000-15010.

APPENDICES

APPENDIX-1

The following Chapters are adapted from previously published work:

Chapter 1: Bohnert KR, McMillan JD, Kumar A: Emerging roles of ER stress and unfolded protein response pathways in skeletal muscle health and disease. *J Cell Physiol* 2017.

Chapter 2: Bohnert KR, Gallot YS, Sato S, Xiong G, Hindi SM, Kumar A: Inhibition of ER stress and unfolding protein response pathways causes skeletal muscle wasting during cancer cachexia. *FASEB J* 2016, 30(9):3053-3068.

APPENDIX-2

Sequence of the primers used in QRT-PCR assay.

Gene Name	Forward primer (5'-3')	Reverse primer (5'-3')
PERK	ACTCCTGTCTTGGTTGGGTCT GAT	CGTGCTCCGATTCCTTTCT
IRE1	CCTTTGCTGATAGTCTCTGCC CAT	TTACCACCAGTCCATCGCCA TT
XBP1	TGTCCATTCCCAAGCGTGTT T	TGGAGCAGCAAGTGGATTT
ATF6	CGTTCCTGAGGAGTTGGATTT G	GCTTCTCTTCCTTCAGTGGCT CTA
GRP78	TGATATTGGAGGTGGGCAAA CC	TTGTCGCTGGGCATCATTGA
GRP94	GGGAGGTCACCTTCAAGTCG	CTCGAGGTGCAGATGTGGG
DR5	AAGCCTTGACAGAGAGGTATT GAC	GCAGTTAGAGCATGACTGGA GAT
ATF4	CTCTTCACGAAATCCAGCAG CA	CCATGAGGTTTCAAGTGCTT G
MAFBx	AAGGCTGTTGGAGCTGATAG CA	CACCCACATGTTAATGTTGC C
MuRF1	TAAGTGCATCTCCATGCTGGT G	TGGCGTAGAGGGTGTCAAAT
MUSA1	TCGTGGAATGGTAATCTTGC	CCTCCCGTTTCTCTATCACG
TRAF6	GCAGTGAAAGATGACAGCGT GA	TCCCGTAAAGCCATCAAGCA
LC3B	CTGGTGAATGGGCACAGCAT G	CGTCCGCTGGTAACATCCCTT
Beclin1	TGAAATCAATGCTGCCTGGG	CCAGAACAGTATAACGGCAA CTCC
MyD88	TATCGCTGTTCTTGAACCCTC G	AGGCATCCAACAAACTGCGA
TLR1	TGATCTTGTGCCACCCAACA GT	CCATAAGCATCTCCTAACA CCAG
TLR2	CACTCCCAGATGCTTCGTTGT T	AACCAGGATTTGAGCCAGAG CT
TLR4	GACTGGGTGAGAAATGAGCT GGTA	ATGATGTTGGCAGCAATGGC
TLR7	CTTGCCTTTGAATGCAGACTG C	GCCAGAGTTCACTGCCATTA AGAG
TLR8	CCAGTGCCATCTTCATAAA GC	TGGGTGCTGTTGTTTGGCAT
TLR9	TCTCGGAACAACCTGGTGAC TATC	TGCTAAAGGGCTGGCTGTTG TA
CHOP	TGAAAGCAGAACCTGGTCCA	CACTGTTTATGCTTGGTGCA

GADD34	CAGAACATCAAGCCACGGAA GA	AAAGTTGTCTCAGGTCCTCCT TCC
sXBP1	AAGAACACGCTTGGGAATGG	CTGCACCTGCGGAC
EDEM	CGGCTATGACAACTACATGG	G TTCAGATTGGAAGGGTCTC
SEC61	AGTCATCAAGCCATTCTGTG	GAAGACATGATGCCAAACAG
p62	AGCACAGGCACAGAAGACAA GAGT	AATGTGTCCAGTCATCGTCTC CTC
IL-6	ATGGCAATTCTGATTGTATG	TGGCTTTGTCTTTCTTGTTA
Tweak	GCTACGACCGCCAGATTGGG	GCCAGCACACCGTTCACCAG
TNF α	GCATGATCCGCGACGTGGAA	AGATCCATGCCGTTGGCCAG
TNFR1		
eMyHC	ACATCTCTATGCCACCTTCGC TAC	GGGTCTTGGTTTCGTTGGGTA T
Myogenin	CATCCAGTACATTGAGCGCC TA	GAGCAAATGATCTCCTGGGT TG
Myf5	TGAAGGATGGACATGACGGAA C	TTGTGTGCTCCGAAGGCTGC TA
MyoD	TGGGATATGGAGCTTCTATC GC	GGTGAGTCGAAACACGGATC AT
Pax7	CAGTGTGCCATCTACCCATGC TTA	GGTGCTTGGTTCAAATTGAG CC
Myomaker	ATCGCTACCAAGCGTT	CACAGCACAGACAAACCAGG
MyHC I	AGTCCCAGGTCAACAAGC	TTCCACCTAAAGGGCTGT
MyHC IIA	GCATGACCAAAGGTTTCA	AGTCCCAGGTCAACAAGC
MyHC IIB	TTTCTCCTGTCACCTCTC	AGTCCCAGGTCAACAAGC
N-Cadherin	CAGCAGATTTCAAGGTGGAC GA	TCCTGGGTTTCTTTGTCTTGG G
Nephronectin	CCAGAACAACCTCCACTACCA CCAA	CTGGGTCGTCCTTTACTTCCT CAT
β -Actin	CAGGCATTGCTGACAGGATG	TGCTGATCCACATCTGCTGG

APPENDIX-3

LIST OF ABBREVIATIONS:

4-PBA.....	4-phenylbutyrate
ALS.....	Autophagy-lysosome system
ATF.....	Activating transcription factor
BSA.....	Bovine serum albumin
BiP.....	Immunoglobulin heavy-chain binding protein
CHOP.....	C/EBP homologous protein
CM.....	Conditioned medium
CSA.....	Cross-sectional area
eIF.....	Eukaryotic translation initiation factor
ER.....	Endoplasmic reticulum
eMyHC.....	Embryonic myosin heavy chain
GA.....	Gastrocnemius muscle
GADD34.....	Growth arrest and DNA-damage inducible protein
GRP78.....	Glucose-regulating protein 78
H&E.....	Hematoxylin and eosin
Hsp.....	Heat shock protein
IL.....	Interleukin
IRE1.....	Inositol-requiring protein 1

LC3B.....Light chain 3B

LLC.....Lewis lung carcinoma

MAPK.....Mitogen associated protein kinase

mKO.....Muscle specific knockout

mTOR.....Mammalian target of rapamycin

MuRF1.....Muscle Ring-finger protein

MyD88.....Myeloid differentiation primary response 88

MyHC.....Myosin heavy chain

myoKO.....Myoblast specific knockout

NF-kB.....nuclear factor kappa-B

Pax7.....paired box protein 7

PERK.....RNA-dependent protein kinase-like ER eukaryotic
translation intitation factor 2 a kinase

rpS6.....Ribosomal Protein S6

shRNA.....short hairpin RNA

QRT-PCR.....Quantitative RT-PCR

sXBP1.....Spliced X-box binding protein

Sunset.....Surface sensing or translation

TA.....Tibialis anterior muscle

TLR.....Toll-like receptor

TNF.....Tumor Necrosis factor

TNFR.....Tumor necrosis factor receptor

TWEAK.....TNF-related weak inducer of apoptosis

UPR.....Unfolded protein response
UPS.....Ubiquitin-proteasome system
XBP1.....X-box binding protein 1

CURRICULUM VITAE

Kyle R. Bohnert, M.S.
3920 Napanee Rd
Louisville, KY 40207
Email: krbohn02@louisville.edu
Phone: 502-852-8594 (Laboratory)
502-724-3773 (Mobile)

Date of Birth: September 19, 1989

Residency Status: US Citizen

A. EDUCATION & TRAINING:

(Month/Year)

- | | |
|-----------------------|---|
| 06/2012 | BA, Exercise Science, Psychology
Hanover College, Hanover, IN |
| 06/2014 | MS, Kinesiology and Health Promotion (Biomechanics),
University of Kentucky, Lexington, KY |
| 08/2016 | MS, Anatomical Sciences and Neurobiology,
University of Louisville, Louisville, KY |
| 08/2018
(Expected) | PhD, Anatomical Sciences and Neurobiology,
University of Louisville, Louisville, KY |

B. RESEARCH EXPERIENCE

- | | |
|-----------|--|
| 2011-2012 | Senior Thesis, Hanover College, Dr. Bryant Stamford laboratory
Department of Exercise Science, Hanover, IN. Study completed in
laboratory of Dr. Jeff Haddad, Purdue University, West Lafayette,
IN
<u>Research Topic:</u> The Effect of a Cognitive and Motor Task on
Postural Stability |
| 2011-2012 | Senior Thesis, Hanover College, Dr. John Krantz laboratory,
Department of Psychology, Hanover, IN
<u>Research Topic:</u> The Effect of Sensory Manipulation on Postural
Sway |

- 2012-2014 Masters Thesis, Dr. Robert Shapiro laboratory, University of Kentucky, Lexington, KY
Research Topic: A Complete Kinematic, Kinetic, and Electromyographical Analysis of the Football Throw in Collegiate Quarterbacks
- 2014-2018 PhD Dissertation, Dr. Ashok Kumar's laboratory, University of Louisville, Louisville, KY
Research Topic: Unfolded Protein Response Pathways in Skeletal Muscle Homeostasis

C. AWARDS AND HONORS

- 2012 Teaching Assistantship, University of Kentucky
 2014 Graduate Fellowship Award, University of Louisville
 2016 Research! Louisville Poster Presentation Third Place
 2018 Ruth L. Kirschstein NRSA Individual Predoctoral Fellowship (F31), National Institute of Health.

D. TEACHING EXPERIENCE

- 2012-2013 Teaching Assistant, Kinesiology and Health Promotion Classes, University of Kentucky
- 2013-2014 Teaching Assistant, Undergraduate Biomechanics Laboratory, University of Kentucky
- 2013-2014 Teaching Assistant, Select Undergraduate Biomechanics Lectures, University of Kentucky
- 2016 Teaching Assistant, Medical Gross Neurobiology Laboratory, University of Louisville

E. PEER-REVIEWED PUBLICATIONS

- 1) **Bohnert KR**, Gallot YS, Sato S, Xiong G, Hindi SM, Kumar A. (2016) Inhibition of ER stress and unfolding protein response pathways causes skeletal muscle wasting during cancer cachexia. *FASEB Journal*, 30: 3053-3068. PMID: 27206451. PMCID: PMC5001510
- 2) Xiong G, Hindi SM, Mann AK, Gallot YS, **Bohnert KR**, Cavener DR, Whittemore SR, Kumar A. (2017). The PERK arm of the unfolded protein response regulates satellite cell-mediated skeletal muscle regeneration. *Elife* pii: e22871. doi: 10.7554/eLife.22871. PMID: 28332979
- 3) Gallot YS, McMillan JD, Xiong G, **Bohnert KR**, Straughn A, Hill B, Kumar A (2017). Distinct roles of TRAF6 and TAK1 in the regulation of adipocyte

survival, thermogenesis program, and high-fat diet-induced obesity. *Oncotarget*, 8:112565-112583. PMID: 29348847

- 4) **Bohnert KR**, McMillan JD, and Kumar A (2018). Emerging roles of ER stress and unfolded protein response pathways in skeletal muscle health and disease. *Journal of Cellular Physiology*, 233:67-78.
- 5) Hindi SM, Sato S, Xiong G, **Bohnert KR**, Gibb AA, Gallot YS, McMillan JD, Hill B, Uchida S, Kumar A (2018). TAK1 is a key regulator of skeletal muscle mass and mitochondrial function. *JCI Insight*. 3(3). pii: 98441. doi:10.1172/jci.insight.98441.
- 6) Gallot YS, Straughn AR, **Bohnert KR**, Xiong G, Hindi SM, and Kumar A (2018). MyD88 is required for satellite cell-mediated myofiber regeneration in dystrophin-deficient mdx mice. *Human Molecular Genetics* (Accepted).
- 7) Gallot YS, **Bohnert KR**, Straughn AR, Xiong G, and Kumar A (2018). PERK regulates skeletal muscle mass and contractile function in adult mice. *FASEB Journal* (under revision).

F. POSTER PRESENTATIONS

- 2015 **Bohnert, KR**, Sato S, Xiong G, and Kumar A. Poster Presented at “2nd Midwest Membrane Trafficking & Signaling Symposium” at the University of Louisville on July 25th, 2015.
- 2015 **Bohnert, KR**, Gallot YS, Sato S, Xiong G, Hindi S, and Kumar A. Presented poster at the “Research Louisville” symposium on October 14th, 2015.
- 2016 **Bohnert, KR**, Gallot YS, Sato S, Xiong G, Hindi S, and Kumar A. Poster Presentation at “Advances in Skeletal Muscle Biology in Health and Disease” conference at the University of Florida from January 20-22, 2016.
- 2016 **Bohnert, KR**, Gallot YS, Sato S, Xiong G, Hindi S, and Kumar A. Poster presentation at the “Neuroscience Day”, University of Louisville on April 7th, 2016.
- 2016 **Bohnert, KR** and Kumar A. Poster Presentation at “3rd Cancer Cachexia” conference in Washington DC from September 23-25, 2016.
- 2016 **Bohnert, KR** and Kumar A. Presented poster at the “Research Louisville” symposium on October 11th, 2016.

- 2017 **Bohnert, KR** and Kumar A. Poster Presentation at “Advances in Skeletal Muscle Biology in Health and Disease” conference at the University of Florida from March 8-10, 2017.
- 2017 **Bohnert, KR** Gallot YS, Xiong G, McMillan JD. Poster Presentation at “Research Louisville” symposium on September 12, 2017